

Analysis of Unplugging as a Common Disassembly Operation

by

Shuihao XU



A thesis submitted to

The University of Birmingham

for the degree of

DOCTOR OF PHILOSOPHY

Department of Mechanical Engineering

School of Engineering

College of Engineering and Physical Sciences

University of Birmingham

December 2023

UNIVERSITY OF
BIRMINGHAM

University of Birmingham Research Archive

e-theses repository

This unpublished thesis/dissertation is copyright of the author and/or third parties. The intellectual property rights of the author or third parties in respect of this work are as defined by The Copyright Designs and Patents Act 1988 or as modified by any successor legislation.

Any use made of information contained in this thesis/dissertation must be in accordance with that legislation and must be properly acknowledged. Further distribution or reproduction in any format is prohibited without the permission of the copyright holder.

Acknowledgements

I would like to thank my PhD supervisor, Prof. Duc Truong Pham. In the final year of my undergraduate studies, I asked Prof. Pham about the possibility of continuing to pursue my doctorate at the University of Birmingham, and I obtained approval from Prof. Pham. With the support of Prof. Pham, I completed my PhD application and admission. His rich academic knowledge and tireless research spirit inspired and directed me to finish my research topic on robotised unplugging throughout the four years of study. Working with Prof. Duc Truong Pham has had a significant impact on my current and future lives.

I would like to thank Dr. Jun Huang for his supervision and guidance during my final year project (Sep 2018–Jun 2019) in my BEng studies at the University of Birmingham. This also allowed me to familiarise myself with the AutoReman Laboratory in advance. I would like to thank Dr. Yongjing Wang for sharing his experience with academic research during my PhD studies. I would like to thank Dr. Shizhong Su for sharing his finite element analysis experience. I would like to thank all the members of the AutoReman Laboratory who helped and stood out during my PhD studies.

I would like to thank the School of Engineering, University of Birmingham, for giving me the opportunity to start my PhD studies. This research was also supported by the UK Engineering and Physical Sciences Research Council (EPSRC), Grant No. EP/N018524/1 - Autonomous Remanufacturing (AutoReman) project.

I would like to thank my parents, my family and my girlfriend, who have always supported and inspired me during this time.

Abstract

Climate change poses a serious existential threat to human societies and the natural environment worldwide. To lessen environmental damage, the circular economy seeks to convert from linear to closed-loop processes in which products, components, and materials circulate for as long as possible at their best value. It is well accepted that remanufacturing, a circular economy strategy that involves returning a product at the end of its service life to its original condition, is economically and environmentally beneficial. Robotising disassembly can make remanufacturing even more cost-effective by removing a substantial proportion of the labour costs associated with dismantling end-of-life products for subsequent processing. As unplugging of press-fitted components is a common operation in disassembly, it is appropriate to investigate how it can be robotised.

For cylindrical plugs and sockets, an unplugging technique, twist-and-pull or twisting-pulling, is proposed to reduce axial friction during the unplugging process. Through theoretical modelling, simulations, and experimental analysis, the interactions among twisting, pulling and axial friction reduction during unplugging are explored. An analysis of the experimental, simulation, and theoretical results confirmed that for small radial interference, twisting and pulling reduces the axial friction and the maximum required unplugging force.

For cuboid plugs and sockets, there are two conditions for the plug: unconstrained and constrained. Correspondingly, two novel disassembly methods, unconstrained wiggling and constrained wiggling, have been proposed. The theoretical models of these unplugging strategies are validated by Finite-Element Modelling. The experimental results prove that

for soft plugs and hard sockets, wiggling reduces the axial friction and the maximum required unplugging force.

In conclusion, this thesis discusses three unplugging techniques for two different plug socket shapes to reduce the axial frictional resistance during the unplugging process and enable a robot to perform unplugging easily.

Declaration

I, Shuihao XU, hereby declare that this PhD thesis titled “Analysis of Unplugging as a Common Disassembly Operation” was carried out by my own for the degree of Doctor of Philosophy at the University of Birmingham. I confirm that:

- The presented work has never been previously included in a thesis or dissertation submitted for a degree or other qualifications.
- Where the thesis is based on joint work done by myself with others, a clear statement has been made to illustrate how the contribution was exactly distributed.
- Except where states are otherwise by reference or acknowledgement, the work presented is entirely composed of myself.

Signed: Shuihao XU.

Date: 28.12.2023.

Table of Contents

Acknowledgements.....	3
Abstract.....	5
Declaration.....	7
Table of Contents	8
List of Figures.....	12
List of Tables.....	16
Acronyms.....	18
Symbols	20
1 Introduction.....	24
1.1 Background.....	24
1.1.1 Climate Change.....	24
1.1.2 Circular Economy	25
1.1.3 Remanufacturing.....	25
1.1.4 Automated disassembly	26
1.1.5 Unplugging	27
1.2 Problem Statement.....	28
1.3 Aims and Objectives of the Research.	29
1.4 Outline of the thesis	30
2 Literature Review	31
2.1 Robotic disassembly	31

2.2	Peg-hole problem.....	33
2.2.1	Origin and development.....	33
2.2.2	Mechanical analysis	34
2.2.3	Force Sensing and Compliance.....	34
2.2.4	Vision-based Approaches.....	35
2.2.5	Robotic Assembly Strategies	35
2.2.6	Applications	35
2.2.7	Summary.....	36
2.3	Interference fit problem	36
2.3.1	Analytical Models.....	37
2.3.2	Finite Element Analysis	38
2.3.3	Contact surface and stress distribution	39
2.3.4	Application and development	40
2.3.5	Combination of theory, simulation and experiment.....	40
2.3.6	Summary.....	41
3	Robotised Unplugging of a Cylindrical Peg Press-Fitted into a Cylindrical Hole	44
3.1	A Case Study on Robotic Disassembly of an EV Battery	45
3.2	Unplugging motion in robotic disassembly	47
3.3	Combined Twisting-Pulling.....	53
3.4	FEM of unplugging.....	56
3.5	Experiments	62

3.5.1	Direct pulling	64
3.5.2	Combined twisting-pulling	65
3.6	Discussion	69
3.7	Conclusion	70
4	Robotised Unplugging of a Cuboid Plug Press-Fitted into a Cuboid Socket with a Disassembly Strategy—Unconstrained Wiggling	72
4.1	Cuboid Unplugging in Robotic Disassembly	73
4.2	Unconstrained wiggling	78
4.3	FEM of cuboid unplugging	81
4.4	Experiments	85
4.4.1	Direct pulling	89
4.4.2	Residual force analysis	91
4.4.3	Unconstrained wiggling	97
4.4.3.1	Single-block unconstrained unplugging experiment	101
4.4.3.2	Multiple-block unconstrained unplugging experiment	104
4.5	Summary	111
5	Robotised Unplugging of a Cuboid Plug Press-Fitted into a Cuboid Socket with a Disassembly Strategy—Constrained Wiggling	113
5.1	Constrained wiggling	114
5.2	FEM of cuboid unplugging	122
5.3	Experiments	126
5.3.1	Experimental setup	126

5.3.2	Constrained wiggling	126
5.3.2.1	7.5 mm-7 mm unplugging experiment	129
5.3.2.2	7.6 mm-7 mm unplugging experiment	133
5.3.2.3	9 mm-8 mm unplugging experiment	135
5.3.2.4	11 mm-10 mm unplugging experiment.....	137
5.3.2.5	18 mm-16.5 mm unplugging experiment	139
5.3.2.6	18 mm-17 mm unplugging experiment	141
5.4	Summary.....	143
6	Conclusion	148
6.1	Conclusions.....	148
6.2	Summary of Achievements	150
6.3	Future Work	151
Appendix A. Experimental data for Chapter 3		154
A.1	Experimental data on directly pulling pins out of the socket.....	154
A.2	Experimental data on twisting pulling pins out of the socket.....	158
Appendix B. Experimental data for Chapter 4 and Chapter 5		168
B.1	Experimental data for residual force analysis	168
B.2	Experimental data for the constrained wiggling unplugging experiment	190
Appendix C. Programming code for calculating variables in Chapter 5		203
References.....		205

List of Figures

Figure 3.1: Inner structure of the battery pack [97].	45
Figure 3.2: Contact force diagram during the unplugging process.	48
Figure 3.3: The interference-fit peg-hole model.	49
Figure 3.4: Schematic diagram of the unplugging.	51
Figure 3.5: The mechanics of twisting-pulling.	53
Figure 3.6: Schematic diagram of the twisting unplugging.	55
Figure 3.7: Mesh of the model and stress distribution in the components due to the interference fit.	58
Figure 3.8: ABAQUS axial resistance friction diagrams (straight pulling, no twisting).	60
Figure 3.9: ABAQUS axial resistance friction diagrams (combined twisting and pulling).	61
Figure 3.10: (a) Experimental setup. (b) Four different sizes of pins used in the experiments.	62
Figure 3.11: Flow charts of the robot programs.	63
Figure 3.12: Variation in the force along the Z-axis (direct pulling).	64
Figure 3.13: Variation in the force along the Z-axis (combined twisting-pulling).	66
Figure 3.14: Changes in the torque on the Z-axis in the case of twisting pulling.	67
Figure 4.1: Cylindrical and cuboid connections	74
Figure 4.2: Contact force diagram in the cuboid unplugging process.	75
Figure 4.3: Interference fit plug-socket model.	76
Figure 4.4: Schematic diagram of unconstrained wiggling and applied force.	78
Figure 4.5: The mechanics of unconstrained wiggling unplugging.	79
Figure 4.6: Dimension of the model and boundary conditions applied.	81
Figure 4.7: Deformation and stress distribution of the model due to the interference fit.	83

Figure 4.8: Stress distribution of the plug due to the interference fit.	83
Figure 4.9: Experimental setup.	85
Figure 4.10: Different sizes of holders used in the experiment.	87
Figure 4.11: Flow charts of the robot programs for direct pulling.	89
Figure 4.12: Two cases in which the 6-axis force change in the PVC block was pulled out directly.	90
Figure 4.13: Contactless grasping experiment with force diagrams.	92
Figure 4.14: Force diagram of the handheld block grasping experiment.	93
Figure 4.15: The motion track of the gripper grabbing the PVC block.	94
Figure 4.16: Force diagrams of the contactless grasping experiment with small displacement.	95
Figure 4.17: Variation in the force along the Z-axis with two different pulling methods. ..	96
Figure 4.18: Experimental setup for unconstrained unplugging.	97
Figure 4.19: Measurement results at three different locations.	98
Figure 4.20: Dimensions of the PVC blocks used in the experiments.	99
Figure 4.21: Flow charts of the robot programs for unconstrained unplugging.	100
Figure 4.22: Variation curves of the force in the first series of experiments.	102
Figure 4.23: Wear of the PVC block after multiple experiments.	103
Figure 4.24: Standard-sized PVC blocks for unconstrained unplugging experiments.	104
Figure 4.25: Variation curves of force for unconstrained unplugging experiments.	105
Figure 4.26: Expected unconstrained pullout trajectory of the PVC block.	108
Figure 4.27: Comparison between the expected pull-out trajectory and the actual pull-out trajectory.	109
Figure 5.1: Schematic diagram of constrained wiggling and force application.	115

Figure 5.2: Schematic diagram of the change in contact surface stress with increasing lateral force.	115
Figure 5.3: Schematic diagram of the contact surface stress distribution.	116
Figure 5.4: Deformation diagram and function on both sides of the plug.....	118
Figure 5.5: Geometry of the distance between two sides' deformation tilt lines.....	121
Figure 5.6: Boundary conditions applied to the plug-socket model.	123
Figure 5.7: Stress distribution of the plug-socket model with a 2 N lateral force.	124
Figure 5.8: Stress distribution of the plug with a 2 N lateral force.....	125
Figure 5.9: Coordinates and gripping direction for constrained wiggling.....	127
Figure 5.10: Flow charts of the robot programs for constrained wiggling unplugging.....	129
Figure 5.11: Variation curves of the force for the 7.5 mm-7 mm constrained unplugging experiments.	130
Figure 5.12: PVC block that broke after applying 4 N of lateral force.	131
Figure 5.13: The bending and recovery of the PVC block at the moment of pulling out..	133
Figure 5.14: Variation curves of the force and torque for the 7.6 mm-7 mm constrained unplugging experiments.....	134
Figure 5.15: Variation curves of the force and torque for the 9 mm-8 mm constrained unplugging experiments.....	136
Figure 5.16: Variation curves of the force and torque for the 11 mm-10 mm constrained unplugging experiments.....	138
Figure 5.17: Variation curves of the force and torque for the 18 mm-16.5 mm constrained unplugging experiments.....	140
Figure 5.18: Variation curves of the force and torque for the 18 mm-17 mm constrained unplugging experiments.....	142
Figure 5.19: Example of using MATLAB to calculate the variables.....	143

Figure 5.20: Error distribution and average error of these sets of experiments..... 146

List of Tables

Table 3.1: Parameters of the materials used in the simulation.....	56
Table 3.2: Dimensions of the pin, hole and receptacle blocks in different sets of simulations.	57
Table 3.3: Maximum axial friction forces (direct pulling).	65
Table 3.4: Maximum axial friction force (combined twisting-pulling).	68
Table 3.5: Axial friction reduction.	68
Table 4.1: Parameters of the material used in the cuboid unplugging simulation.	82
Table 4.2: Material properties of the PVC block and the aluminum angle.....	88
Table 4.3: Measurement results at different locations.	98
Table 4.4: Design of the movement parameters.....	101
Table 4.5: Results of the first series of experiments and calculations for friction.....	102
Table 4.6: Results of measurements of PVC blocks in unconstrained unplugging experiments.	104
Table 4.7: Results of the unconstrained unplugging experiments and calculations for friction.	106
Table 4.8: Theoretical and Experimental Errors of Maximum Friction.	107
Table 4.9: Reduction in the maximum axial friction.	107
Table 5.1: Dimensions and measurements for the 7.5 mm-7 mm unplugging experiments.	130
Table 5.2: Results of the 7.5 mm-7 mm constrained unplugging experiments.....	132
Table 5.3: Dimensions and measurements for the 7.6 mm-7 mm unplugging experiments.	134
Table 5.4: Results of the 7.6 mm-7 mm constrained unplugging experiments.....	135

Table 5.5: Dimensions and measurements for the 9 mm-8 mm unplugging experiments.	135
Table 5.6: Results of the 9 mm-8 mm constrained unplugging experiments.....	137
Table 5.7: Dimensions and measurements for the 11 mm-10 mm unplugging experiments.	137
Table 5.8: Results of the 11 mm-10 mm constrained unplugging experiments.....	139
Table 5.9: Dimensions and measurements for the 18 mm-16.5 mm unplugging experiments.	139
Table 5.10: Results of the 18 mm-16.5 mm constrained unplugging experiments.....	141
Table 5.11: Dimensions and measurements for the 18 mm-17 mm unplugging experiments.	141
Table 5.12: Results of the 18 mm-17 mm constrained unplugging experiments.....	142
Table 5.13: Summary of the theoretical, actual, and experimental results for all the sets of experiments.	144

Acronyms

2D	Two-dimensional
3D	Three-dimensional
AI	Artificial intelligence
Al	Aluminium
AutoReman	Autonomous Remanufacturing
CO ₂	Carbon dioxide
DOF	Degree of freedom
EoL	End of life
EPSRC	Engineering and Physical Sciences Research Council
EV	Electric vehicle
EVA	Ethylene Vinylacetate
FDM	Fused deposition modelling
FE	Finite element
FEA	Finite element analysis
FEM	Finite element modelling
IPCC	Intergovernmental Panel on Climate Change
LF	Lateral force
LiB	Lithium-ion battery
PHEV	Plug-in hybrid electric vehicle

PVC	Polyvinyl Chloride
rad	Radians (measure of angle)

Symbols

A	Contact area (Chapter 4)
d	Distance between the inclined lines formed by deformation at both ends of the plug (Chapter 5)
d_2	Diameter of the hole (Chapter 3)
D_1	Diameter of the pin (Chapter 3)
D_2	Diameter of the plate (Chapter 3)
D_z	Displacement on the Z-axis (Chapter 5)
E	Young's modulus
E_1	Young's modulus of EVA (Chapter 3)
E_2	Young's modulus of steel (Chapter 3)
f	Friction force (Chapter 4)
f_Y	Friction force on the Y-axis (Chapter 4)
f_Z	Friction force on the Z-axis (Chapter 4)
F	Applied lateral force (Chapter 5)
F	Axial pulling force (Chapter 3)
F	Total contact force (Chapter 4)
F_1	Upwards pulling force
F_2	Lateral force
F_r	Total applied force (Chapter 3)

F_T	Tangential force (Chapter 3)
F_Y	Force on Y-axis (Chapter 4)
F_Z	Axial friction force
h_1	Deformation height on the right side (Chapter 5)
h_2	Deformation height on the left side (Chapter 5)
H	Height of the contact
k	Slopes of the deformation (Chapter 5)
l	Length of the PVC block
l_1	Length of the PVC block after contact (Chapter 4)
L	Depth of the contact (Chapter 3)
M	Applied external moment (Chapter 5)
P	Contact pressure
r	Nominal radius of the contact (Chapter 3)
r_2	Original radius of the hole (Chapter 3)
R	Axial friction Reduction
R_1	Original radius of the pin (Chapter 3)
R_2	Radius of the steel block (Chapter 3)
Rf	Resistance friction
Rf_1	Axial friction force
Rf_2	Tangential friction force

Rf_{max}	Maximum axial resistance friction
S	Contact area (Chapter 3)
T_z	Axial torque
u_r	Radial displacement
u_{r_1}	Radial displacement of the pin (Chapter 3)
u_{r_2}	Radial displacement of the hole (Chapter 3)
ν	Poisson's ratio
ν_1	Poisson's ratio of EVA (Chapter 3)
v_1	Upwards velocity (Chapter 4)
v_2	Lateral velocity (Chapter 4)
ν_2	Poisson's ratio of steel (Chapter 3)
v_c	Resultant velocity of the plug (Chapter 4)
v_c	Resultant velocity of the selected point on the pin (Chapter 3)
w	Angular velocity (Chapter 3)
w	Width of the PVC block (Chapter 4 and Chapter 5)
Δl	Change in length (Chapter 4)
Δl_1	Deformation length on the right side (Chapter 5)
Δl_2	Deformation length on the left side (Chapter 5)
δ	Interference on one side (Chapter 5)
δ	Radial interference

μ_d Coefficient of dynamic friction

μ_s Coefficient of static friction

1 Introduction

1.1 Background

1.1.1 Climate Change

Climate change poses an existential threat to human societies and natural ecosystems worldwide. According to the Intergovernmental Panel on Climate Change (IPCC), human activities have warmed the atmosphere, ocean and land by approximately 1°C above pre-industrial levels as of 2017 [1]. This dramatic disruption of the earth's energy balance has been driven primarily by greenhouse gas emissions from fossil fuel combustion, deforestation, agricultural practices, and other human activities since the Industrial Revolution [2]. Atmospheric carbon dioxide (CO₂) levels have risen to more than 400 parts per million, far exceeding the natural range of the past 800,000 years [3]. The impacts of climate change, including sea level rise, more frequent extreme weather events, and ecosystem shifts, are already apparent across physical and biological systems on all continents [4]. Warming on this scale would increase the risk to human health and survival through heat stress, the spread of infectious diseases, severe economic damage, and geopolitical instability [5]-[9].

Achieving the rapid, far-reaching transitions required to reduce emissions will entail massive shifts across technological, economic, political, and social domains [10]. Incremental improvements are insufficient; fundamental transformation of industrial systems toward sustainability is imperative [11].

1.1.2 Circular Economy

The take-make-use-dispose model relies on extracting maximum virgin resources to make short-lived products that are ultimately discarded as waste [12]. The circular economy aims to transition from linear to closed-loop flows where products, components, and materials circulate at their highest value for as long as possible [13], [14]. Resources are regeneratively designed to enable continuous recovery, renewal, and reuse during cycling. Waste and pollution are controlled by superior material selection, product longevity, reparability, and closed energy and material loops [15].

The climate change benefits of circularity are significant across mitigation and adaptation [16]. Circular strategies, including energy efficiency, renewables, resource optimisation, product longevity, reuse, remanufacturing, and recycling, can reduce greenhouse gas emissions by nearly 50% over business-as-usual projections for some sectors [17].

1.1.3 Remanufacturing

Remanufacturing is a circular economy strategy. Compared with traditional manufacturing, remanufacturing is one of the most effective approaches for reducing embodied material and energy use. Remanufacturing entails rigorous processes whereby end-of-life (EoL) or discarded products are restored to similar or better conditions with warranties to match [18]. This allows reused components and recycled materials to displace new inputs, avoiding duplication of high-impact extraction and processing. Studies consistently demonstrate the sustainability benefits of remanufacturing versus manufacturing new products. Greenhouse gas emissions are reduced for remanufactured goods [19]. Raw material and energy savings occur across product categories from vehicle engines to photocopiers, while water use decreases [20], [21]. These advantages make remanufacturing a key circular economy strategy for climate change mitigation.

However, remanufacturing faces barriers restricting broader adoption [12]. The variable availability, quality, and integrity of cores and components can inhibit process efficiency and reliability [22]. Remanufacturing also entails specialised facilities [23], skillsets, and regulatory compliance [24], [25]. However, a primary obstacle is the efficient and automated disassembly of end-of-life products to enable component reuse.

1.1.4 Automated disassembly

The disassembly stage strongly influences remanufacturing feasibility, economics, and environmental performance [26]. Manual disassembly is often slow, costly, and hazardous for workers with the potential for damage to recoverable parts. [27]. Increasing labour costs, turnover, variability, and availability constrain manual disassembly scalability for remanufacturing [28].

Automating the disassembly process through robotic work cells or on-demand systems can deliver major advantages over manual approaches [29]. Robotic disassembly automates skilled disassembly tasks for faster, more consistent, and reliable outcomes independent of operator conditions. Robots can be programmed to expertly separate target components without damage using optimal sequences, tools, grippers, and forces [30]. Sensors allow real-time monitoring of connection points and component states [31]. The integration of artificial intelligence (AI) techniques such as machine vision and machine learning enable adaptive control and decision making [32].

Automated disassembly substantially improves remanufacturing productivity and reliability while lowering costs and error rates [33]. Automation also reduces occupational hazards associated with difficult disassembly operations in harsh or hazardous environments [27].

1.1.5 Unplugging

Automated disassembly includes many different disassembly operations, among which there have been a few studies and research on unscrewing and removing. However, studies on unplugging are very rare, although unplugging is a common disassembly operation that occurs in the dismantling of both mechanical and electrical products [34].

Significant research is needed to develop unplugging strategies and evaluate the suitability of unplugging strategies for a variety of conditions and environments. In this thesis, two unplugging strategies, twisting and wiggling, and two plug-socket models with different shapes, cylinders and cuboids, are studied.

1.2 Problem Statement.

Unplugging is a disassembly operation that occurs in many applications, for instance, in industry, removing wires from controllers or power supplies, removing hoses from valves, and separating connectors from corresponding connecting objects; and in daily life, unplugging the network cable from the computer, unplugging the desk lamp plug from the socket, and unplugging the wine bottle stopper from the wine bottle. These various examples include different connection methods, shapes, and material combinations. In this paper, the most common wire interface connection is chosen as the research object. The fitting method of its model is interference fit, and the plug is applied for softer materials while hard materials are chosen for the socket. Electric wires are generally composed of an insulated outer shell and a conductive inner core. In this study, in order to simplify the theoretical model, the material of the plug is applied to the same soft material, and the conductive inner core will be ignored.

As a common operation in disassembly, unplugging is rarely mentioned and studied in academic articles. Therefore, in order to study this topic, it is necessary to draw inspiration from other related issues, such as interference fit and peg-hole problems.

Automated disassembly is an important part of remanufacturing, and it is also meaningful to consider using robots to complete automated unplugging. This article will propose some new disassembly strategies to provide robots with more references and choices when performing the unplugging operation.

1.3 Aims and Objectives of the Research.

The hypothesis of this research is that for plug-socket models of different shapes, using the corresponding unplugging strategy can reduce the maximum axial friction force on the plug during the pull-out process, thus making robotised unplugging easier. The following objectives were set to help prove this hypothesis.

- i. Establishing an interference-fit peg-hole theoretical model to conduct a mechanical analysis of a disassembly strategy, twisting-pulling (Objective 1)
- ii. Based (i), designing a series of unplugging experiments to study the effect of twisting-pulling on the reduction in maximum axial friction (Objective 2).
- iii. Building an interference-fit cuboid plug-socket theoretical model (two surfaces in contact) to analyse an emerging approach, wiggling, for unplugging (Objective 3).
- iv. Designing unconstrained unplugging experiments based on the theoretical model of (iii) to prove that wiggling can reduce the plug's maximum axial friction during the pull-out process, when two surfaces of the plug are unconstrained (Objective 4).
- v. Designing constrained unplugging experiments according to the results of (iii) to demonstrate that wiggling can reduce the maximum axial friction of the plug when all four surfaces of the plug are constrained (Objective 5).

1.4 Outline of the thesis

The remaining sections of this thesis are structured as follows:

- Chapter 2 reviews the literature about the topics investigated in this thesis, including robotic disassembly, peg-hole problems, interference-fit models, calculations of interference fits, friction analysis, Finite Element simulation, and software usage.
- Chapter 3 illustrates the theoretical model of a cylindrical interference-fit peg-hole. A disassembly strategy, twisting-pulling, for decreasing the maximum axial friction of the plug during the robotised unplugging process is demonstrated (addressing Objectives 1 and 2).
- Chapter 4 presents a mechanical model of a cuboid plug socket, in which two surfaces of the plug have interference contact with the socket while the other two surfaces have no contact. A disassembly approach, unconstrained wiggling, is introduced when the non-contacting two sides of the plug are unconstrained (addressing Objectives 3 and 4).
- Chapter 5 describes another disassembly strategy, constrained wiggling. This approach is based on the basic interference model in Chapter 4, and the difference is that the two noncontact sides of the plug are constrained; hence, the wiggling direction can be the same as the interference direction.
- Chapter 6 summarises the achievements of this thesis in the field of unplugging and provides potential research directions for further study.

2 Literature Review

2.1 Robotic disassembly

Disassembly is an essential step in remanufacturing in which the scrapped products are separated into subassemblies or useable parts using manual or robotic procedures [35]. Manual disassembly, which is time-consuming, expensive and boring, is commonly adopted in industrial remanufacturing to handle end-of-life products [36]. Compared with manual disassembly, robotised disassembly can improve the efficiency of disassembly [37]. For this reason, robotised disassembly, which uses intelligent manipulators to disassemble items, is being developed, and its technology needs to be promoted to meet the requirements of industrial remanufacturing [38].

There have been many existing studies on and advancements in robotic disassembly, covering various operations, techniques, challenges [39] and reviews. Unscrewing is a common disassembly operation. Apley et al. [40] analysed unscrewing operations and studied various methods for diagnosing faults. Chen et al. [41] designed a multihead tool on a robot for unscrewing, drilling and grinding. Schumacher and Jouaneh [42], [43] analysed unscrewing operations by developing a robotic system equipped with force sensing resistors to release snap-fit covers on electronic devices. Huang et al. [44] proposed strategies for handling common failure modes in robotised unscrewing operations, including screwdrivers missing the screw head, slipping on the head, or encountering screws that are too tight to remove. Li et al. [45] presented a new method for automating the unfastening of hexagonal headed screws using a collaborative robot. They developed a spiral search strategy to compensate for uncertainties in screw positioning and implemented a control strategy

combining torque, position, and active compliance control. Removing operations such as prying or snapping components apart are also widely studied. Vongbunyong et al. [46] presented a platform for operators to demonstrate full disassembly processes, captured via computer vision. This approach enables the transfer of skills such as removing operations to robots by extracting tool motions and sequences.

Researchers have developed techniques to improve robotic disassembly performance. Marconi et al. [47] presented a method for calculating the effective disassembly sequence and time for industrial products. Merdan et al. [48] proposed an ontology-based automated disassembly system to handle the dynamic nature and variability of disassembly environments. Kececi et al. [49] presented an approach for improving visually servoed robotic disassembly operations using an independently mobile camera. Huang et al. [50] developed a new experimental human–robot collaborative disassembly cell with two collaborative robots and a human operator working together flexibly. Klas et al. [51] introduced a multifunctional gripper for disassembly tasks that is able to perform actions such as grasping, tool change, levering and unscrewing.

Poschmann et al. [52] provided a comprehensive literature review on the use of robotics in disassembly tasks for remanufacturing, covering 178 papers. They surveyed robotic assembly and disassembly planning, execution, and design considerations and discussed the importance of these technologies for sustainability and a circular economy. Daneshmand et al. [53] also reviewed the state of the art in robotic assembly and disassembly, examining aspects such as sequence planning, robot types, grasping, human-robot collaboration, and sustainability.

In summary, robotic disassembly research covers diverse operations, techniques for enhancing performance, and strategies for handling uncertainties and reviews. However, few

studies have considered unplugging and its role in robotic disassembly. As a common manual disassembly operation, an in-depth study of the mechanical principles and strategic approaches related to the process of unplugging can significantly enrich the use of options and strategies in robotic disassembly.

2.2 Peg-hole problem

Considering that there are few papers specifically studying robotic unplugging, theoretical and mechanical models regarding unplugging can only draw inspiration from other related directions. One of the research focuses, single-cylinder unplugging, can be approximately regarded as the reverse of the peg-hole insertion problem and has been investigated by many researchers.

2.2.1 Origin and development

The peg-hole problem is a classic challenge in robotics involving the insertion of a peg into a hole. This problem was first described in the 1980s as researchers began exploring solutions for robots to perform complex insertion tasks. In 1979, McCallion, Johnson and Pham [54] presented a simple solution to the problem of inserting a peg in a hole. One of the other early works on peg-hole insertion was by Whitney [55], who proved that the peg-hole insertion process was affected by the location of the compliance centre, which should be at or near the tip of the peg. Since then, numerous researchers have developed different strategies and models to address the peg-hole problem.

2.2.2 Mechanical analysis

Mechanical analysis and the establishment of theoretical models are crucial to solving the peg-hole problem. Lozano-Pérez, Mason and Taylor [56] investigated an automatic synthesis of the fine-motion approach and developed a mathematical model of peg-hole insertion. The strategy includes correctness criteria for compliant motion strategies. Zohoor and Shahinpoor [57] analysed the dynamic insertion of a peg into a hole for manufacturing automation applications. They derived governing equations for various contact configurations between the peg and hole. Pitchandi et al. [58] studied insertion force analysis for a compliantly supported peg-in-hole assembly using a dynamic model. These parameters included the damping coefficient and elastic property of the compliance material in the model. Zhang et al. [59] developed a theoretical model based on active compliance for peg-hole disassembly.

2.2.3 Force Sensing and Compliance

Force sensing and compliance play crucial roles in the peg-hole problem. Li et al. [60] proposed a human-inspired compliant strategy for peg-hole assembly using environmental constraints and coarse force information. They designed a constraint region based on geometric information to reduce uncertainty in initial peg positioning. A coarse force sensor provides contact force direction to guide peg adjustments. Abdullah et al. [61] presented an automated peg-hole assembly approach using force/torque sensing and machine vision guidance. They developed a 6-phase algorithm inspired by human operators using force data to determine hole location. The experiments showed improved contact position estimation compared to that of force map methods.

2.2.4 Vision-based Approaches

Vision-based approaches have been widely used in peg-hole assembly tasks. Su et al. [62] proposed a sensorless strategy for inserting an eccentric peg into a hole with tight clearance. Experiments have shown successful high-precision assembly without force sensors using vision and an open-loop insertion device. Wang et al. [63] proposed an uncalibrated visual servoing method for microassembly of a micropeg and microhole. The experiments showed that the micropeg was successfully assembled into the mating hole using the uncalibrated visual servoing method. Chang et al. [64] developed an automatic visual-servo microassembly system for peg-in-hole tasks. The experiments demonstrated the automatic alignment, grasping, transport, and assembly of micropegs into mating holes.

2.2.5 Robotic Assembly Strategies

Several robotic assembly strategies have been proposed for multiple peg-hole insertion problems. Fei and Zhao [65] presented an assembly process modelling and analysis approach for robotic multiple peg-in-hole insertion. Contact forces were analysed using screw theory and small motion rules to overcome redundancy. A simulation and an experiment involving a triple peg-hole task validated the methods. Zhang et al. [66] developed fuzzy force control strategies for rigid dual peg-hole assemblies. Contact states and forces were analysed to prove the feasibility of the strategy. Impedance control was used in free, contact, and mated states with appropriate force/moment references.

2.2.6 Applications

Peg-hole assembly tasks have been applied to various robotic systems. Zhao et al. [67] explored a peg-in-hole approach for six-leg robots using vision and force/torque sensors to navigate the hole, plan the trajectory, and ensure smooth insertion and assembly. Li et al. [68] studied the robotic assembly of an irregularly shaped peg into a hole with partial constraints.

They developed kinematic models for the partial constraints between the peg and hole parts. Zhang et al. [69] discussed a two-phase assembly scheme for the Baxter robot utilising force/torque sensors to ensure accurate positioning and successful assembly of peg and hole pieces.

2.2.7 Summary

In general, the model establishment, mechanical analysis, visual application and automated assembly strategies included in the peg-hole problem are of great help and inspiration to the unplugging research of this thesis. Based on the experience and guidance provided by the literature, vision (camera) was used during the unplugging research experiment to assist the robot in finding and grasping the corresponding target. The use of sensors enables real-time force and torque data to be acquired and used to determine the real-time position and status of the target using certain programming strategies. The model establishment and mechanical analysis of the peg-hole problem can serve as a reference for the unplugging problem. However, the main difference between the two models is that the peg-hole contact is more of a clearance fit, while the unplugging contact is an interference fit. In this case, further research on the interference-fit model is needed.

2.3 Interference fit problem

Interference fit, also known as press fit or shrink fit, is a common mechanical assembly technique used to join cylindrical or tapered parts by creating intentional interference between their mating surfaces [70]. The inner component is forcibly pressed or shrunk into the outer component, generating compressive contact stresses that provide friction and adhesion to resist relative motion between the parts [71]. Interference-fitted joints are utilised

in a wide range of applications, such as mounting gears and pulleys on shafts, hub-shaft connections, fastening machine elements to shafts, and installing bearings. Hence, the interference fit has been studied extensively due to its wide application in engineering.

2.3.1 Analytical Models

A number of studies have developed analytical models to estimate the stresses, contact pressures and axial forces generated in interference fit assemblies. Goel [72] presented a closed-form analytical solution for estimating the initial contact force in an interference-fit pin connection, including the effects of pin shape, stiffness, interference fit, hole shape and plate material. Song et al. [73] developed an analytical model based on complex potential theory to investigate the stress distribution in the interference-fit area around a composite laminate joint. Jiang and Bi [74] theoretically analysed an elastic-plastic interference fit model treating the pin as an elastic body, deriving equations for contact stress, elastic limit interference and plastic zone radius, and verified the results with FEA. Croccolo and Vincenzi [75] presented a generalised mathematical model to calculate the stresses and contact pressures in shaft-hub couplings made of multiple elements of different materials. The model accounts for static loads, rotation, and interference fits. The results were validated against finite element analysis. Paredes et al. [76] studied the axial load capacity of interference fit and adhesively bonded joints between carbon-epoxy composite bushes and steel housings. They found that adding anaerobic adhesive alone did not significantly increase the push-out force, but incorporating axial grooves in the composite bush to host the adhesive improved the push-out force.

Goel's theoretical model used 'spring' model to simulate the contact condition of the interference fit pin joint, the approach is worth learning from but only for initial contact stage. Song's model combined analytical and numerical methods. However, this model is analysed

for the material of composite laminates. Jiang and Bi's model considered the elastic-plastic behaviour of the materials. The section for the elastic deformation of the interference fit joint is regarded as one reference for the model establishment in this thesis. The mathematical model presented by Croccolo focused on the analysis of shaft-hub couplings; it analysed axial rotation, and the axial displacement, which is the concern of this research, was neglected. Paredes's research simplified the fastener bolt into a tip to simulate the installation process and analyse the actual axial force loss. The influence of the thread on the contact surface is ignored.

2.3.2 Finite Element Analysis

Finite element analysis (FEA) has been employed to design and analyse interference fits. Sen and Aksakal [77] developed a finite element model to analyse the transient thermal stress distribution in an interference-fitted shaft-hub system during the shrink-fitting process. Zhang et al. [78] compared FEA results versus traditional analytical methods for an interference-fitted ring gear, finding that FEA provides more complete and accurate stress results and proposed new safety factors and tolerance guidelines to improve the interference fit design. Shen et al. [79] performed FEA contact analysis with different interferences, shaft diameters, wall thicknesses and mating lengths using orthogonal testing and regression analysis to investigate the relationships between parameters and contact stress for shaft-sleeve interference fits. Lanoue et al. [80] performed a 3D FEA study focused on mesh convergence, submodelling and contact algorithms to obtain accurate displacement and stress results for an interference-fitted assembly under bending. Pedersen [81] analysed 3D shrink-fit joints using axisymmetric finite element models. The studies determined the shrinkage fit surface geometry needed to produce the desired contact pressure distribution. A superelement technique was also presented to directly calculate contact pressures for a given interference fit. Niu [82] developed a finite element model to study the stress

distribution in an interference-fitted shaft-sleeve assembly. The results showed high stresses at the ends of the sleeve and a W-shaped contact pressure distribution. Mackerle [83] provided an extensive bibliography on finite element analyses of various mechanical fastening techniques published between 1990 and 2002, including bolted joints, rivets, fittings, and tubular joints. More than 700 references were classified into relevant categories.

2.3.3 Contact surface and stress distribution

The analysis of the contact surface and stress distribution is essential for improving and supplementing theoretical models of interference fit. Lewis et al. [84] measured the interface pressure in interference fits using ultrasound reflection. The authors showed that the interface behaves like a spring, with higher stiffness and ultrasound transmission indicating higher pressure. Their results matched predictions and showed edge effects but the ability to detect surface damage. Bottini and Boschetto [85] examined the effects of surface morphology and interference on assembly forces for fused deposition modelling (FDM) parts. The deposition angle strongly affects the deviation and roughness. Jiang et al. [86] analysed the hole deformation and residual stresses during interference fit bolt insertion. They observed that higher interference levels result in increased nonuniformity in hole expansion and larger protuberances. Parsons and Wilson [87] presented a method for determining the surface contact stresses resulting from interference fits using finite element analysis for the sleeve and classical elasticity analysis for the shaft. They analysed sleeves of rectangular, stepped and tapered sections fitted to a solid shaft and compared the results to known solutions. Sogalad and Udupa [88] performed a comparative study of the stress distribution in interference-fitted assemblies using Lamé's approach and finite element analysis. The authors evaluated the principal and von Mises stresses for different combinations of pin and bush materials, cryogenic treatment, and geometric parameters such as contact length and interference.

2.3.4 Application and development

There are also many applications of interference fit that have been researched, including some assembly strategies and conclusions drawn from the integration of theoretical, simulated and experimental results. Hüyük et al. [89] studied elastic–plastic interference-fit joints experimentally and numerically, identifying three distinct stages as pins that are pushed into a tube and finding an optimum geometry that maximises joint strength. Liu et al. [90] proposed a screw insertion method to reduce axial friction in peg-in-hole assemblies. Analysis and experiments showed that the imposed screw motion redistributed friction from the axial to the tangential direction. Clearance-fit and interference-fit tests verified decreased axial friction with screw insertion. Croccolo et al. [91] investigated the axial push-out force in hybrid joints made using carbon-epoxy composite bush interference fitted into a steel housing. Grooved bushes were proposed to increase the push-out force. Yang et al. [92] analysed the contact pressure between two rough surfaces in a cylindrical interference fit, which is used for torque transmission in machine assemblies. They developed a new model accounting for the plastic deformation of asperities to calculate the tight fitting pressure using the surface bearing area ratio to relate the radial deflection to the contact area.

2.3.5 Combination of theory, simulation and experiment

Madej and Sliwka [93] analysed interference-fit joints, which are commonly used in engineering constructions for connecting shafts and hubs. They performed finite element method (FEM) simulations of pressing a shaft into a hub for various interference fit types. The simulation results were verified experimentally using an MTS testing device, confirming the correctness of the numerical model. The load capacities obtained from the FEM simulations were compared to the analytical results using Lamé's formulas. The comparisons showed that plastic deformation can occur during pressing, affecting the load capacity; therefore, the design should not rely solely on Lamé's elastic assumptions. Wang

et al. [94] proposed a new analytical method to accurately predict the pressure-fit curve for interference fitting part assembly. Compared to the commonly used thick-walled cylinder theory, the new method accounts for the influence of noncontact regions that induce a constant resistance force. The analytical results agreed well with the numerical and experimental results, with a relative error in the maximum press-mounting force less than 3%. Regalbuto and Wheeler [95] presented an approximate model to predict interference stresses in tapered-bolt assemblies, which was compared with experimentally measured stress distributions. They also analysed techniques to determine the maximum stress due to interference plus uniaxial tension. Wu et al. [96] proposed an analytical method based on complex potential theory to calculate the stress around interference fit holes in pinned composite plates under tensile loading. Displacement and load transfer conditions were analysed. The method was verified using 3D finite element analysis and experimental data, which showed good accuracy.

2.3.6 Summary

Although the literature review of interference fit has been conducted mainly from the perspective of assembly, it has also provided useful guidance for the research direction and methodology of this thesis. First, the analytical model of interference fit serves as a reference for the mechanical analysis of the unplugging theoretical model, especially for the initial static force analysis. Different from the force changes during the assembly process, the maximum force during the disassembly process generally occurs in the initial stage to overcome the maximum static friction. Therefore, static mechanical analysis of the initial state is particularly important for studying the unplugging problem. Second, the finite element analysis of interference fit provides references and suggestions for model establishment, contact modelling and boundary conditions for the simulation analysis of

unplugging problems. The deformation and stress analysis of the interference-fit contact surface can improve the understanding of unplugging contact problems and simplify the theoretical model.

3 Robotised Unplugging of a Cylindrical Peg

Press-Fitted into a Cylindrical Hole

This chapter discussed an unplugging technique, twist-and-pull or twisting-pulling, to reduce the axial frictional resistance during the unplugging process and enable a robot to perform it easily. In Section 3.1, a case study on the automated disassembly of an electric vehicle (EV) battery is introduced as the basis of the research. In Section 3.2, a theoretical model of the unplugging process is established, which is similar to the peg-hole model. In Section 3.3, the impact of twisting on axial friction during unplugging is described. In Section 3.4, simulation results for unplugging with and without twisting are presented. In Section 3.5, an overview of the experiments is conducted to validate the simulation, and a presentation of the experimental results is obtained. In Section 3.6, an analysis of the differences between the experimental, simulation, and theoretical results, as well as potential causes, is provided. The final section of this chapter (Section 3.7) concludes the chapter and suggests areas for further investigation.

3.1 A Case Study on Robotic Disassembly of an EV Battery

The case study, which has been published in the journal ‘Automation’ as ‘Robotic Disassembly Platform for Disassembly of a Plug-In Hybrid Electric Vehicle Battery: A Case Study’, presents a comprehensive study on the development and evaluation of a robotic platform designed for the disassembly of plug-in hybrid electric vehicle (PHEV) lithium-ion batteries (LiB) [97].

The study is structured around several key components, including the disassembly process, the design of a non-destructive robotic disassembly platform, and a comparison between robotic and human disassembly performance. Among them, the disassembly process is divided into four main stages, each involving specific steps such as unscrewing, removal, and disconnection of various components of the battery pack. The process begins with the removal of the top cover, followed by circuit breaking, junction box removal, and finally, the extraction of battery modules.

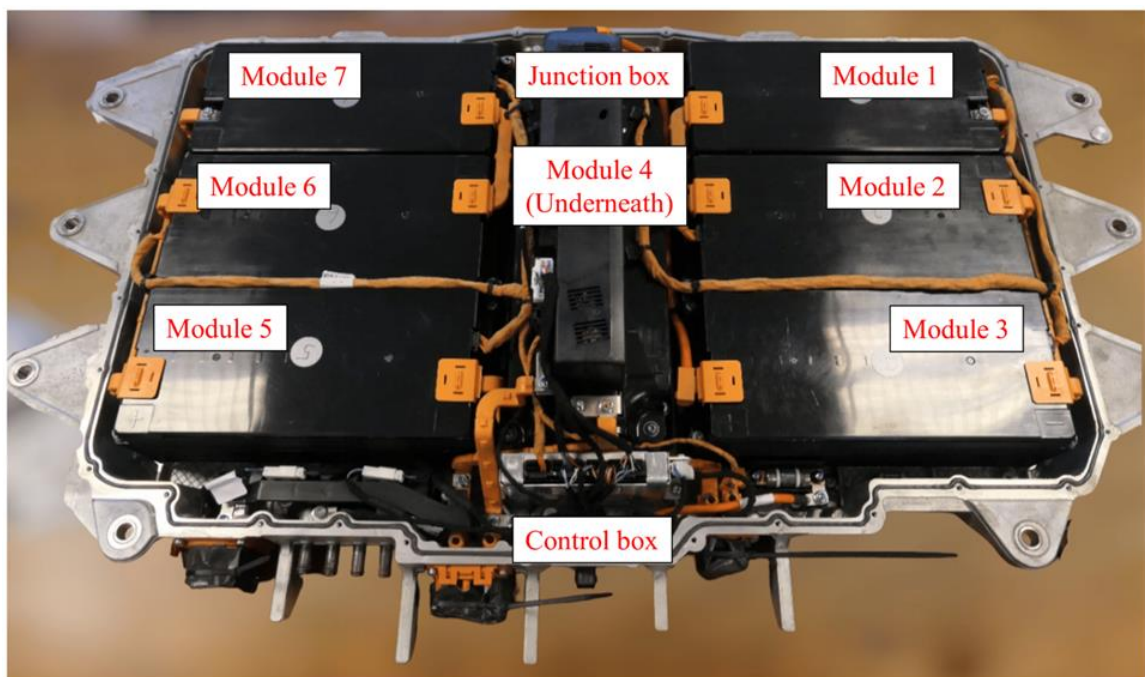


Figure 3.1: Inner structure of the battery pack [97].

During the disassembly process, a problem occurred: it is difficult to unplug the signal cable and some power cables from the control box, even with human hands. One of the solutions to this problem is to use side cutters to cut the cable ties [98, 99]. However, threading multiple signal wires into one interface can be labour-intensive and increase production costs, while keeping the complete interface or connection is another choice. Then, the research into ‘unplugging’ this disassembly operation thus started.

As mentioned in Section 1.2, the research object of this thesis is the combination of the hard socket and the soft plug. Ethylene vinyl acetate (EVA), which is commonly used in EV lithium-ion batteries for many different functions [100], is selected as the material of the plug.

3.2 Unplugging motion in robotic disassembly

Although a large amount of literature has been published about assembly and disassembly (Chapter 2), the definition of unplugging in the context of disassembly has still not been mentioned. After searching the Collins English Dictionary, the meaning of ‘unplug’ was “to disconnect (an electrical appliance) by taking the plug out of the socket” [101]. Therefore, unplugging is an elementary operation in disassembly that involves pulling a male component (the plug) out of a female receptacle (the socket). In a ‘plug-socket’ disassembly operation, the fit type is generally a fixed fit or a press fit, both of which are interference fits relying on the deformation of the mating components to provide a secure connection [102].

In this work, the unplugging problem was simplified, and the classic cylindrical peg-hole model was adopted to describe the relationship between the plug and socket. The difference is that the steel peg has been replaced with a plug made of a soft material, and the unplugging motion takes place with slight interference throughout the peg (Figure 3.2).

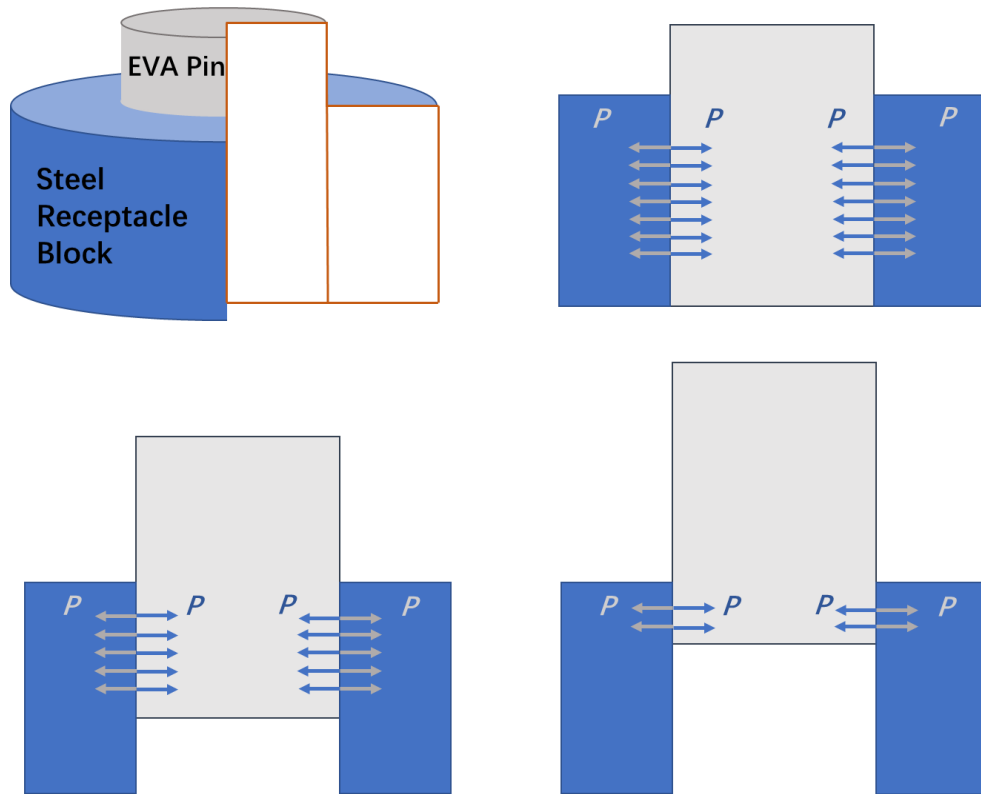


Figure 3.2: Contact force diagram during the unplugging process.

An interference-fit peg-hole model (Figure 3.3) was built to study the unplugging operation [74]. In addition to the diameter of the peg being slightly larger than the inner diameter of the hole, ethylene vinyl acetate (EVA) was used as the peg material in this model. In this theoretical model, since the radial interference (δ) is small and the material of the pin has good elasticity, only elastic deformation occurs in the pin and the hole block [103]. Therefore, ‘Modulus of Elasticity’ will be used as a reference for theoretical calculations [104].

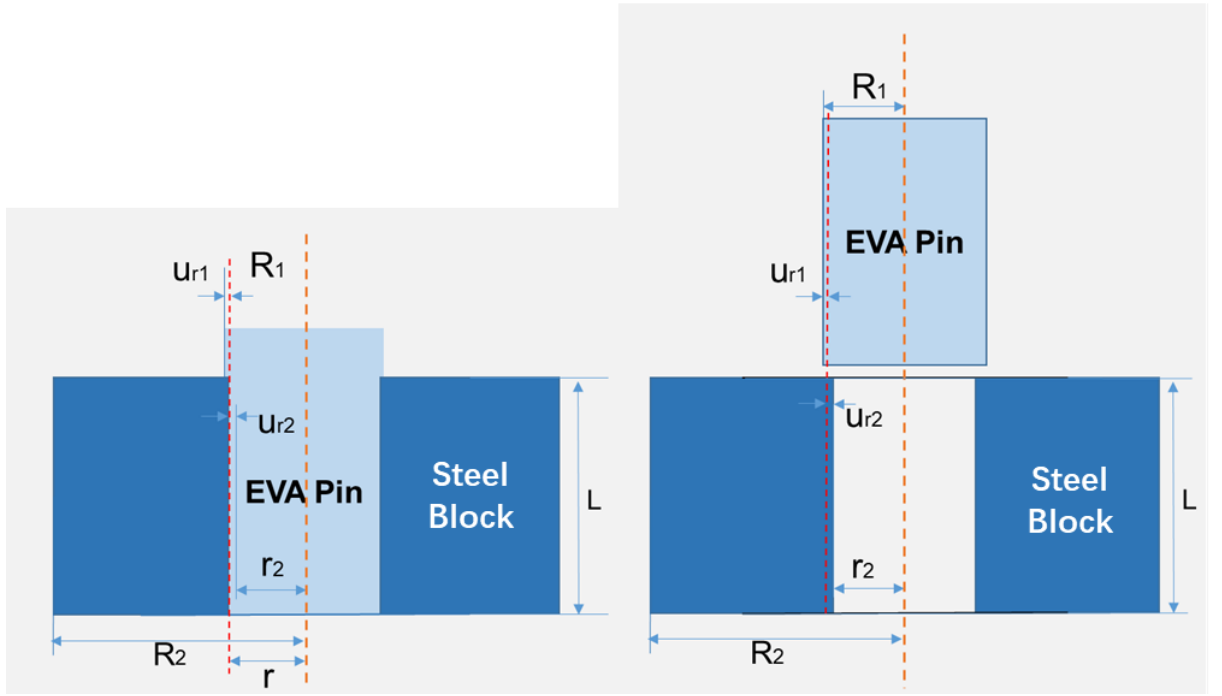


Figure 3.3: The interference-fit peg-hole model.

By using Lamé's equation and the thick-wall cylinder theory [105, 106], the displacement of the pin (u_{r_1}) is given by:

$$u_{r_1} = -\frac{P(1 - \nu_1) \cdot r}{E_1} \quad (3.1)$$

where P is the contact pressure, r is the nominal radius, and E_1 and ν_1 are the Young's modulus and Poisson's ratio of the EVA, respectively.

The radial displacement of the hole (u_{r_2}) is given by:

$$u_{r_2} = \left(\frac{R_2^2 + r_2^2}{R_2^2 - r_2^2} + \nu_2 \right) \frac{Pr}{E_2} \quad (3.2)$$

where r_2 is the original radius of the hole, R_2 is the radius of the steel block, and E_2 and ν_2 are the Young's modulus and Poisson's ratio of steel, respectively.

In this model, the interference fit size is small, and it is possible to assume in the calculation that [74]

$$r = r_2 = R_1 \quad (3.3)$$

The radial interference consists of the displacement of the pin and the hole:

$$\delta = -u_{r_1} + u_{r_2} \quad (3.4)$$

Combining Equations (3.1) – (3.4) gives the contact pressure as follows:

$$P = \frac{\delta}{\frac{(1 - \nu_1)r_2}{E_1} + \left(\frac{R_2^2 + r_2^2}{R_2^2 - r_2^2} + \nu_2\right)\frac{r_2}{E_2}} \quad (3.5)$$

Substituting Equation (3.5) into Equation (3.1) and Equation (3.2), the displacement of the pin and the hole can be expressed as:

$$u_{r_1} = -\frac{\delta}{1 + \frac{E_1}{E_2(1 - \nu_1)}\left(\frac{R_2^2 + r_2^2}{R_2^2 - r_2^2} + \nu_2\right)} \quad (3.6)$$

$$u_{r_2} = \frac{\delta}{1 + \frac{E_2(1 - \nu_1)(R_2^2 - r_2^2)}{E_1[R_2^2 + r_2^2 + \nu_2(R_2^2 - r_2^2)]}} \quad (3.7)$$

After obtaining the contact pressure P from Equation (3.5), the total contact force can be calculated from:

$$F = 2\pi rLP \quad (3.8)$$

where $2\pi rL$ is the total contact area before unplugging.

Hence, the maximum axial resistance friction can be obtained:

$$Rf_{max} = \mu_s F = \mu_s 2\pi rLP \quad (3.9)$$

where μ_s is the coefficient of static friction between the EVA and steel.

The system transforms from static to dynamic as soon as the pin begins to move. The axial resistance friction decreases rapidly because the dynamic friction coefficient is smaller than the static friction coefficient [107]. Then, as the pin is gradually pulled out, the contact area shrinks, resulting in a decreased friction resistance. Figure 3.4 shows a schematic diagram of the unplugging process.

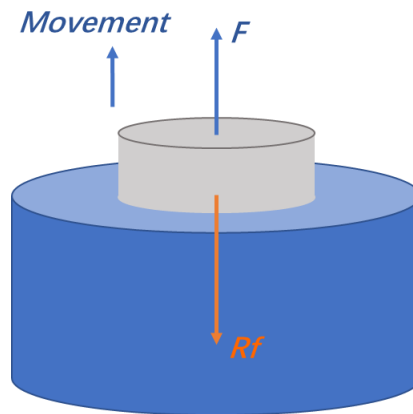


Figure 3.4: Schematic diagram of the unplugging.

At the beginning of the extraction process, a large force is required to resist static friction, which could exceed the capacity of the robot. Consequently, if there is a method to lower the maximum friction in the axial direction, the burden on the robot will be reduced.

3.3 Combined Twisting-Pulling

Twisting is a manoeuvre often adopted by people in the process of unplugging. This means that both axial force and torque are applied on the plug to make it rotate and move up at the same time. The pin is pulled out in a spiral motion, which is presumed to require less effort than straight pulling. The simple theoretical model shown in Figure 3.5 was built to analyse the change in frictional resistance and explore the mechanics of this unplugging method.

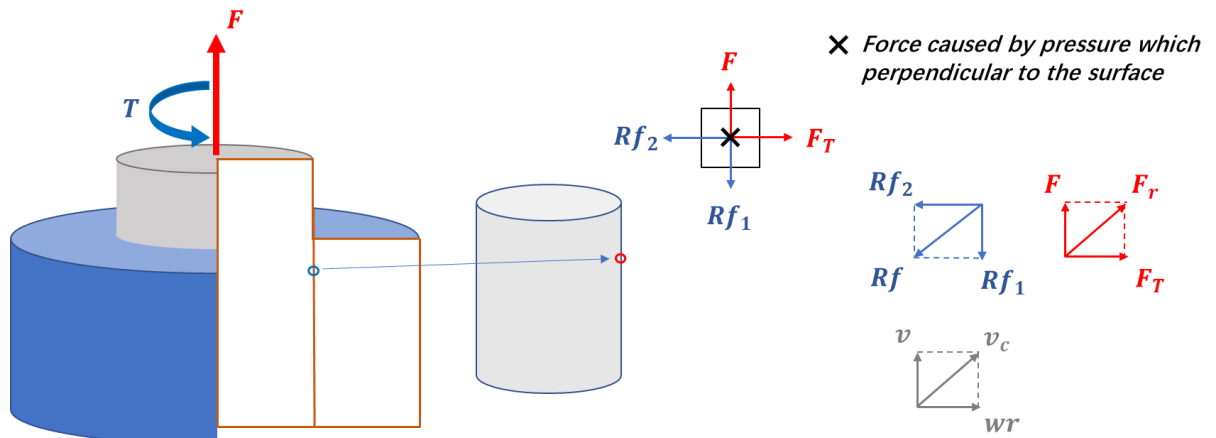


Figure 3.5: The mechanics of twisting-pulling.

In this theoretical model, a point on the surface of the pin is selected for analysis. When both torque and force are applied to the pin, the force tangent to the cylindrical surface is added together with the axial force. The frictional resistance divided into two components Rf_1 and Rf_2 opposes the applied force and torque, respectively. The overall resistance friction can be obtained as follows:

$$Rf = \sqrt{Rf_1^2 + Rf_2^2} \quad (3.10)$$

where Rf denotes the overall resistance friction, Rf_1 is the axial friction force and Rf_2 is the tangential friction force.

The total applied force F_r is the result of the axial pulling force and twisting force:

$$F_r = \sqrt{F^2 + F_T^2} \quad (3.11)$$

Similarly, when a constant velocity v in the axial direction and a constant angular velocity w about the axis are applied to the pin, the resultant velocity of the selected point on the pin is given by

$$v_c = \sqrt{v^2 + (wr)^2} \quad (3.12)$$

The axial frictional resistance in twisting-pulling is lower than that in direct pulling. The percentage reduction can be calculated as follows (Figure 3.4):

$$\text{Axial friction reduction } (R) = \frac{Rf - Rf_1}{Rf} \times 100\% \quad (3.13a)$$

$$R = \frac{F_r - F}{F_r} \times 100\% = \frac{v_c - v}{v_c} \times 100\% \quad (3.13b)$$

Figure 3.6 shows the spiral trajectory of the pin during the twisting unplugging. The rate at which the maximum axial frictional resistance decreases is equal to the factor R mentioned above (Equation 3.13).

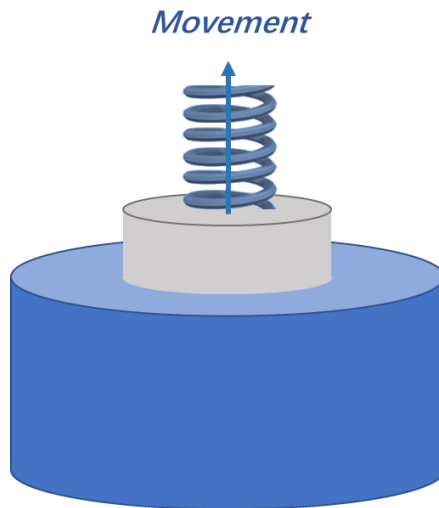


Figure 3.6: Schematic diagram of the twisting unplugging.

3.4 FEM of unplugging

Finite element modelling (FEM) was used to simulate twisting-pulling. Abaqus/Standard 2D/3D FEM software [108,109] was adopted in this study.

In addition to the movement in the Z direction, the pin needs to rotate around the Z-axis. This is a 3D problem; therefore, a 3D model was created to simulate the operation. Although unplugging is a dynamic process, static analysis was adopted to obtain the change in friction force for small movement increments.

The material parameters of the pin and the plate used in the FEM from the GRANTA EduPack [110] are shown in Table 3.1.

Table 3.1: Parameters of the materials used in the simulation.

Part	Material	Young's Modulus	Poisson's Ratio	Density
Pin	EVA	2×10^7 Pa	0.4	900 kg/m^3
Block	Steel	2×10^{11} Pa	0.25	7800 kg/m^3

Considering the load capacity of the robot, relatively small pins were employed. Under the condition that all the other parameters remain unchanged, four different sizes of pins were utilised to run four sets of simulations. The dimensions of the components are presented in Table 3.2.

Table 3.2: Dimensions of the pin, hole and receptacle blocks in different sets of simulations.

	Pin (D_1)	Hole (d_2)	Radial Interference	Block (D_2)	Depth (L)
Set1	7.02 mm	7 mm	0.01 mm	25 mm	10 mm
Set2	7.04 mm	7 mm	0.02 mm	25 mm	10 mm
Set3	7.06 mm	7 mm	0.03 mm	25 mm	10 mm
Set4	7.08 mm	7 mm	0.04 mm	25 mm	10 mm

After building the model, two static steps were created. The first step involved applying an interference fit [78,79], and the second step involved adding displacement and rotation. Next, the interaction between the pin and the hole was set up as ‘surface-to-surface’ [80,104]. Then, according to the GRANTA EduPack [110], the static and dynamic friction coefficients were set to 0.4 and 0.15, respectively. Meshing of the receptacle block was performed by applying 0.5 as the mesh size. For the hole and the pin, a finer mesh size of 0.4 was used. Figure 3.7 illustrates the mesh of the model and the static contact stress distribution in the pin and receptacle block caused by the interference fit.

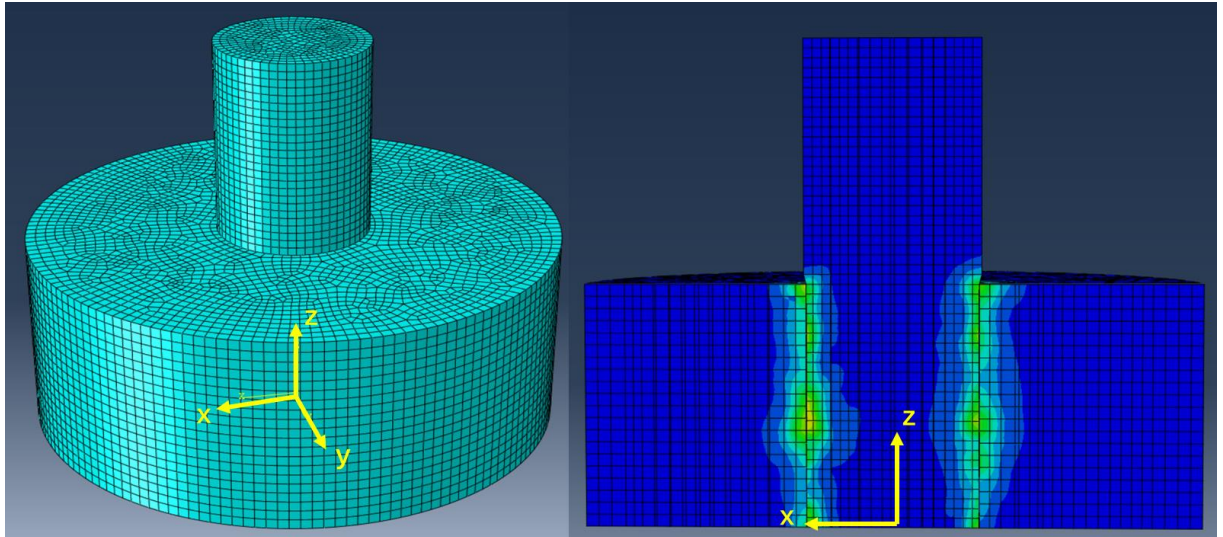


Figure 3.7: Mesh of the model and stress distribution in the components due to the interference fit.

In every set of simulations, two different conditions were applied to the pin. One was to add a linear displacement (+10 mm) in the Z+ direction to the pin. The other was to apply both a linear displacement (+10 mm) in the Z+ direction and a rotation ($+\pi$ rad) in the RZ+ direction. In addition, the linear and angular velocities were set as constant boundary conditions.

Figure 3.8 shows that the axial friction force changes with pin size when the pin is directly pulled out. With a smaller pin size, the axial resistance friction decreases throughout the process. The simulation process can be separated into four stages. In the first stage, the model only applied the interference fit, as mentioned above. No axial friction was generated at this stage. The second stage was a transformation from a static to a dynamic process. The axial resistance friction first increased substantially until the pin started to move and then decreased rapidly as the pin continued to move. This is the linear motion stage. Ideally, at this stage, the pin moved up at a constant speed, which also reduced the contact area between

the pin and the hole uniformly. According to Equation (3.8) and Equation (3.9), the following equations can be obtained:

$$S = 2\pi rD \quad (3.14)$$

where D is the contact depth between the pin and the hole and S is the contact area.

$$D = L - vt \quad (3.15)$$

$$Rf = \mu_d SP \quad (3.16)$$

where t is time and μ_d is the coefficient of dynamic friction between the EVA and steel.

Combining Equations (3.14)–(3.16) gives the following linear relationship between the friction force and time:

$$Rf = \mu_d P * 2\pi r(L - vt) \quad (3.17)$$

The third stage is the stage in which the resistance friction decreases linearly, as characterised by Equation (3.17). In the final stage, the pin was pulled out completely, and there was no contact between the pin and the plate.

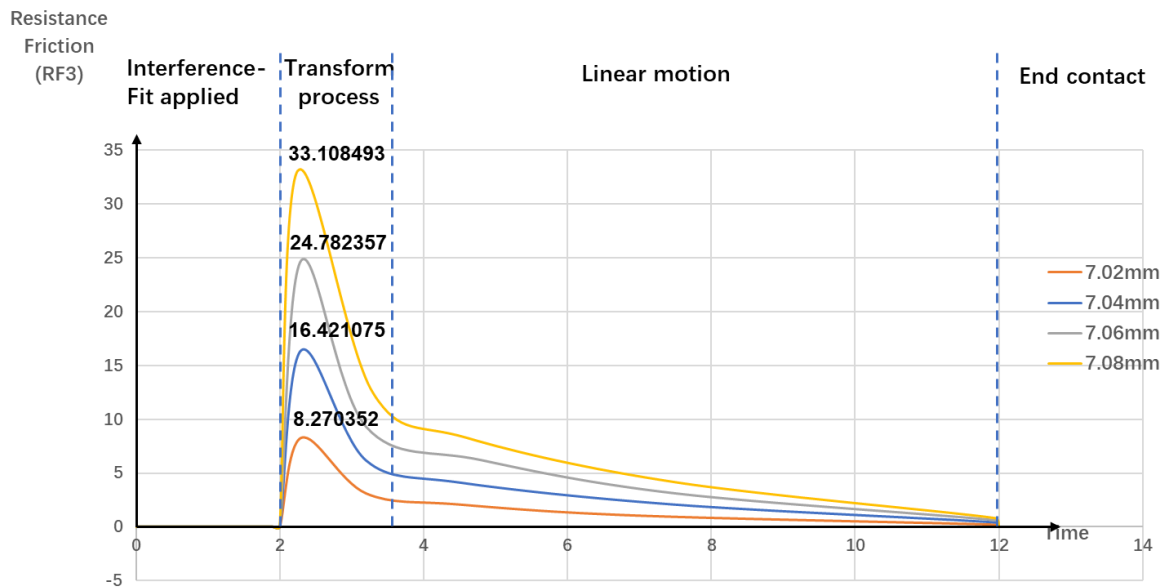


Figure 3.8: ABAQUS axial resistance friction diagrams (straight pulling, no twisting).

Figure 3.9 shows the simulation results of the axial friction change in the case of twisting-pulling. Compared with the trends of the curves in Figure 3.8, the axial friction change trends in Figure 3.9 are generally similar, and the process is divided into four stages. The difference is that rotation was applied, causing the pin's movement to shift from linear to spiral. Moreover, because the tangential friction generated by rotation contributes to the resultant friction, the axial friction is reduced, lowering the highest points of the curves.

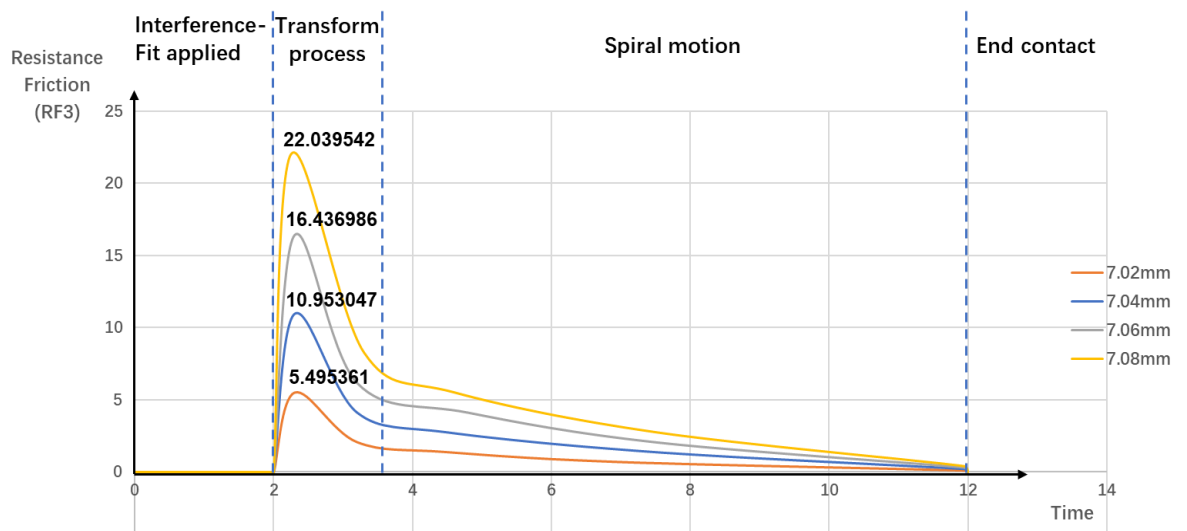


Figure 3.9: ABAQUS axial resistance friction diagrams (combined twisting and pulling).

3.5 Experiments

To verify that twisting can reduce the axial friction force during unplugging, experiments involving direct pulling, combined twisting and pulling interference-fit pins from receptacles were conducted.

In the experiments, a 6-DOF robot (TM 14) with a two-finger gripper (ROBOTIQ 2F-85) was used to grab the pin and perform the unplugging process. A 6-Axis Force/Torque sensor (ATI axia80-m20) was installed on the wrist of the robot to record the forces and torques in real time. The experimental setup for unplugging is shown in Figure 3.10(a). As in the FEM simulation, the inner diameter of the receptacle was 7 mm. Figure 3.10(b) shows the four different sizes of pins ($\Phi 7.02$ mm, $\Phi 7.04$ mm, $\Phi 7.06$ mm, and $\Phi 7.08$ mm), again matching the simulation conditions.

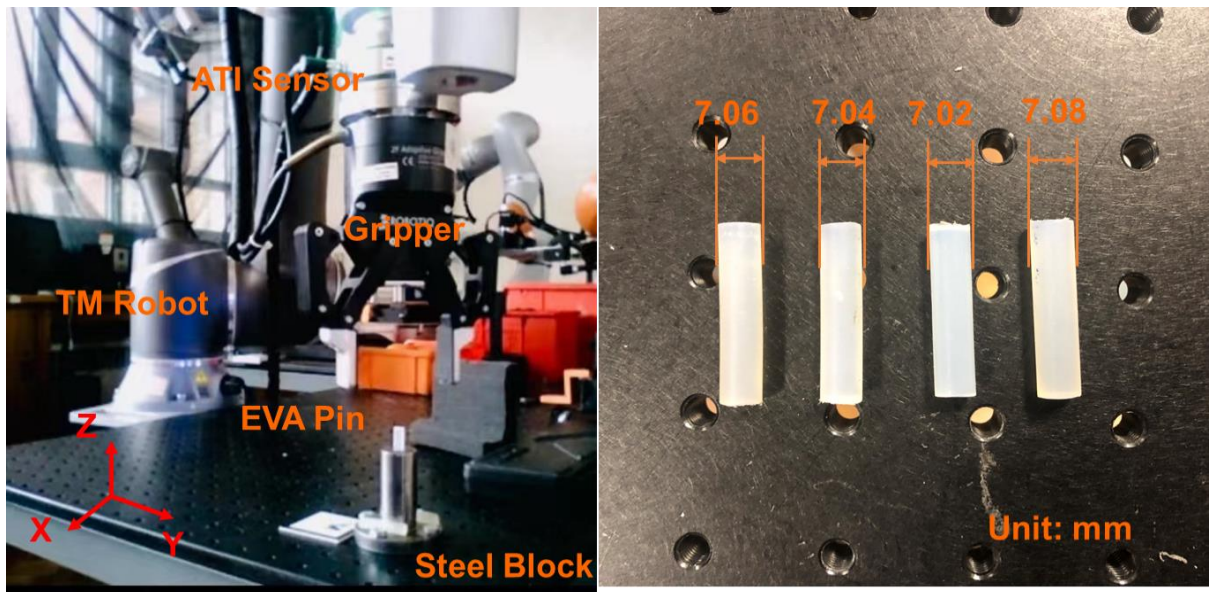


Figure 3.10: (a) Experimental setup. (b) Four different sizes of pins used in the experiments.

In the experiments, a Vernier calliper was used to measure the diameter of the pin at different positions, and the average diameter was determined. For the receptacle block, a 25 mm-diameter metal cylinder with a base was used.

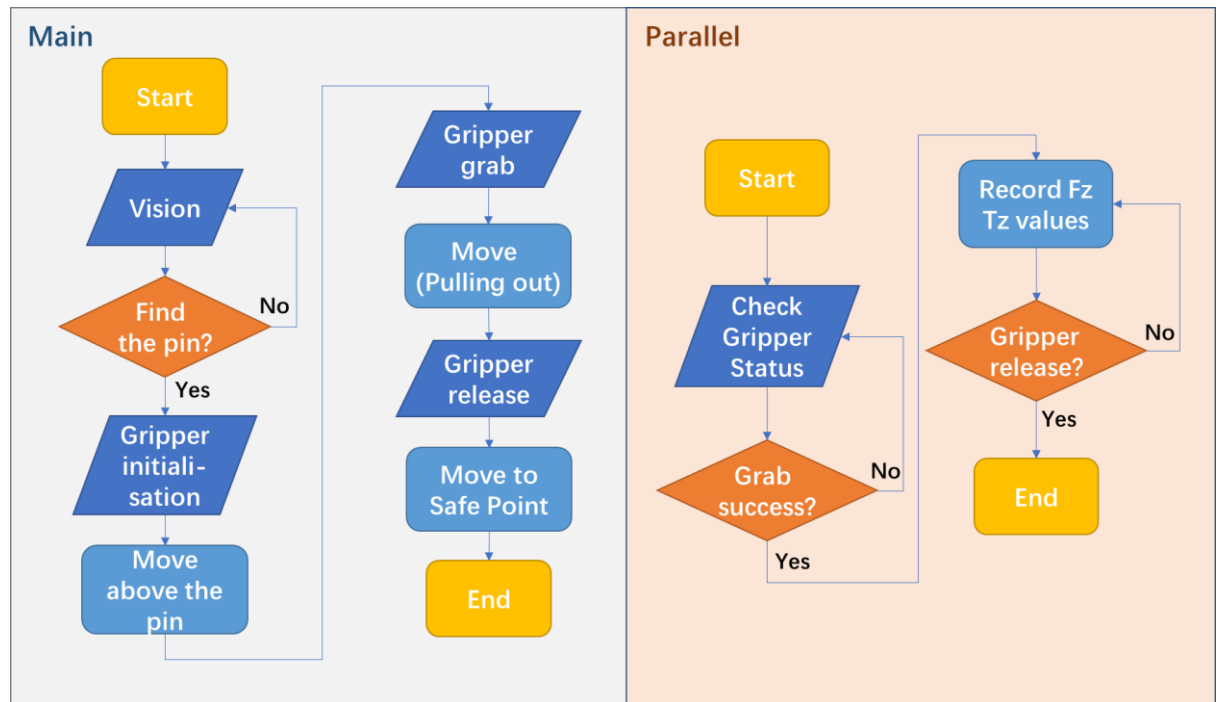


Figure 3.11: Flow charts of the robot programs.

The flow charts of the TM robot programs are shown in Figure 3.11. The main program was used to control the robot to locate the pin with its vision system, grab it and pull it out of the receptacle block, while the parallel program recorded force/torque data during the unplugging process.

3.5.1 Direct pulling

In the first step of the experiment, the vision system on the TM robot was used to locate the pin's position. Then, the gripper clamped the pin tightly to ensure that the centre of the gripper was on the centreline of the pin. The robot moved the gripper along the Z+ direction at a constant speed of 0.25 mm/s and stopped after moving 10 mm.

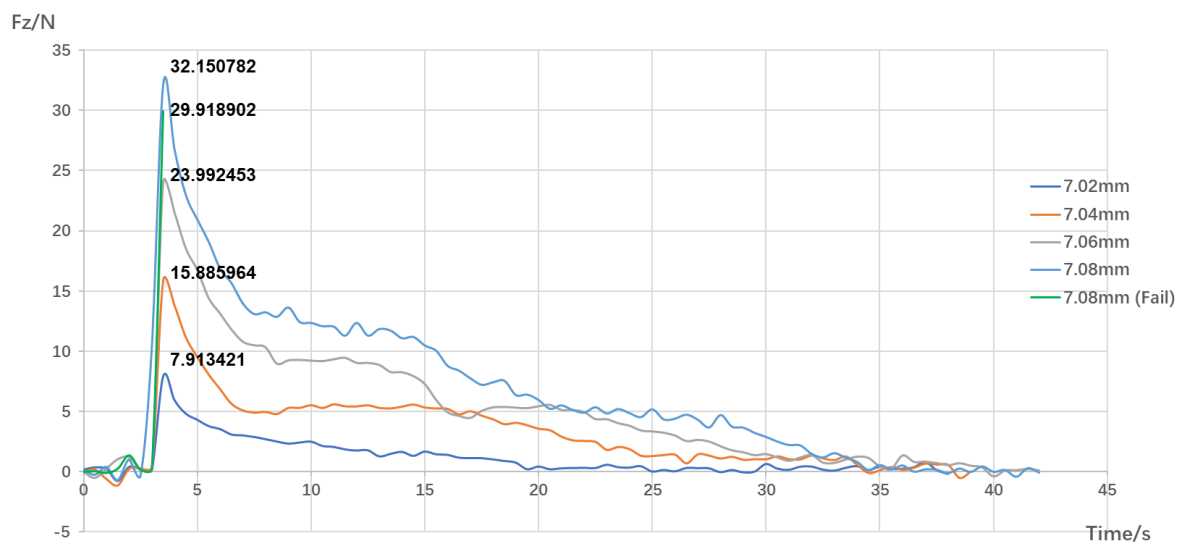


Figure 3.12: Variation in the force along the Z-axis (direct pulling).

Figure 3.12 shows that the force along the Z-axis changes throughout direct pulling. In this set of experiments, the 7.02 mm, 7.04 mm and 7.06 mm diameter pins were directly pulled out by the robot, and the axial friction forces in the respective experiments are shown in Figure 3.12. However, the 7.08 mm diameter pin could not be pulled out of the receptacle block. Since the friction force generated by the gripper's clamping pressure was not sufficient to offset the friction between the pin and the hole, slippage occurred between the gripper and the pin. Therefore, the operation of the robot was paused, producing a force

break, as shown in Figure 3.12. A 7.08 mm pin was subsequently bonded to the gripper, and the unplugging operation was completed successfully.

The maximum axial friction forces obtained from the theoretical model, FEM simulation and experiments are shown in Table 3.3. Errors are defined as:

$$Error = \left| \frac{Theoretical\ value - Simulated\ or\ Experimental\ value}{Theoretical\ value} \right| \times 100\% \quad (3.18)$$

Table 3.3: Maximum axial friction forces (direct pulling).

Pin size (mm)	Maximum Axial Resistance Friction (N)		
	Theoretical model	Simulation (Error)	Experiment (Error)
7.02	8.375836	8.270352 (1.26%)	7.913421 (5.52%)
7.04	16.751671	16.421075 (1.97%)	15.885964 (5.17%)
7.06	25.127507	24.782357 (1.37%)	23.992453 (4.52%)
7.08	33.503342	33.108493 (1.18%)	32.150782 (4.04%)
Avg. Error	/	1.45%	4.81%

3.5.2 Combined twisting-pulling

Combined twisting-pulling experiments necessitate the addition of the rotation of the robot end joint to the operation procedure compared with direct pulling experiments. The constant speed of movement in the +Z direction was reduced from 0.25 mm/s to 0.15 mm/s, and a $+\pi$ rad rotation at an angular velocity of $+\frac{3\pi}{200}$ rad/s was superimposed on the linear

motion. Low extraction speeds were specified because of the rotational range and torque constraints on the robot joints. Another reason for selecting these speeds was to ensure that the parameters in the experiments and simulations were consistent. In addition to the axial friction force F_Z , the axial torque T_Z was also recorded.

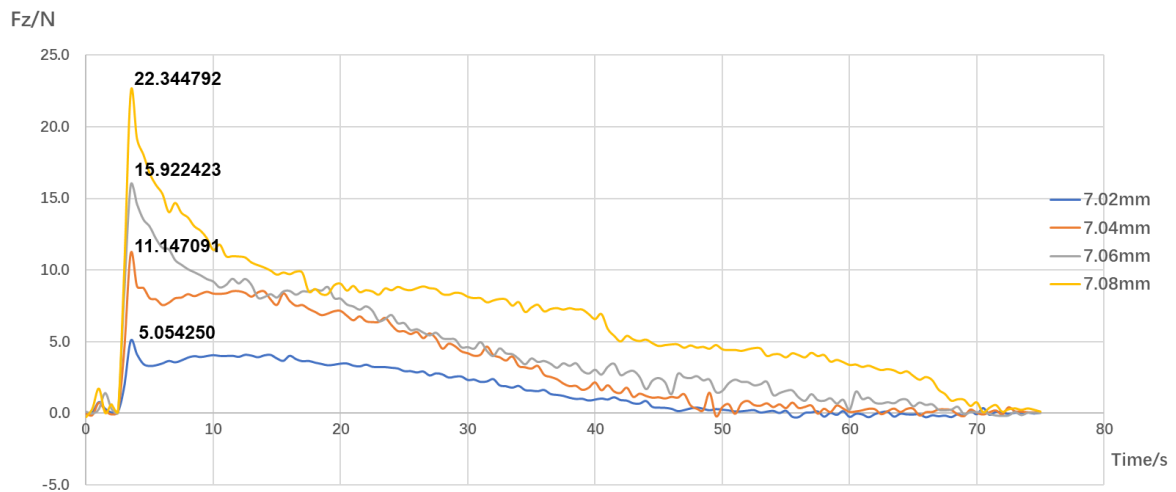


Figure 3.13: Variation in the force along the Z-axis (combined twisting-pulling).

Figure 3.13 and Figure 3.14 show F_Z and T_Z for different pin sizes in the case of twisting-pulling. In this group of experiments, the pins were all successfully pulled out. Compared with direct pulling, twisting pulling decreased the maximum axial friction force produced by twisting-pulling. The $\Phi 7.08$ mm pin that failed to pull out in the direct pulling experiment was easily removed from the receptacle block by the twisting-pulling method. However, the latter led to large fluctuations in friction throughout this group of experiments, especially for the T_Z curves. The fluctuations occur because the torque generated by the unplugging motion is low (less than 0.1 Nm), and the sensor used in the experiments is very sensitive. Second, due to the use of EVA, a polymer material, the deformation and surface roughness of the pin would undergo directional and dimensional alterations as a consequence of twisting.

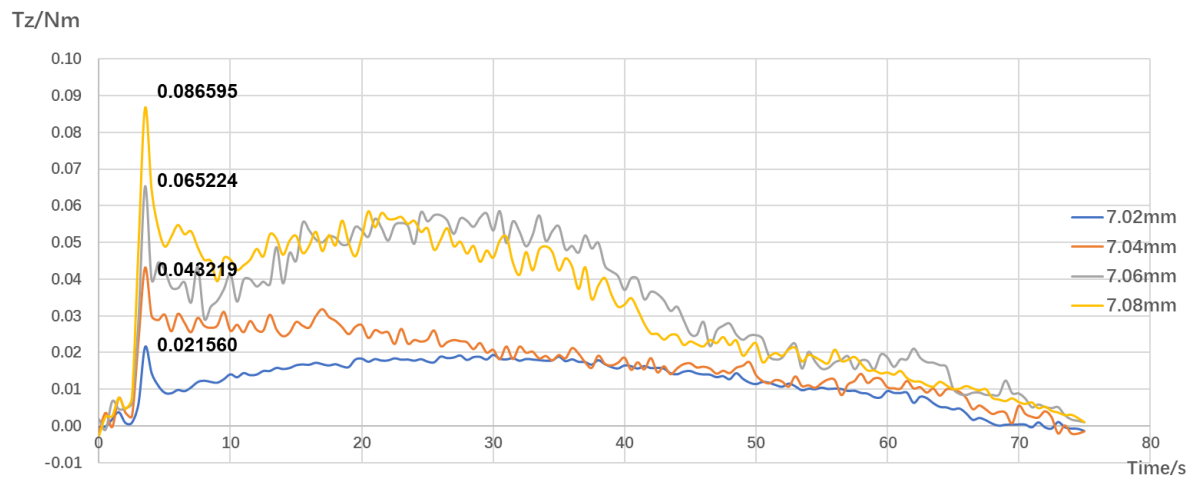


Figure 3.14: Changes in the torque on the Z-axis in the case of twisting pulling.

Table 3.4 lists the maximum axial friction forces obtained from the theoretical model, simulation and experiments.

The axial friction reduction (R), an important measure of whether the twisting-pulling method is effective, is shown in Table 3.5.

Table 3.4: Maximum axial friction force (combined twisting-pulling).

Pin size (mm)	Maximum Axial Resistance Friction (N)		
	Theoretical model	Simulation (Error)	Experiment (Error)
7.02	5.635262	5.495361 (2.48%)	5.054250 (10.31%)
7.04	11.270524	10.953047 (2.82%)	11.147091 (1.10%)
7.06	16.905787	16.436986 (2.77%)	15.922423 (5.82%)
7.08	22.541049	22.039542 (2.22%)	22.344792 (0.87%)
Avg. Error	/	2.57%	4.53%

Table 3.5: Axial friction reduction.

Pin size (mm)	Axial friction reduction (<i>R</i>)		
	Theoretical model	Simulation	Experiment
7.02	32.72%	33.55%	36.14%
7.04	32.72%	33.30%	29.83%
7.06	32.72%	33.67%	33.64%
7.08	32.72%	33.43%	30.50%
Avg. R	32.72%	33.49%	32.53%

3.6 Discussion

In the FEM simulation, Granta Edupack was employed as the reference for material selection. The EVA was selected as the pin material because of its good tensile and torsional elasticity. To make the simulation more realistic, chamfering was used to build the pin and the receptacle block. The actual maximum contact area between the pin and the hole was reduced due to the insertion of the chamfer. As a result, the value of the maximum friction force in the simulation is slightly lower than the theoretical value, as shown in Table 3.3 and Table 3.4.

The plots in Figure 3.12 show that during the first few seconds of the experiment, the values of F_z fluctuated slightly because of the gripper operation. After that, the F_z values exhibited sudden increases of different magnitudes according to the different radial interferences, and the maximum value was lower than the theoretical and simulated maximum values. The reasons for the error include the uneven interference caused by the deformation of the material, the position error between the robot gripper and the experimental model, and the trajectory and speed error of the robot motion. The reasons for the large fluctuations include the small size of the model in the experiment, which causes a small torque to be applied on the pin, and the high accuracy of the sensor, which means that although the distance error and operation error are small, they can produce large numerical changes. Furthermore, the simultaneous action of tensile deformation and torsional deformation causes the pin to slide and rebound in multiple stages during the unplugging process, which is also the reason why the moment curve is jagged. Although the difference in the maximum resistance friction between the different sizes and the theoretical value varies greatly in this set of experiments, the average error is 4.53%, which is within an acceptable range. In addition, the average axial friction reduction is 32.53%, which is very close to the theoretical reduction of 32.72%.

3.7 Conclusion

This paper studies the twist-and-pull method of unplugging a cylindrical peg press-fitted into a cylindrical hole. FEM simulations and experiments have confirmed the theoretically predicted reduction in axial friction and pulling effort when the amount of radial interference is small.

Although twisting causes the friction force to fluctuate more during the unplugging process, the overall friction in the axial direction is significantly decreased. In addition, utilising the same axial velocity and angular velocity as those of unplug pins with different amounts of radial interference results in similar axial friction reductions.

This paper first proposed the definition of unplugging in robotic disassembly and provided an improved understanding of robotised unplugging. A novel disassembly strategy that involves twisting and pulling to reduce axial friction was introduced and developed. This disassembly strategy enables robots to perform cylindrical unplugging more easily, and it can be applied to automatically disassemble products with wires, power cables and wire connectors, such as electric vehicle batteries and computer mainframes.

There are also several shortcomings in the theoretical model established in this paper, as well as in the disassembly strategy employed. A limitation of this research is that only a simplified linear-elastic model was used to verify the twisting-pulling method. While the model is applicable if there is no plastic deformation, large errors may be observed in practice when local stresses exceed the plastic threshold. On the experimental side, as the material of the peg is ethylene vinyl acetate (EVA) and is much softer than the material of the receptacle block, which is steel, repeated tests could not be performed on the same peg to determine

the effect of the twist-and-pull operation on surface wear. Moreover, the twisting-pulling method is applicable only to single-cylinder unplugging and cannot be adapted to multiple-cylinder or cuboid unplugging. Future work will address the identified shortcomings.

To address these identified shortcomings, a theoretical model that includes both elastic and plastic deformation could be developed to adapt to situations where local stresses exceed plastic thresholds. Different materials should be investigated to verify the applicability of this twisting method. Wear analysis of unplugging is necessary to determine the extent to which the damage to the plug is twisted and pulled out. In addition, the development of a disassembly method that can be adapted for multiple cylinders is considered in future work.

4 Robotised Unplugging of a Cuboid Plug Press-Fitted into a Cuboid Socket with a Disassembly Strategy—Unconstrained Wiggling

This chapter introduces an unplugging technique, unconstrained wiggling, for cuboid plug-socket connections to reduce axial friction. In Section 4.1, an introduction to cuboid unplugging is presented. In addition, a theoretical model of cuboid unplugging is established. In Section 4.2, a disassembly technique, unconstrained wiggling, is described and analysed. In Section 4.3, the FEM is used to validate the theoretical model built in Section 4.1. In Section 4.4, several groups of experiments are presented, including the analysis of the residual force. An error analysis is conducted along with the experimental results. In Section 4.5, a summary of this chapter is provided.

4.1 Cuboid Unplugging in Robotic Disassembly

Unplugging, a common step in disassembling objects, entails removing a male component, known as the plug, from a female receptacle, referred to as the socket [101]. This disassembly process, often referred to as 'plug-socket' operation, typically involves either a fixed fit or a press fit, both of which rely on interference fits and the deformation of the mating components to establish a firm and secure connection [102].

In the problem of unplugging, there are different disassembly strategies for different unplugging structures or shapes. In addition to common cylindrical unplugging, the problem of unplugging with cuboids often occurs during disassembly (Figure 4.1). This study considers a more elastic interference fit, which involves employing a softer material for the cuboid plug and a harder metal for the socket. This type of plug-socket combination is widely applicable to wire or cable connections and connections that require frequent and convenient operation [111].



Figure 4.1: Cylindrical and cuboid connections

It is also considered that the cuboid interference connection is frequently adopted for fastening cables or plugs; thus, two of the four sides of the cuboid connections are typically interference fit, making it possible to install with a hammer or by hand. Therefore, the model of cuboid unplugging can be simplified to a mechanical model with only two sides in interference-fit contact (Figure 4.2).

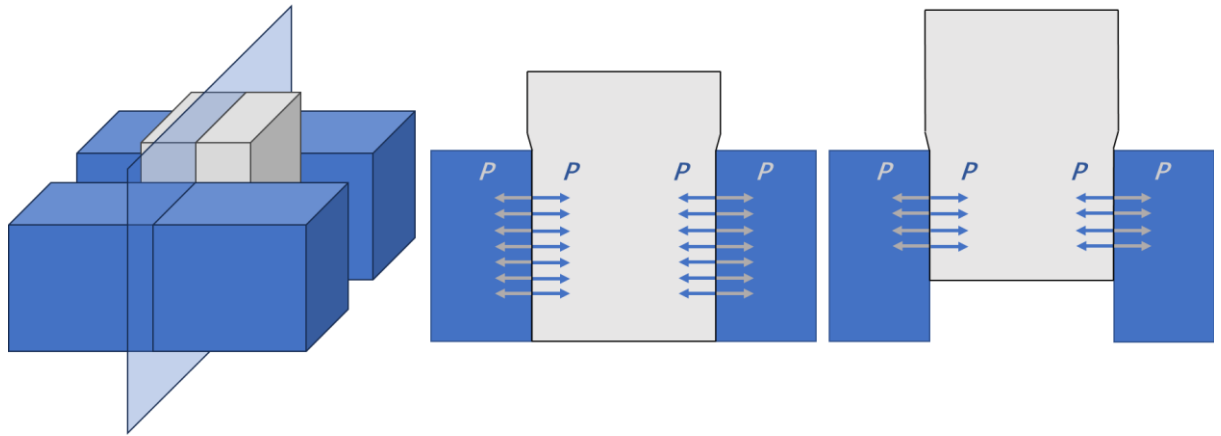


Figure 4.2: Contact force diagram in the cuboid unplugging process.

In this work, a soft material, polyvinyl chloride (PVC) elastomer, was used as the plug material. Grade 6082 T6 aluminium, a medium strength alloy, was chosen as the socket material. Considering the significant variation in hardness between the two materials, the deformation of the socket was neglected in this study. Therefore, it is only necessary to consider how the interference fit size and plug deformation affect the unplugging process.

An interference-fit plug-socket model (Figure 4.3) is built to analyse the cuboid unplugging operation. Although PVC, as a polymer material, has an unstable stress–strain curve different from that of metal materials, elastomers have good elasticity and a wide elastic deformation range, which causes only elastic deformation to occur in the plug and the socket [112].

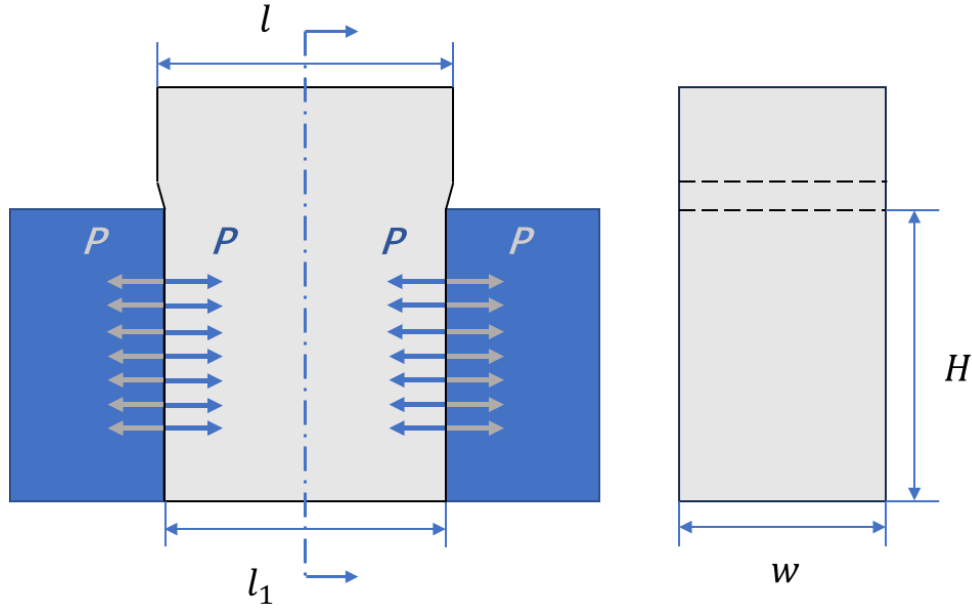


Figure 4.3: Interference fit plug-socket model.

After applying Hooke's law [113] to this interference-fit plug-socket model, the PVC plug with good elasticity can be regarded as a 'spring', and combined with the definition of Young's modulus, the following formula can be obtained:

$$P = \frac{F_N}{A} = E \frac{\Delta l}{l} \quad (4.1)$$

where P is the contact pressure, A is the contact area, Δl is the change in length, and E is the Young's modulus of the PVC.

Therefore, the following formulas can also be given:

$$A = H \times w \quad (4.2)$$

$$\Delta l = l - l_1 \quad (4.3)$$

Since there are two contact surfaces in this cuboid unplugging model, the total contact force can be expressed by:

$$F = 2PA \quad (4.4)$$

Combining Equations (4.1) and (4.4), the original or maximum axial resistance friction can be calculated from:

$$Rf_{max} = \mu_s F = 2\mu_s E \frac{l - l_1}{l} Hw \quad (4.5)$$

where μ_s is the coefficient of static friction between the PVC and aluminium.

Equation (4.5) shows that when the dimension and material of the plug and socket are determined, the value of the maximum resistance friction that needs to be overcome to pull out the plug will not change.

When the plug is moved upwards at a constant velocity v , the following equations can be obtained:

$$A = (H - vt)w \quad (4.6)$$

$$Rf = \mu_d F = 2\mu_d E \frac{l - l_1}{l} (H - vt)w \quad (4.7)$$

where μ_d is the coefficient of dynamic friction between the PVC and aluminium.

4.2 Unconstrained wiggling

Wiggling is a technique or method used to assist in removing the plug from the socket. This refers to alternating forward and backwards forces while maintaining an upwards pulling force throughout the unplugging process, causing the object to be easily removed.

As mentioned above, the interference between cuboid plugs and sockets always occurs on two of the four contact surfaces, so the contact conditions of the other two sides are not in contact or clear. When the lateral force is applied perpendicular to these two noncontact surfaces, the plug will have space for lateral displacement; this process can be referred to as unconstrained wiggling. Therefore, when an upwards pulling force and a periodically applied lateral force act on the plug at the same time, the motion trajectory will increase, as shown in Figure 4.4.

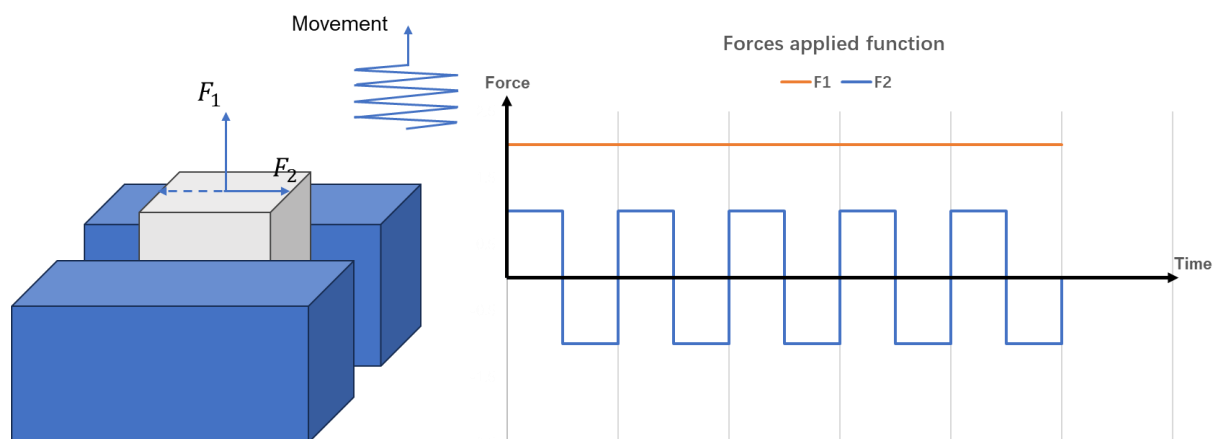


Figure 4.4: Schematic diagram of unconstrained wiggling and applied force.

To analyse whether this unconstrained wiggling method can reduce axial resistance friction during unplugging so that the robot can pull out the plug more easily, a theoretical model was established for mechanical analysis (Figure 4.5). In this theoretical model, one random point on the contact surface of the plug was selected for further force analysis. When the upwards pulling force F_1 and the lateral force F_2 are applied on the plug, regardless of whether the direction of the lateral force is positive or negative, a resultant force with a certain oblique angle is generated. Because the direction of the friction force is always opposite to the direction of the applied force, two separate resistance frictions, Rf_1 and Rf_2 , occur and can be combined with the resultant resistance friction (Rf).

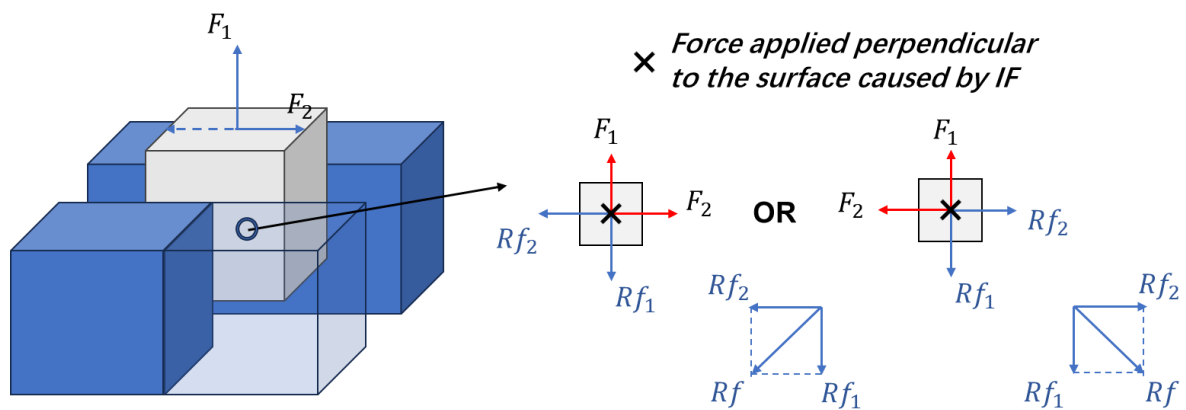


Figure 4.5: The mechanics of unconstrained wiggling unplugging.

Then, the total resistance friction can be expressed by:

$$Rf = \sqrt{Rf_1^2 + Rf_2^2} \quad (4.8)$$

Equation (4.5) indicates that the value of the maximum frictional resistance does not vary as the plug moves but rather that the direction of the frictional resistance does. The friction generated by the lateral force becomes part of the total frictional resistance while also reducing the axial frictional resistance.

Hence, the reduction in the axial friction can be calculated as:

$$\textbf{Reduction (R)} = \frac{\textbf{Rf} - \textbf{Rf}_1}{\textbf{Rf}} \times 100\% \quad (4.9)$$

Similarly, when the upwards velocity \textbf{v}_1 and the lateral velocity \textbf{v}_2 are applied, the reduction is given by:

$$\textbf{Reduction (R)} = \frac{\textbf{v}_c - \textbf{v}_1}{\textbf{v}_c} \times 100\% \quad (4.10)$$

where \textbf{v}_c is the resultant velocity of the plug.

.

4.3 FEM of cuboid unplugging

Finite element modelling (FEM) was used to validate the theoretical model of cuboid unplugging. In this study, Abaqus/Standard 2D/3D was chosen as the FEM software [108], and static analysis was adopted. A 3D plug-socket model was created to demonstrate changes in stress and deformation. The dimensions of the model and the boundary conditions imposed during the simulation are shown in Figure 4.6.

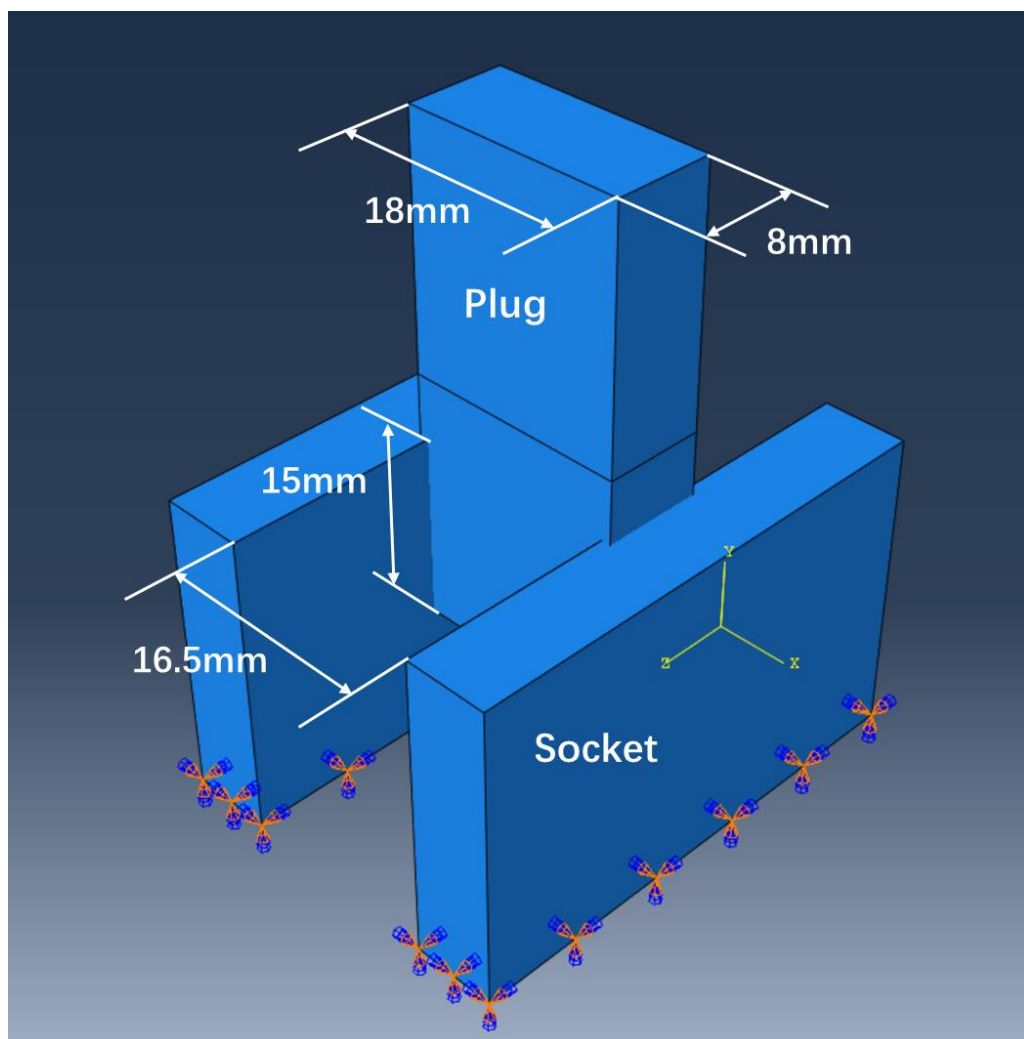


Figure 4.6: Dimension of the model and boundary conditions applied.

The size of the plug was 18 mm × 8 mm × 40 mm, and the initial insertion depth was 15 mm. The gap of the socket was set at 16.5 mm, which generated a total of 1.5 mm of interference (0.75 mm for both sides). The base of the socket was fully fixed throughout the analytical simulation. In the theoretical model, due to the difference in material hardness between the plug and the socket, the deformation of the socket is neglected. However, in the simulation, the socket was not directly established into the solid body; instead, the parameters of the corresponding material were applied to ensure the accuracy of the results of the simulations and the feasibility of ignoring socket deformation in the theoretical model. The material parameters of the plug and the socket used in the FEM from GRANTA EduPack [110] are displayed in Table 4.1.

Table 4.1: Parameters of the material used in the cuboid unplugging simulation.

	Material	Young's Modulus	Poisson's ratio
Plug	PVC elastomer	2 MPa	0.45
Socket	aluminium	7×10^4 MPa	0.3

After completing the mesh of the components and contact modelling between the plug and the socket [109], the simulation results of the static interference fit were obtained and are illustrated in Figure 4.7. The deformation graph shows that the maximum displacement occurred on both sides of the plug, and there was almost no displacement in the socket. The maximum deformation on the plug was 0.7473 mm, which is very close to the set value (0.75 mm). When there is a large difference in material strength between two objects that have an interference fit, the deformation of the object with greater hardness can be regarded as negligible.

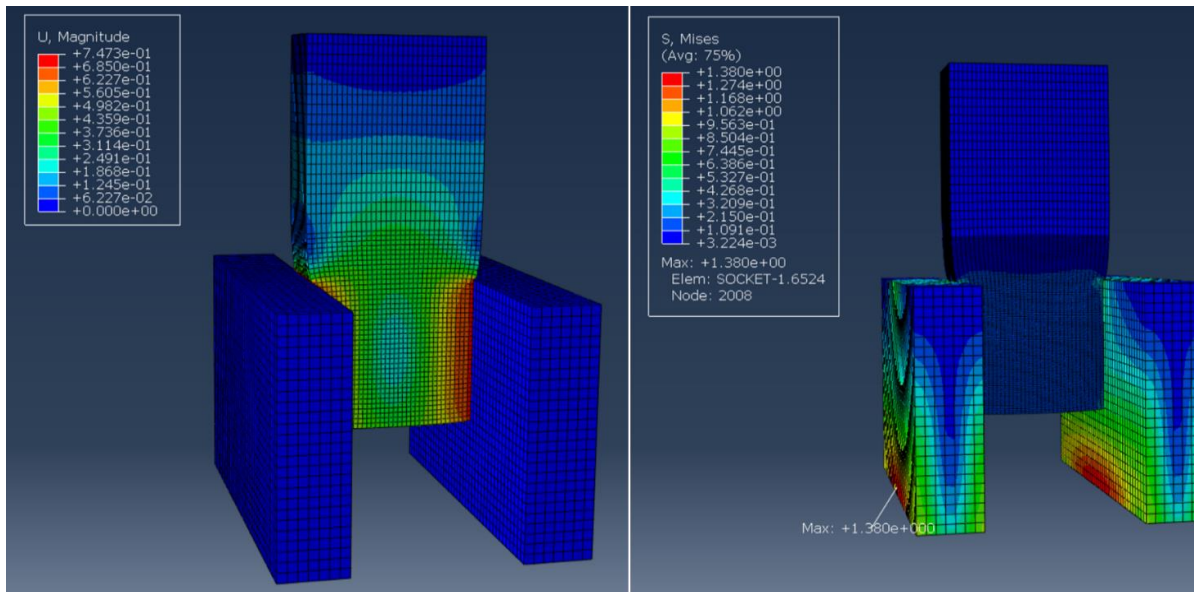


Figure 4.7: Deformation and stress distribution of the model due to the interference fit.

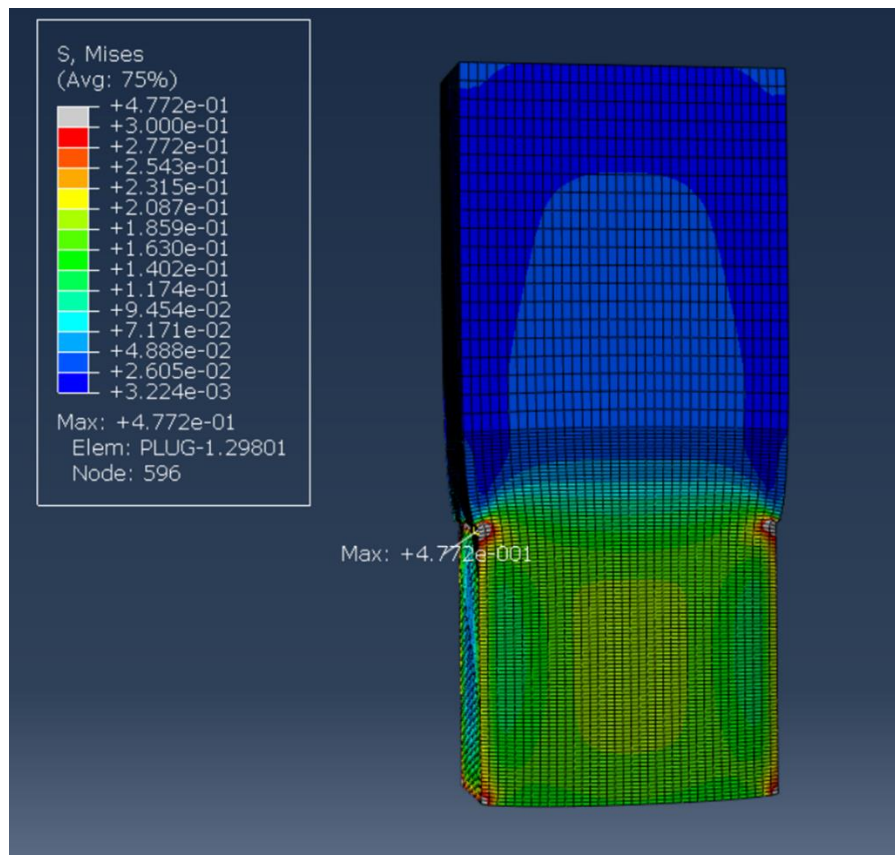


Figure 4.8: Stress distribution of the plug due to the interference fit.

The stress distribution of the model (Figure 4.7) indicated that the stress on the socket, particularly on the bottom of the socket, was significantly greater than that on the plug. The reason is that in the simulation, the stress situation of the socket is similar to that of the cantilever beam. The bottom end of the socket and one end of the cantilever beam are both fixed, and the force generated by the deformation of the plug is equivalent to the load on the other end of the cantilever beam. Therefore, the maximum stress is generated at the fixed end of the cantilever beam [114] and at the bottom of the socket.

To better demonstrate the stress distribution of the plug, the socket is temporarily hidden, and the maximum value of stress shown in red is changed to 0.3 in the illustration (Figure 4.8). The stress on both sides of the interference contact is average and corresponds to the stress distribution of the theoretical model. Although the stress on the contact edge of the plug and the socket is greater, the impact on the average contact pressure of the surface is not apparent.

4.4 Experiments

To verify whether unconstrained wiggling can reduce axial friction, experiments involving direct pulling and wiggling while unplugging the interference-fit plug out of the socket were performed.

In the experimental setup, a 6-DOF robot (TM 14) equipped with a two-finger gripper (ROBOTIQ 2F-85) was adopted to apply lateral and upwards forces during the unplugging process. An ATI sensor (axia80-m20), which is a 6-axis force/torque sensor, was mounted between the end of the robot and gripper to record the force and torque data during the experiment. Two aluminium angles were fixed on the special stable table with threaded holes to simulate the socket. The PVC block was pressed into the gap by a hammer (Figure 4.9).

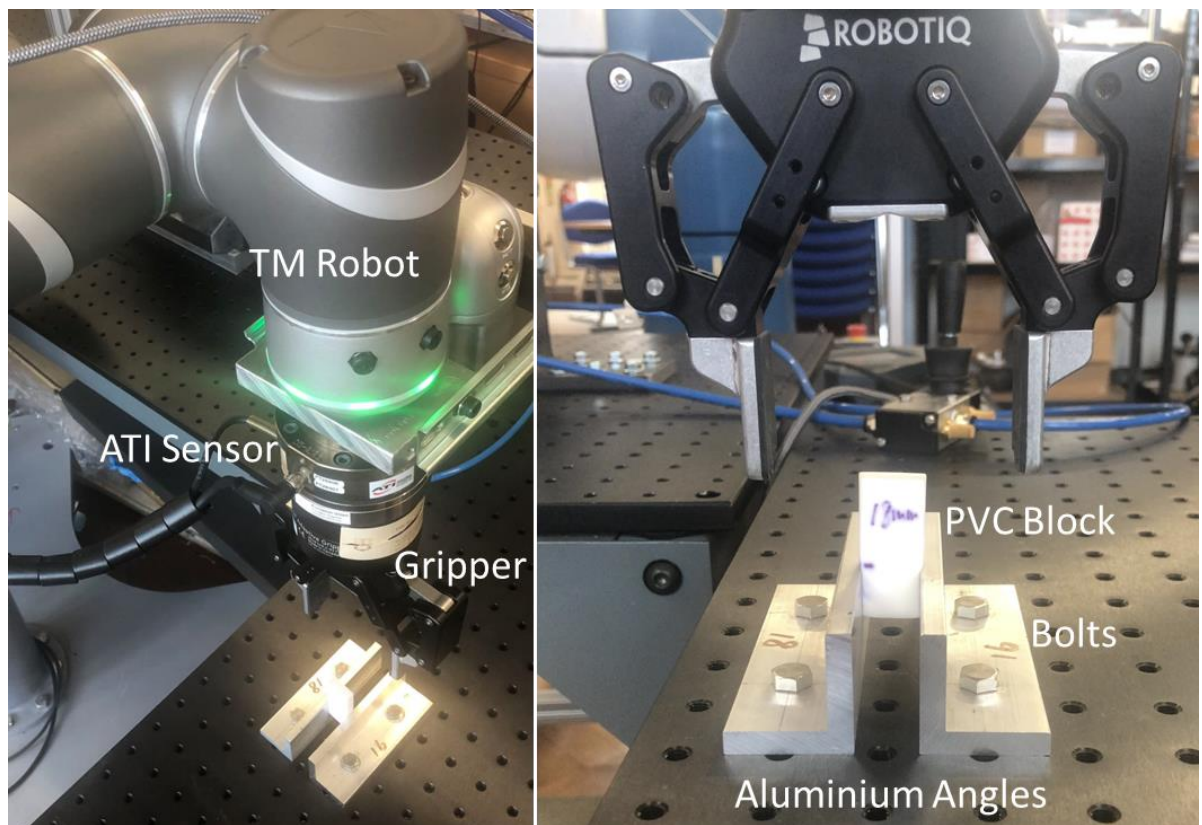


Figure 4.9: Experimental setup.

To facilitate adjustment of the dimension of the gap between two L-shaped holders and simulate sockets of different sizes, a 1/4 in (31.75 mm) \times 1/4 in (31.75 mm) \times 1/4 in (6.35 mm) aluminum angle was cut into several pieces, each with a length of 100 mm (Figure 4.10). The threaded hole spacing of the table is 25 mm. To stably fix the holder, two holes were drilled on each holder, and the distance between the two holes was 50 mm.

Because the production size of the PVC block is limited, the width w is fixed at 8 mm, the length l ranges from 7 to 18 mm, and the total height of the block is 20 mm or 40 mm; thus, the height H or insertion depth can be artificially controlled to 10 mm or 15 mm while it is necessary to set aside a section for the gripper to clamp. Therefore, the size of the gap needs to match the length range of the block. For different holders, the distance between the contact surface and the drilled hole varies from 16 mm to 22 mm. Since the fixed distance between the two holders in each experiment is 50 mm, when the gap or width of the socket needs to be set to 7 mm, a 21 mm and a 22 mm holder can be adopted (Figure 4.10). Because M6 bolts were used to mount the holders on the table, the holes drilled on the holders were all 6.5 mm long. In this case, after the holder is installed on the table, it is still necessary to use a Vernier calliper to measure the gap multiple times at different positions. After confirming the dimension of the gap, the PVC block was pressed in.

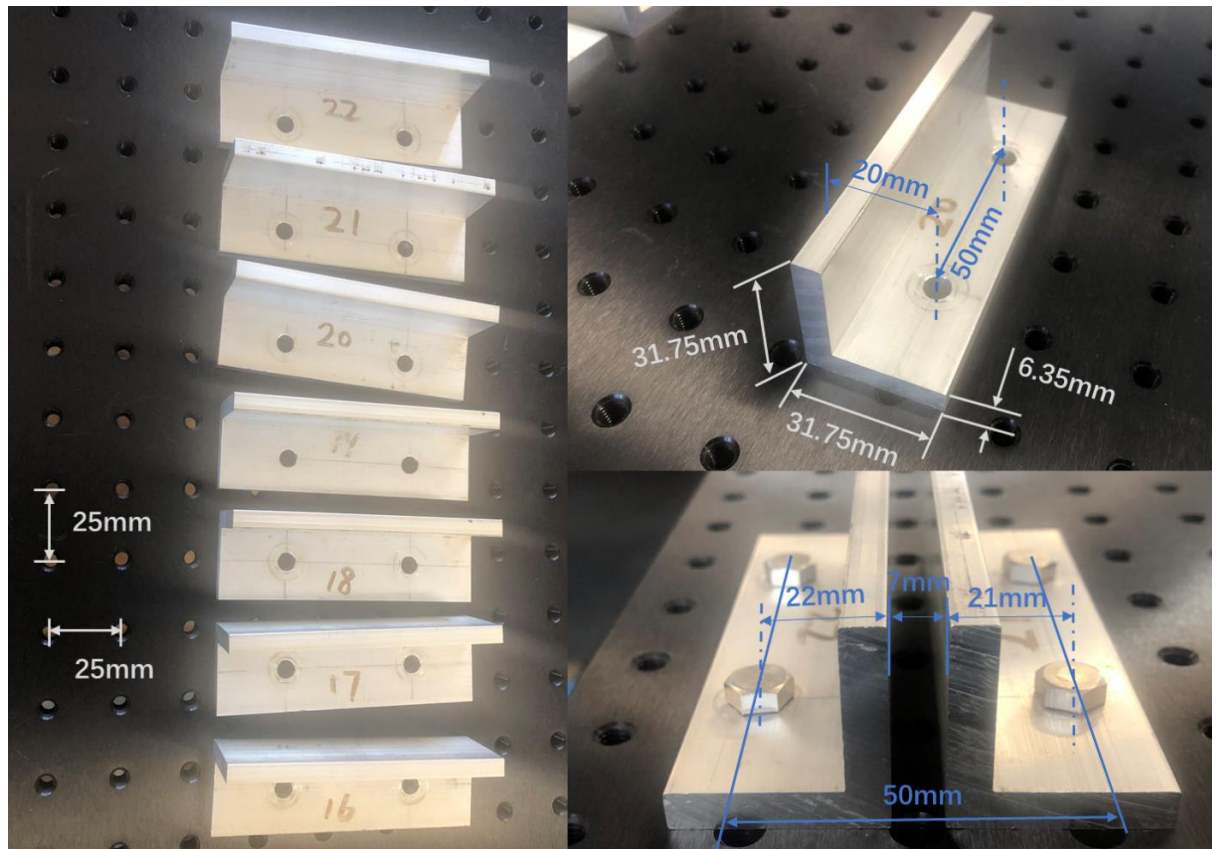


Figure 4.10: Different sizes of holders used in the experiment.

The material properties of the PVC block and the aluminium angle are shown in Table 4.2.

Table 4.2: Material properties of the PVC block and the aluminum angle.

	Material	Young's Modulus	Density
PVC block	PVC elastomer (soft)	$2 \cdot 10^6$ Pa	1380 kg/m^3
Al holder	Grade 6082 T6 aluminium	$7 \cdot 10^{10}$ Pa	2700 kg/m^3
Static coefficient of friction	0.23	Dynamic coefficient of friction	0.4

4.4.1 Direct pulling

To judge whether unconstrained wiggling can reduce axial friction, a controlled test of direct pulling is needed. On the basis of not applying any lateral force, the robot and gripper were used to firmly clamp the PVC block, which was then moved upwards at a constant speed of 0.1 mm/s. The 6-axis sensor was used to obtain the force status of the PVC block in all directions while moving upwards and being completely pulled out. The flow chart of the robot programs is shown in Figure 4.11.

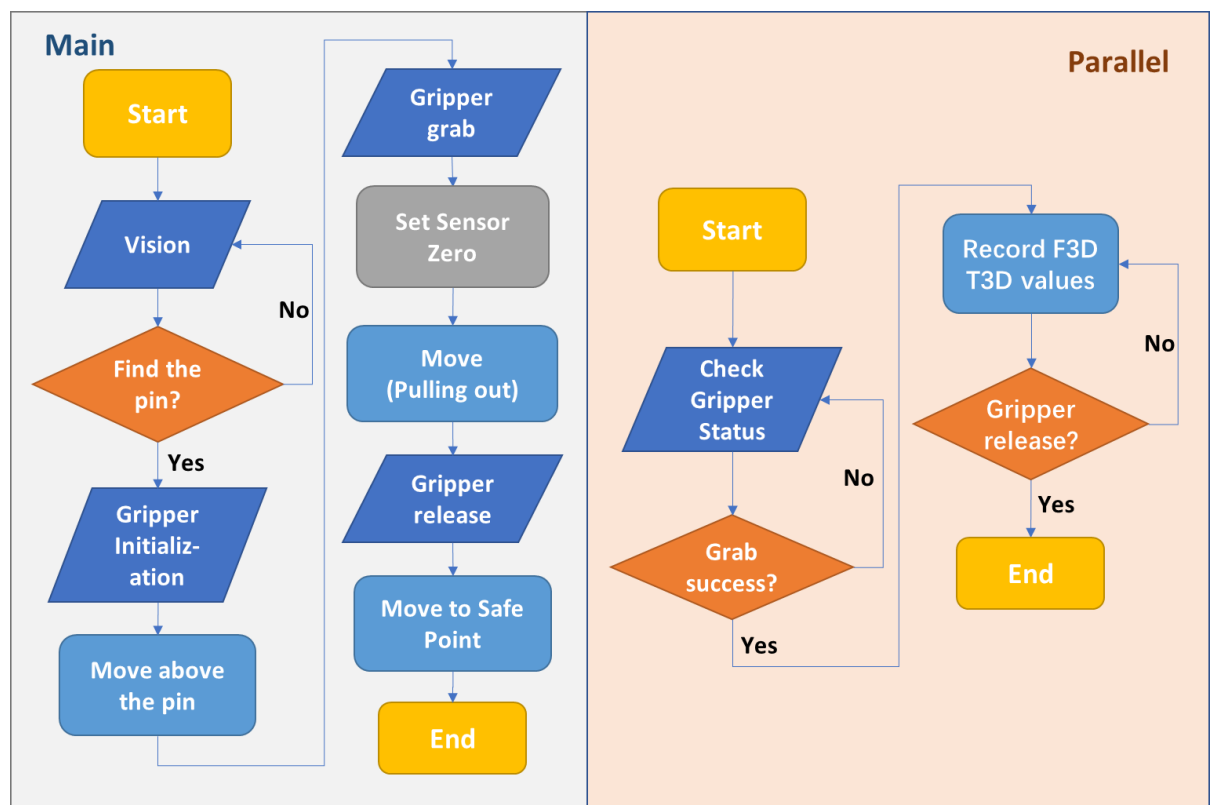


Figure 4.11: Flow charts of the robot programs for direct pulling.

For each set of experiments, a direct pulling test is required for comparison, depending on the size of the PVC block. As a result of performing numerous groups of comparable tests

and finding that the trends of the force curves are extremely similar, two cases were selected for display and further analysis (Figure 4.12).

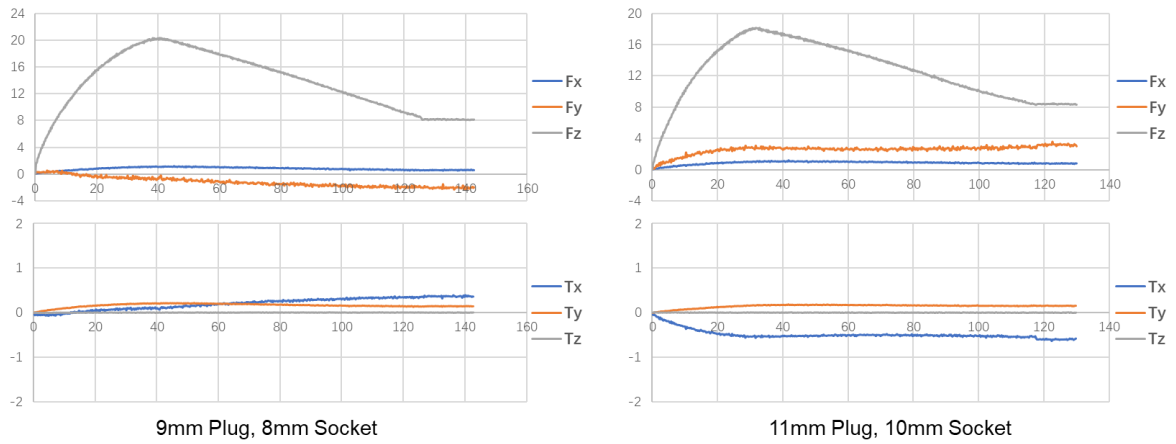


Figure 4.12: Two cases in which the 6-axis force change in the PVC block was pulled out directly.

Figure 4.12 shows two cases of the change in the 6-axis force of the PVC block during the direct pulling process. In these two sets of experiments, the same interference agent (1 mm) was applied, and the depth of the PVC block was 10 mm. The figure shows that the force on the z-axis first increases relatively rapidly from 0 N, reaches the maximum peak value at 30 to 40 seconds, and then begins to decrease gradually. After approximately 120 s, the PVC block was completely pulled out from the support, and the value of F_z began to remain constant but did not drop to 0 N, which exceeded expectations. To analyse the cause of this residual force, a series of analyses and experiments were conducted.

4.4.2 Residual force analysis

The appearance of residual force affects the determination of the maximum axial friction in the nonplugging experiment. To clearly understand the composition and origin of the residual force, a series of experiments were performed.

The weight of the equipment mounted on the robot, including a flange plate with two supports and an external camera, is first believed to be the main cause of this residual force because the installation and calibration of the sensor were completed before the installation of this equipment. After removing the flange plate and the external camera, a set of contactless grasping experiments was conducted.

A smaller PVC block was placed on the table and kept at a distance from the holders on both sides. The gripper was used to grip the PVC block and move it upwards. The force diagrams obtained by the sensor are shown in Figure 4.12. When the PVC block moved upwards without contact with both sides, it was not affected by friction except for its own gravitational field in the Z direction. However, in this experiment, the force in the z direction increased rapidly from 0 N to more than 4 N and then remained at this magnitude, which decreased slightly because of removing the equipment; additionally, the force did not match its own mass of less than 20 g.

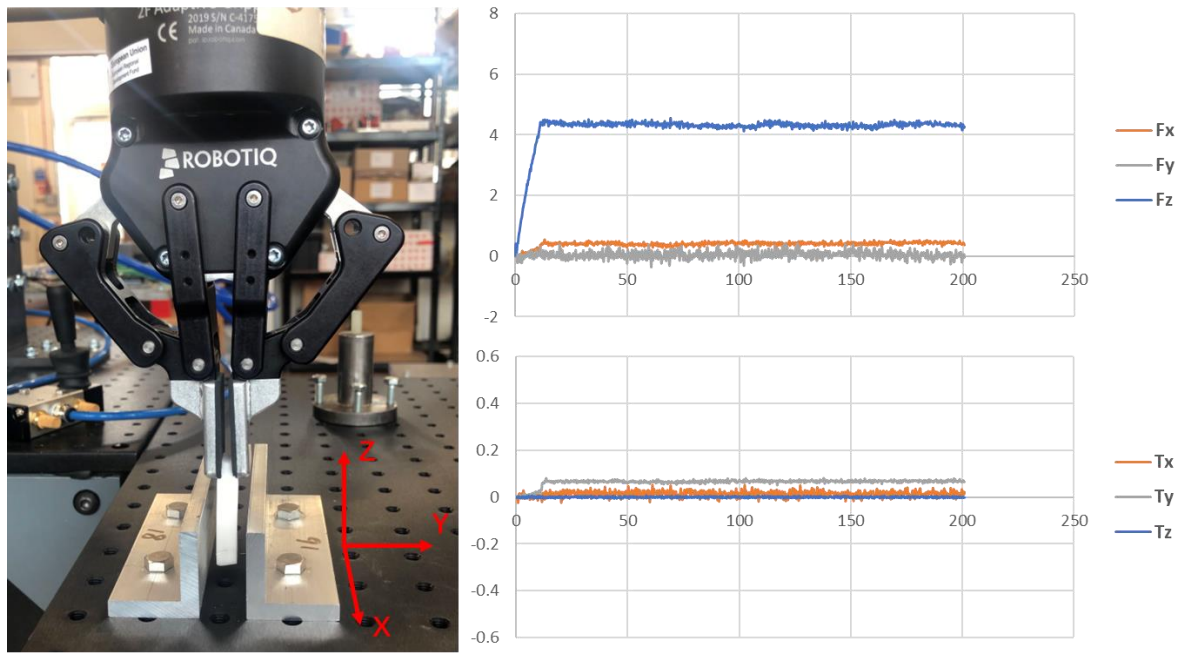


Figure 4.13: Contactless grasping experiment with force diagrams.

Based on this, another experiment was implemented to rule out the possibility that the values given by the sensor were inaccurate. The difference from the previous experiment is that in this experiment, the PVC block was held by hand without contact with the table. When the robot was controlled to clamp the PVC block with the gripper, the hand was immediately released without affecting the force of the PVC block. Then, the PVC block moved upwards. Figure 4.14 indicates that nearly no force was applied to the block during the movement, as expected.

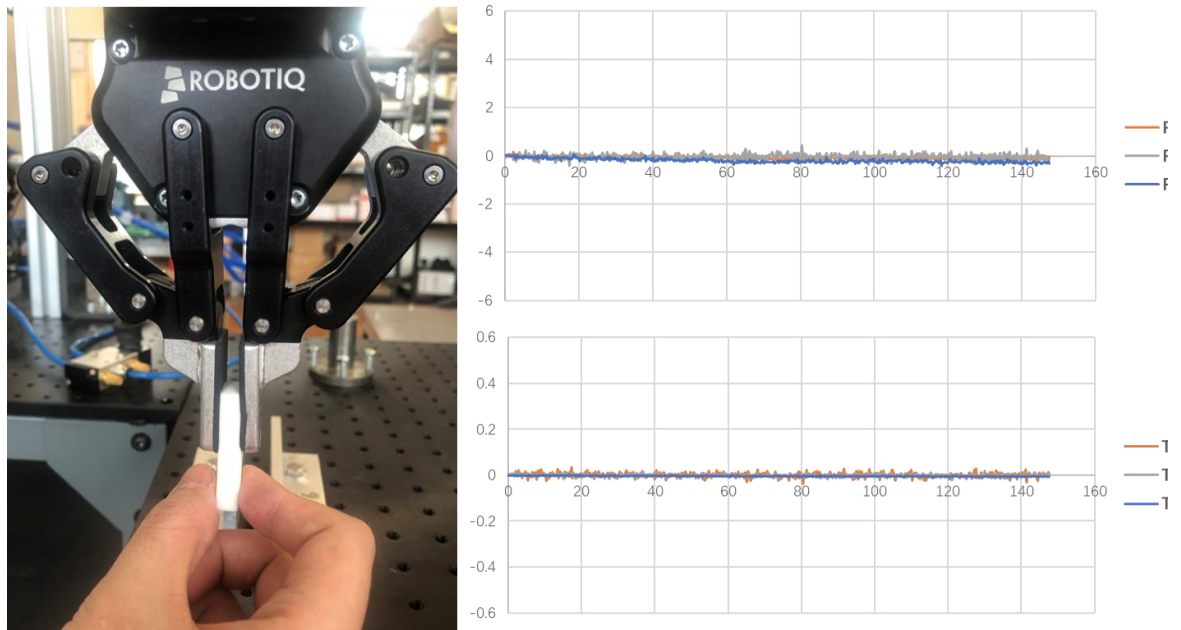


Figure 4.14: Force diagram of the handheld block grasping experiment.

Since the only difference between the above two experiments was that the table was replaced by hands, after careful observation, it was found that when the gripper grabbed the PVC block, its motion was oblique downwards (Figure 4.15); therefore, in addition to applying a lateral gripping force, a downwards force was also applied. Figure 4.11 illustrates that the sensor is zeroed after the gripper grabs. Therefore, after the gripper clamped the PVC block, the applied lateral and downwards forces were applied to the PVC block, which subsequently deformed the block and acted on the table. After the sensor was zeroed, the deformation of the PVC block still occurred. Hence, when the PVC block started to be lifted upwards, the force that had accumulated as a result of the deformation burst out rapidly, increasing the force in the Z direction to a point where the deformation was fully released and maintaining this value nearly unchanged, as shown in Figure 4.13.

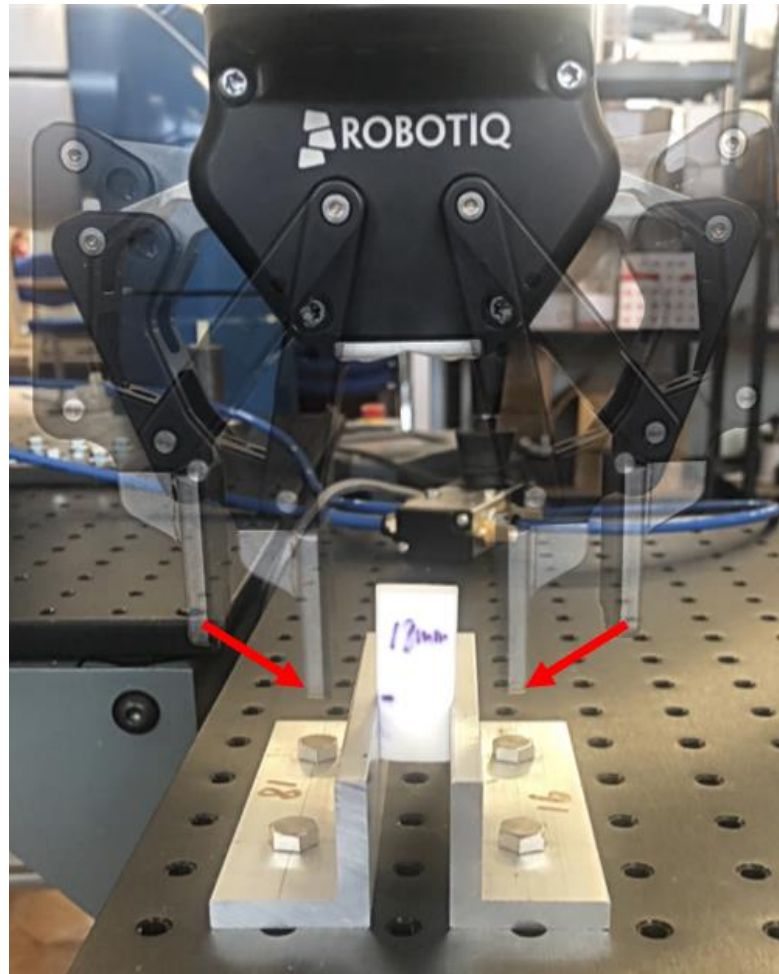


Figure 4.15: The motion track of the gripper grabbing the PVC block.

To further verify that the deformation of the PVC block caused by the gripping force produced part of the residual force, the experiment with the small PVC block placed on the table was repeated, and an upwards movement of a small displacement was added between the gripper grab and the sensor zeroing to try to overcome the deformation resulting from the grip. The force diagrams (Figure 4.16) demonstrate that the gripping force is indeed one of the reasons for the residual force because the gripping force is overcome by a small displacement while the force of the PVC block is almost 0 N.

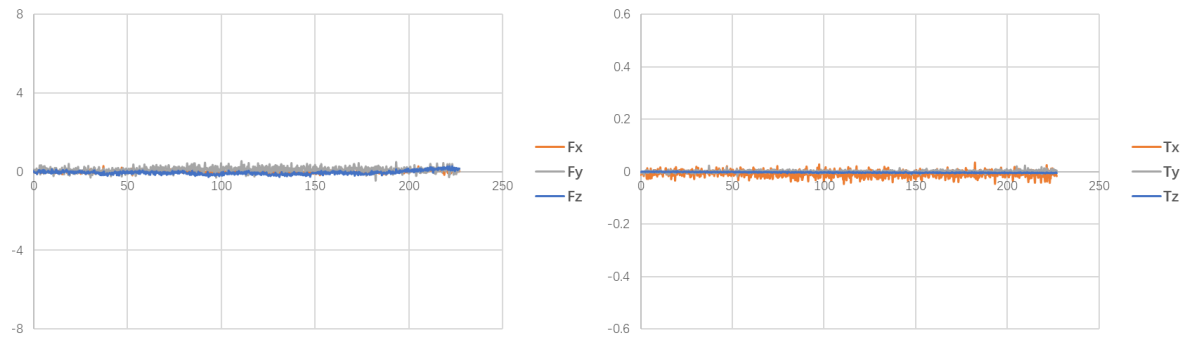


Figure 4.16: Force diagrams of the contactless grasping experiment with small displacement.

Based on the above experiments and verification, another set of control experiments was conducted. PVC blocks with a 16.5 mm gap were used. One experiment used the direct pulling method, and the other experiment involved the addition of a small upwards displacement of 0.8 mm between the grasping and sensor zeroing. The results are shown in Figure 4.17. Compared with the force diagrams obtained by direct pulling, the residual force in the z-axis of the PVC block with a small displacement was greatly reduced. Although the reduced F_z value did not drop to 0, this is because the predisplacement of 0.8 mm is only a test amount, and the magnitude of the residual force generated by the deformation caused by the grasping force cannot be accurately estimated.

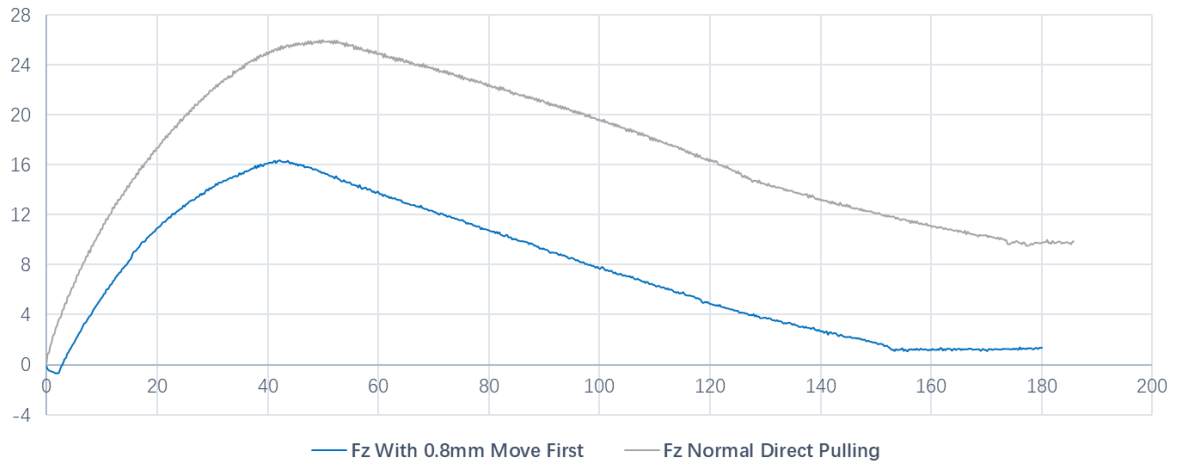


Figure 4.17: Variation in the force along the Z-axis with two different pulling methods.

In general, although the deformation caused by the gripping force cannot be accurately estimated and cannot be completely overcome by applying a displacement in advance, the residual force can be attributed to the weight of the additional equipment and the deformation caused by the gripping force. In addition, the actual maximum friction force during the pullout process of the PVC block can be obtained by subtracting the residual force from the maximum value on the z-axis in the experiment.

$$\text{Maximum Axial Friction} = \text{Maximum value in Z direction} - \text{Residual force} \quad (4.11)$$

4.4.3 Unconstrained wiggling

According to the theoretical model analysis of Section 4.1, it can be inferred that in unconstrained unplugging, the addition of horizontal force changes the direction of movement of the plug, thereby reducing the axis friction by changing the orientation of the friction force while the value of the maximum friction remains unchanged. Therefore, in the unconstrained unplugging experiment, axial and horizontal displacements were programmed and applied to the PVC blocks to replace upwards forces with periodic horizontal forces.

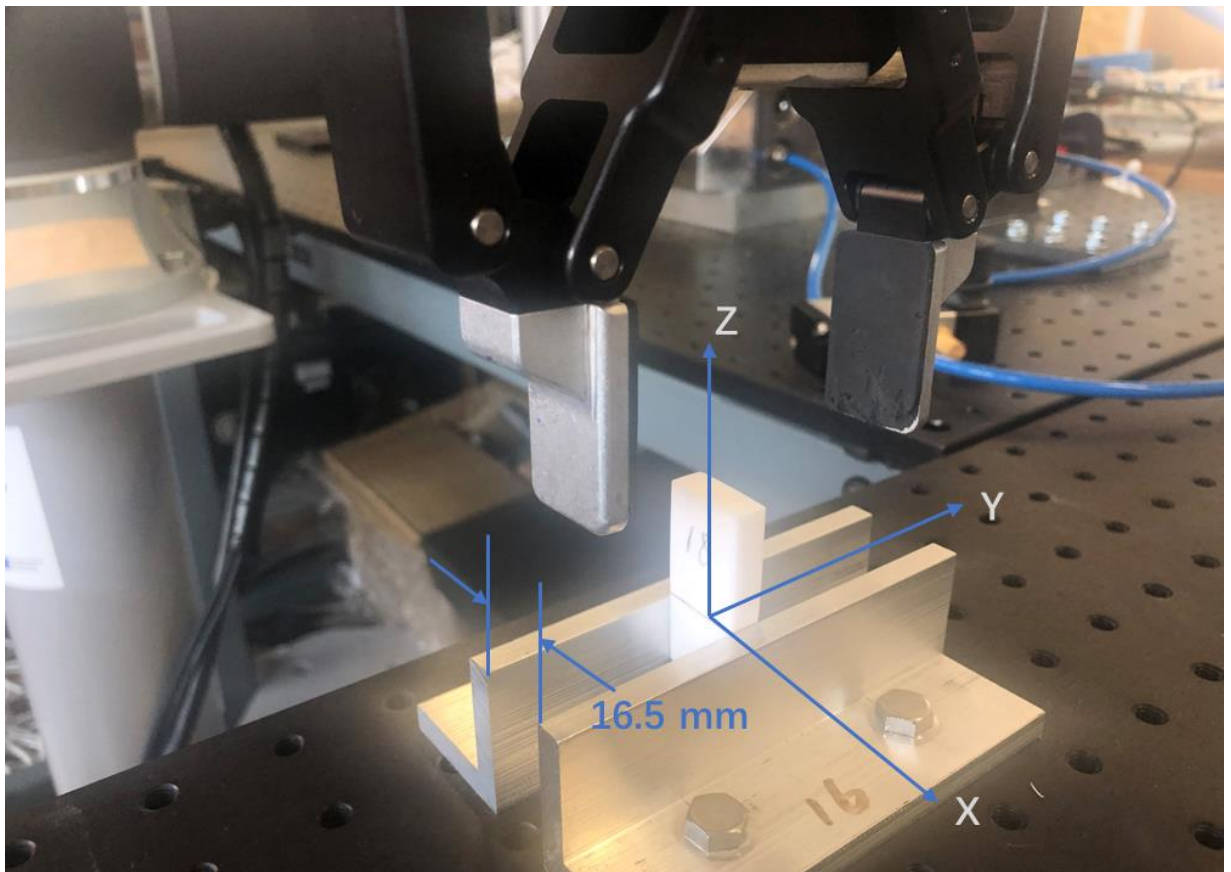


Figure 4.18: Experimental setup for unconstrained unplugging.

Figure 4.18 demonstrates the experimental setup for unconstrained unplugging. In the experiment, 18 mm PVC blocks and a 16.5 mm gap were adopted because 2 mm of

interference will cause the deformation of the PVC block to exaggerate and the contact pressure to increase; moreover, it is not easy to use a hammer to reach its contact depth to the required value (15 mm). As mentioned above, for M6 bolts, because the hole diameter on the aluminium plate was 6.5 mm, there was a certain gap in the connection. It is necessary to use a calliper to accurately measure the distance from different locations (Figure 4.19).



Figure 4.19: Measurement results at three different locations.

Table 4.3 shows the measurement results of the gap (distance between two aluminium angles) at different locations. For the middle-bottom position, the measuring end of the Vernier calliper is not long enough to reach and measure. The average distance between the other eight locations is 16.4975 mm, which is very close to the expected value.

Table 4.3: Measurement results at different locations.

Position Height	Left	Middle	Right
Top	16.49 mm	16.50 mm	16.50 mm
Middle	16.48 mm	16.51 mm	16.51 mm
Bottom	16.50 mm	x	16.49 mm
Average	16.4975 mm		

In the unconstrained unplugging experiment, PVC blocks of standard size (18 mm * 8 mm * 40 mm) were utilised, as shown in Figure 4.20. Since the contact depth in the experiment was determined to be 15 mm, each block used in the experiment was drawn at a depth of 15 mm in advance.

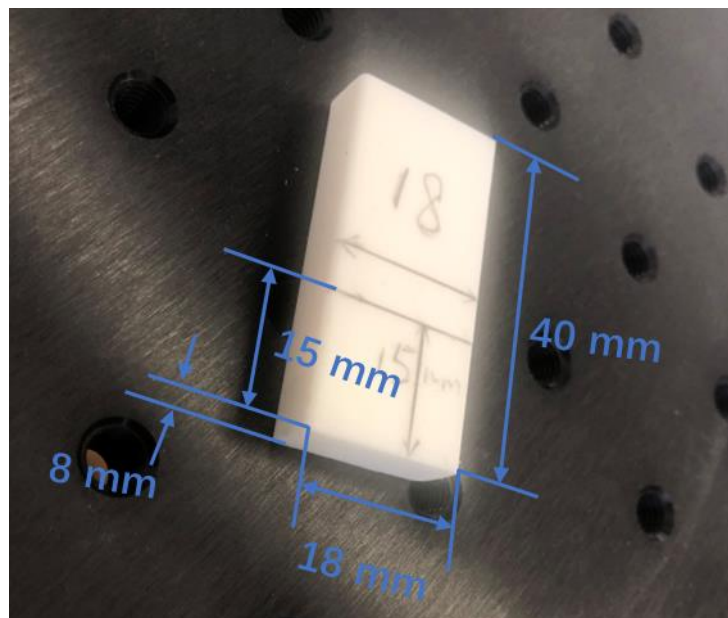


Figure 4.20: Dimensions of the PVC blocks used in the experiments.

Figure 4.21 describes the logic of the robot's programming for unconstrained unplugging. After using a camera to find the block, the gripper was controlled by the robot to move above the block, after which the robot grabbed the block. Then, based on the set displacements in the z direction and y direction, the movement mode of the robot was changed to 'line movement' so that the PVC block was expected to move upwards obliquely.

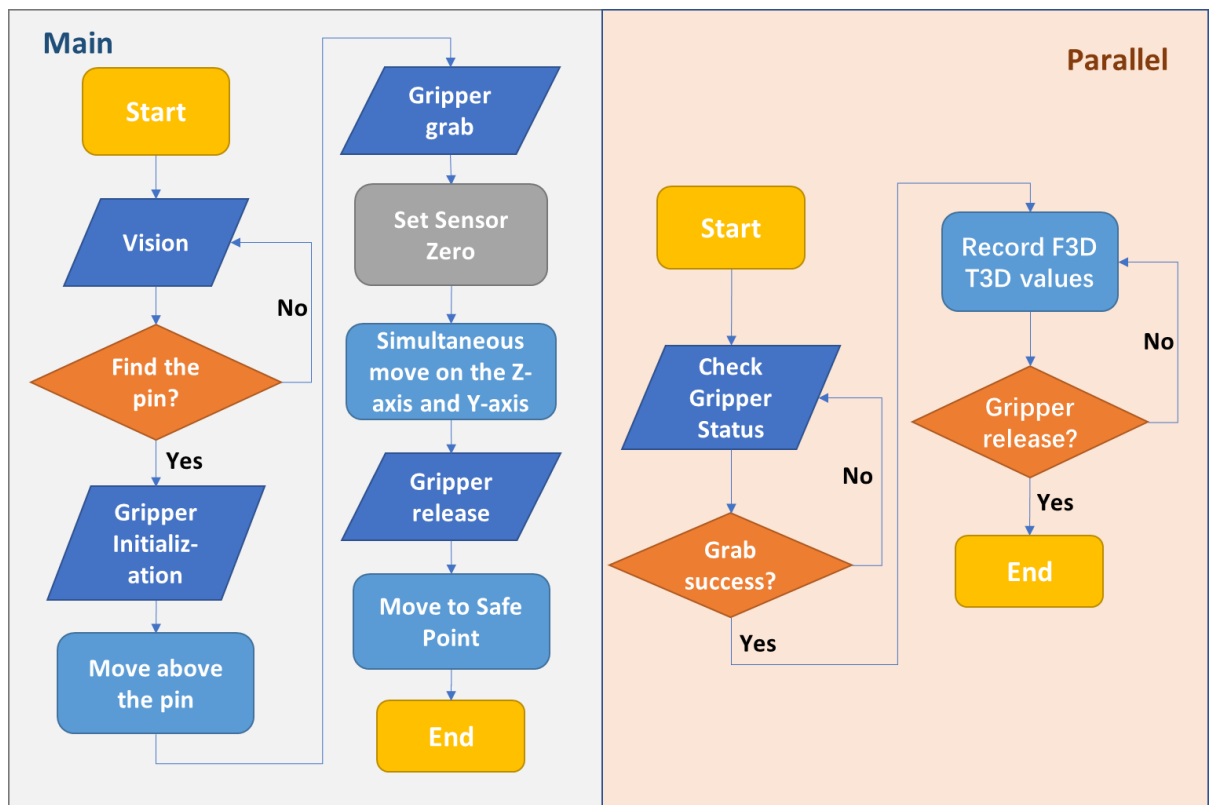


Figure 4.21: Flow charts of the robot programs for unconstrained unplugging.

4.4.3.1 Single-block unconstrained unplugging experiment

Although the standard size of the PVC block is given by the manufacturer, it is still necessary to accurately measure the specific length of the PVC block before the test. For the first series of experiments, one PVC block was used for all tests, and its length was 18.14 mm, which is 0.14 mm greater than the standard value. As mentioned above, the displacement of the robot was adopted to move the PVC block. The design of the movement parameters is detailed in Table 4.4. The longitudinal displacement was set to 30 mm instead of 15 mm to ensure that the PVC block could be pulled out completely during the experiment. The amount of displacement applied laterally changes the movement direction of the PVC block.

Table 4.4: Design of the movement parameters.

Set No.	1	2	3	4	5	6	7
Z-axis movement	30 mm	30 mm	30 mm	30 mm	30 mm	30 mm	30 mm
Y-axis movement	0 mm	5 mm	10 mm	15 mm	20 mm	25 mm	30 mm

The experimental results for the force change in the PVC block in seven sets of experiments are illustrated in Figure 4.22. From Equation (4.11), the maximum axial friction and lateral friction can be obtained. The resultant maximum friction can be calculated by Equation (4.8) and is shown in Table 4.5.

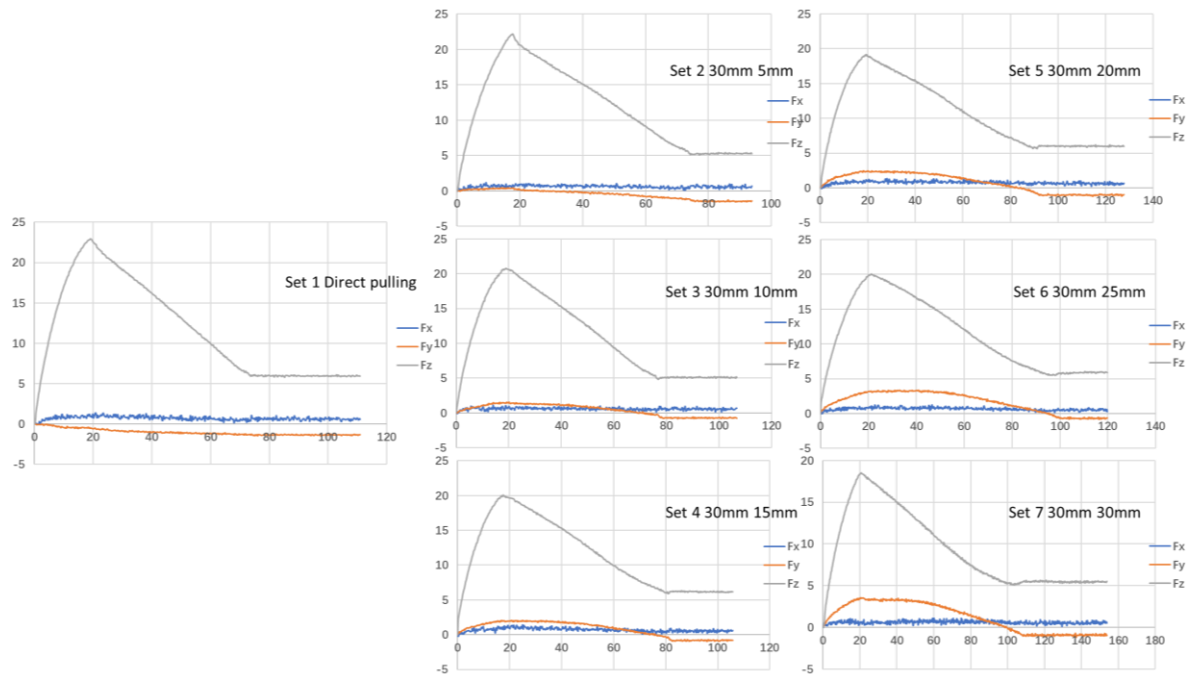


Figure 4.22: Variation curves of the force in the first series of experiments.

Table 4.5: Results of the first series of experiments and calculations for friction.

Set No.	1	2	3	4	5	6	7
MaxF_Z	22.96459	22.22075	20.81086	20.09364	19.17927	20.03287	18.52351
ResidualF_Z	5.98359	5.29552	5.11296	6.19686	6.03319	5.89269	5.47969
Actualf_Z	16.98100	16.92523	15.69790	13.89678	13.14608	14.14018	13.04382
MaxF_Y		0.47725	1.53725	2.03923	2.44711	3.40040	3.52933
ResidualF_Y		-1.47538	-0.68664	-0.82166	-1.02369	-0.71190	-0.92031
Actualf_Y		1.95263	2.22389	2.86089	3.47079	4.11230	4.44964
Totalf	16.98100	17.03749	15.85465	14.18820	13.59653	14.72602	13.78189

Unit: N

According to the first series of experimental results, with increasing lateral displacement, the lateral friction force indeed increases. According to Equation (4.5), the theoretical maximum frictional force for an 18.14 mm PVC block could be calculated as 17.3583 N. The total friction values of sets 1 and 2 are relatively close to the theoretical values, but in the next few sets, the error between the experiment and theory is relatively large. The observation of the PVC block used in this series of experiments revealed that the PVC block was obviously worn, and some debris was left on the two aluminium plates (Figure 4.23).

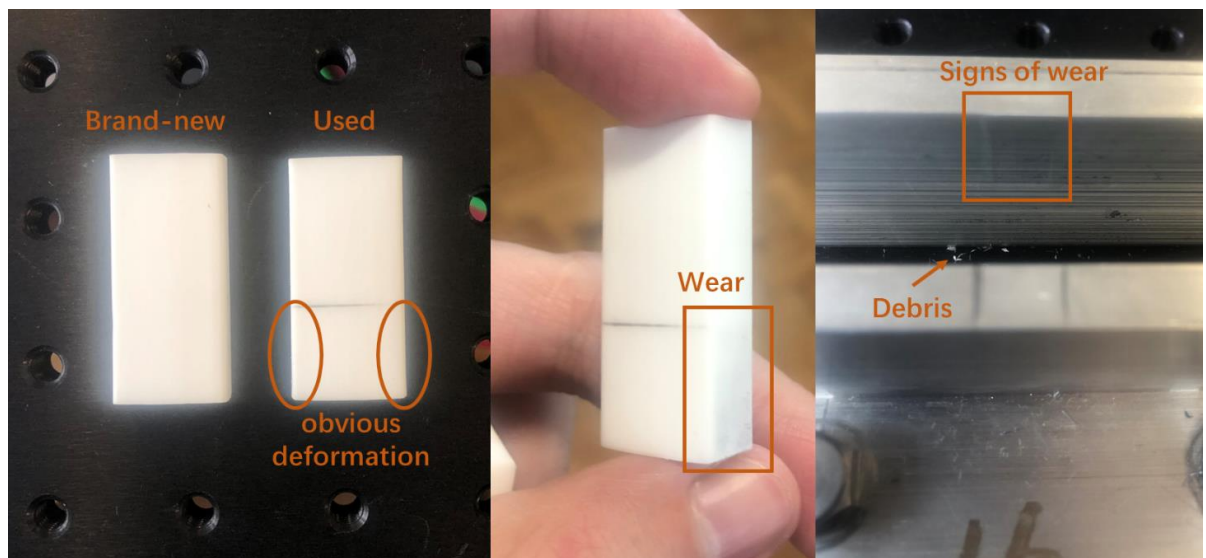


Figure 4.23: Wear of the PVC block after multiple experiments.

4.4.3.2 Multiple-block unconstrained unplugging experiment

To reduce the impact of PVC block wear on the experimental results, seven standard-sized PVC blocks were used to conduct corresponding experiments separately (Figure 4.24), and their measurement results are shown in Table 4.6.

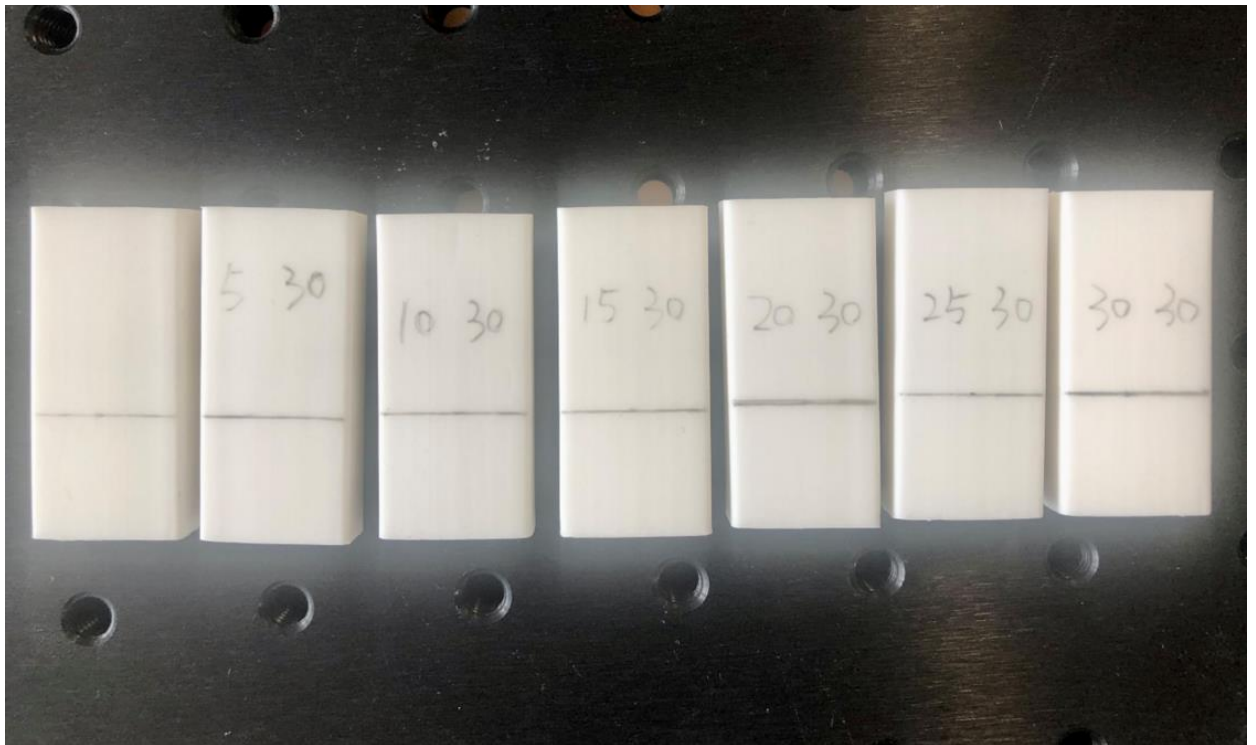


Figure 4.24: Standard-sized PVC blocks for unconstrained unplugging experiments.

Table 4.6: Results of measurements of PVC blocks in unconstrained unplugging experiments.

Set No.	1	2	3	4	5	6	7
Length (mm)	18.24	18.18	18.15	17.98	18.16	18.30	18.28

After obtaining the measurement data of these PVC blocks, according to the different lateral displacements of each set, as shown in Table 4.4, a new group of unconstrained unplugging experiments was performed, and the experimental results are shown in Figure 4.25 and Table 4.7.

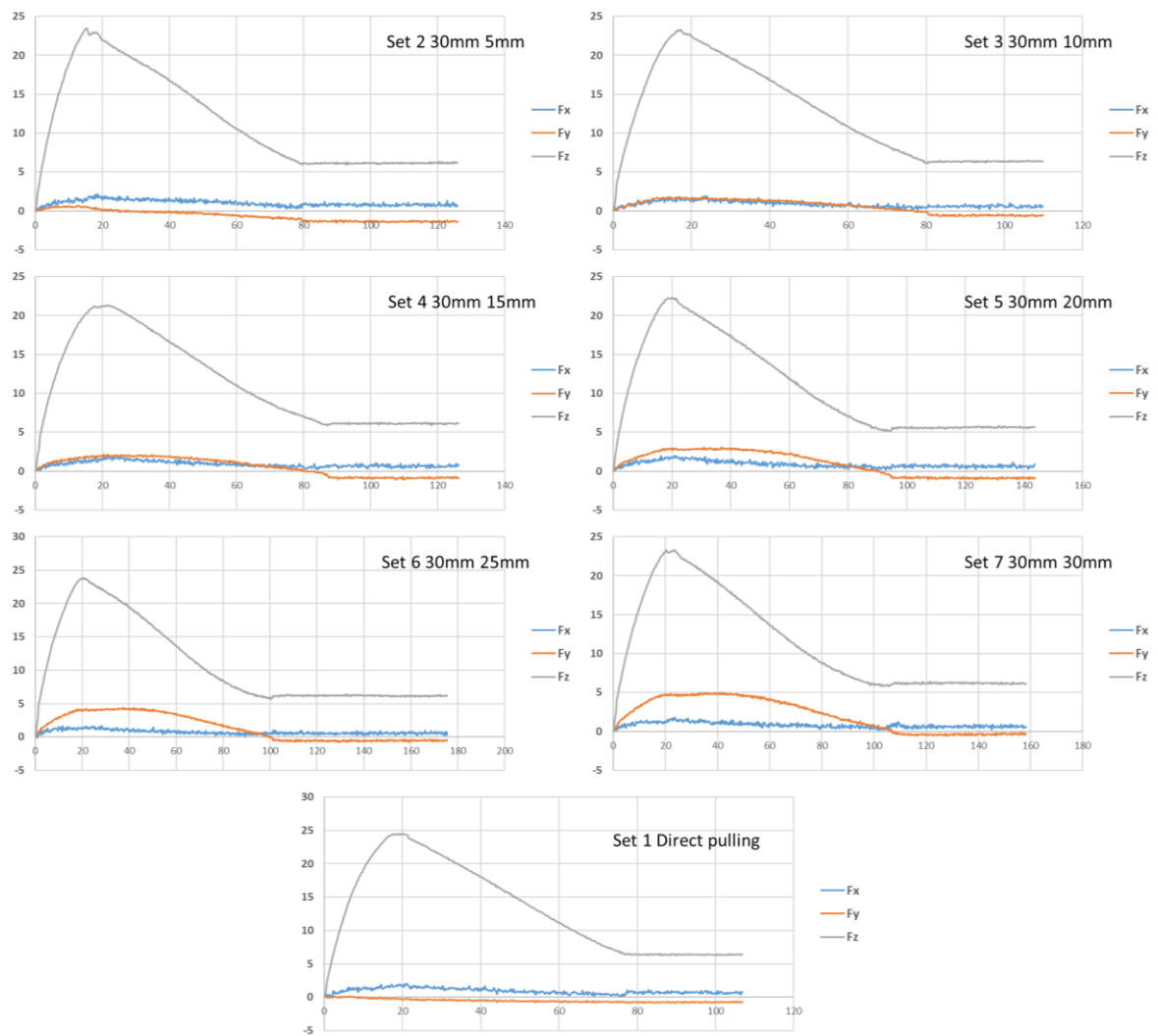


Figure 4.25: Variation curves of force for unconstrained unplugging experiments.

Table 4.7: Results of the unconstrained unplugging experiments and calculations for friction.

Set No.	1	2	3	4	5	6	7
MaxF_Z	24.54152	23.48003	23.25788	21.30593	22.29074	23.79398	23.33224
ResidualF_Z	6.41328	6.16372	6.36103	6.12269	5.61229	6.19383	6.20395
Actualf_Z	18.12824	17.31631	16.89685	15.18324	16.67845	17.60015	17.12829
MaxF_Y		0.63919	1.78444	2.13200	3.02942	4.37470	5.01572
ResidualF_Y		-1.39187	-0.59134	-0.87233	-0.89214	-0.57806	-0.34780
Actualf_Y		2.03106	2.37578	3.00433	3.92156	4.96176	5.36352
Unit: N							

Since the size of the PVC block used in each set of experiments is different, it is not necessary to compare the magnitude of the maximum friction force obtained by different sets. However, the difference between the theoretical and experimental results can be obtained (Table 4.8) by comparing the theoretical maximum friction of each set with the experimental maximum friction. Equation (4.5) can be employed to generate the theoretical results, and the experimental resultant maximum friction can be calculated by using Equation (4.8) and the data from Table 4.7.

Table 4.8: Theoretical and Experimental Errors of Maximum Friction.

Set No.	1	2	3	4	5	6	7
Theory f	18.3158	17.7426	17.4545	15.8042	17.5507	18.8852	18.6958
Expt. f	18.12824	17.43502	17.06305	15.47763	17.13329	18.28618	17.94842
							Unit: N
Error	1.024%	1.734%	2.243%	2.066%	2.378%	3.172%	4.000%

In the experiment, the displacement was applied to control the movement direction of the PVC block to change the direction of the friction force. The reduction in theoretical axial friction can therefore be calculated as the ratio of the applied axial and lateral displacements. For example, in Set 2, the lateral displacement is 5 mm, and the axial displacement is 30 mm; then, the total displacement can be calculated by the Pythagorean theorem. The axial displacement is subtracted from the total displacement, and the result is divided by the total displacement so that the theoretical axial friction reduction is obtained.

Table 4.9: Reduction in the maximum axial friction.

Set No.	1	2	3	4	5	6	7
Theory R	0	1.361%	5.132%	10.557%	16.795%	23.178%	29.289%
Expt. R	0	0.681%	0.974%	1.902%	2.655%	3.752%	4.567%
Actual R	0	2.400%	3.195%	3.929%	4.970%	6.805%	8.384%

Table 4.9 presents the theoretical, experimental, and actual reductions in the maximum axial friction. The experimental and actual axial friction reductions greatly differ from the theoretical reduction. To understand the reason for this difference, a further analysis was conducted.

Figure 4.26 depicts the setting of the displacement direction for the PVC block at the beginning of the experiment, the direction of the friction force during the pull-out process, and the expected trajectory of the PVC block. The robot is programmed to move simultaneously in the Z+ and Y+ directions after the gripper grabs the PVC block, and the motion mode is linear motion rather than point-to-point motion, which makes the motion of the PVC block oblique upwards straight-line movement, while the amount of horizontal displacement also determines the slope of this straight line.

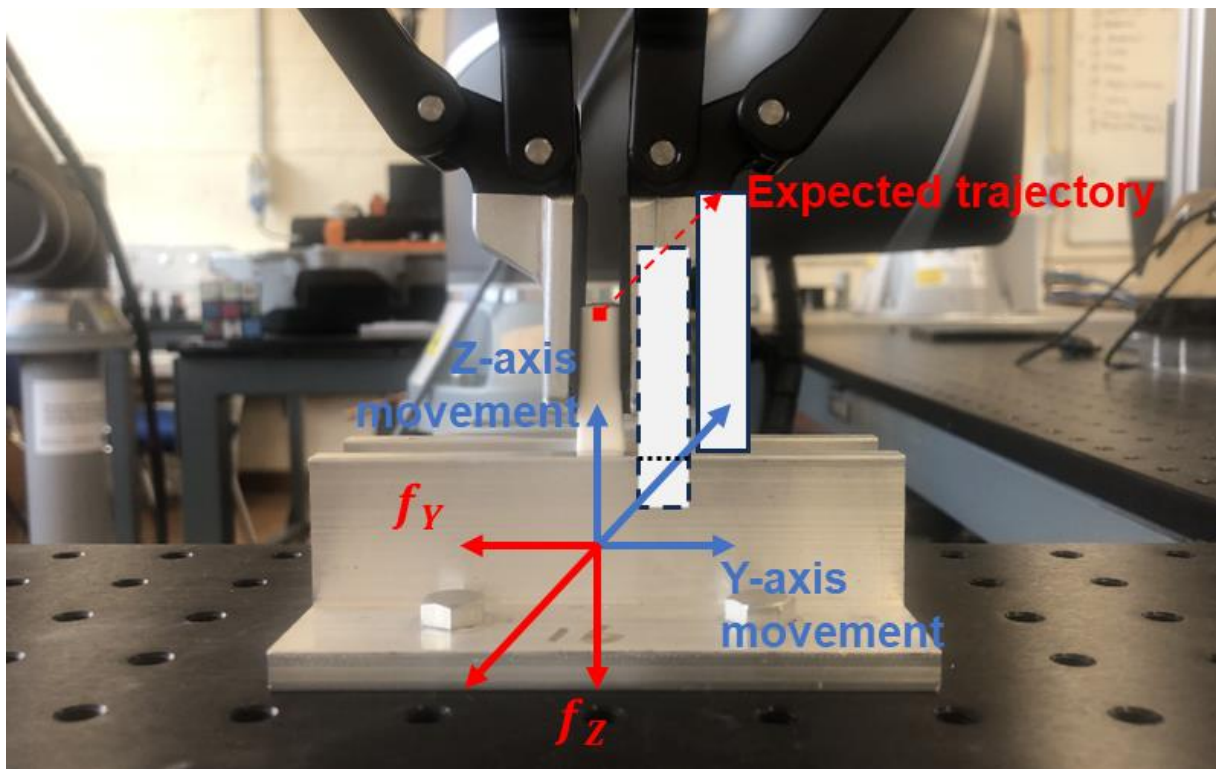


Figure 4.26: Expected unconstrained pullout trajectory of the PVC block.

However, in the experiment, the PVC blocks did not move completely along the expected trajectory. Figure 4.27 shows the moment of motion in this experiment, in which part of the PVC block is grabbed by the gripper, following the given direction of displacement, sloping upwards. Because the material of the PVC block is very soft and has high elasticity, the middle part of the block experiences bending and deformation, so that the displacement angle of the part of the PVC block that is in contact with the aluminium plate is much smaller than the set value.

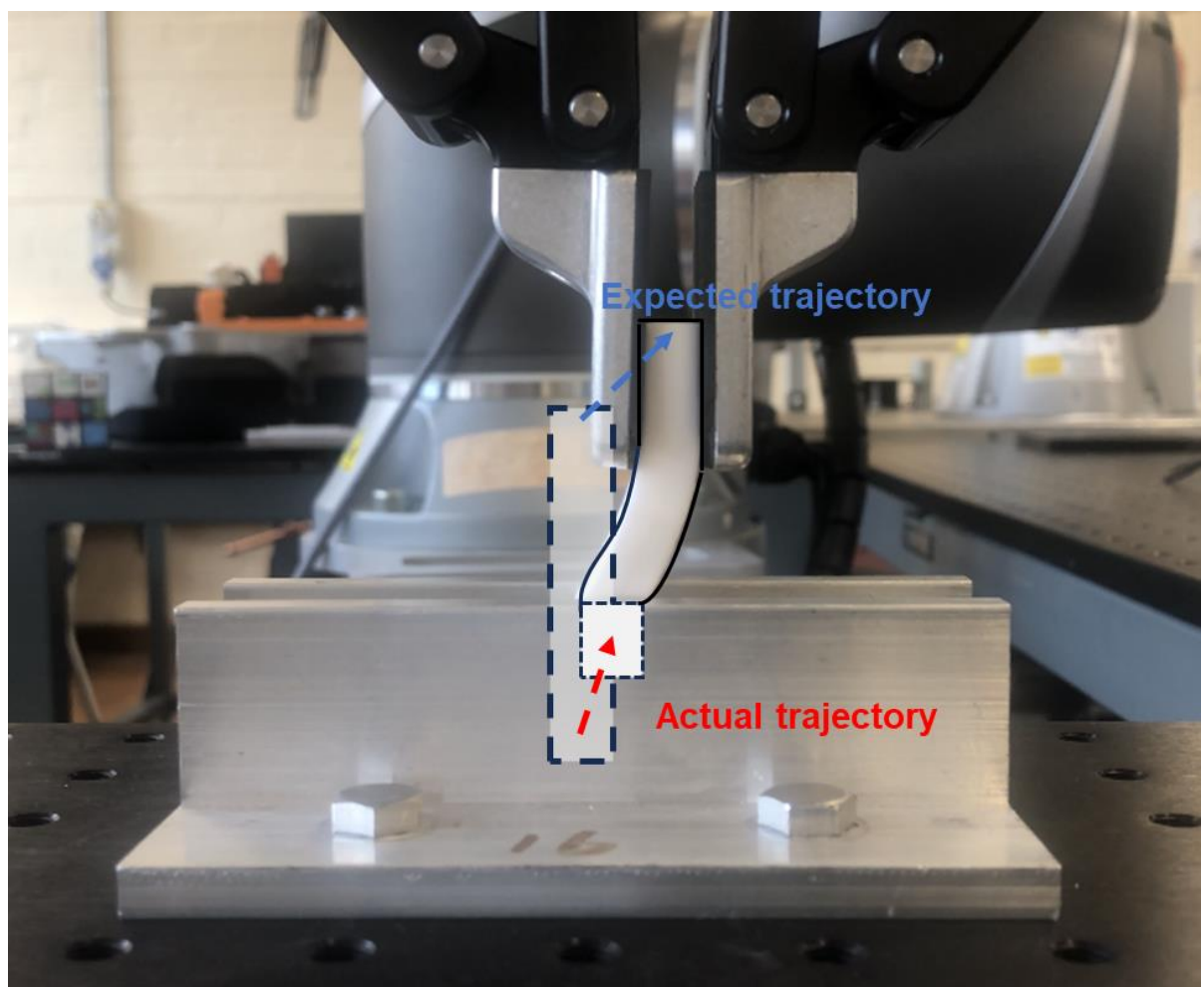


Figure 4.27: Comparison between the expected pull-out trajectory and the actual pull-out trajectory.

In general, due to the softness of the material, the PVC block bends and deforms when stressed. Although this deformation and bending affect the displacement direction of the contact part, such that the experimental and actual reductions in the maximum axial friction are much smaller than the theoretical reductions, it is also proven that the larger the lateral displacement applied is, the greater the reduction in the maximum axial friction.

4.5 Summary

In this chapter, the cuboid plug-socket unplugging problem was investigated. To study the stress distribution of the plug during extraction, an interference-fit cuboid plug-socket model was developed. The simulation results of the plug stress distribution generated in ABAQUS are consistent with the stress distribution described by the theoretical model.

The weight of the additional equipment and the deformation caused by the gripping force are the main causes of the residual force, as proven by several sets of experiments with control variables. The same size plugs and varied lateral forces were adopted in unconstrained wiggling trials, and the results illustrated that this disassembly technique can reduce the axial friction force during the extraction process; the greater the lateral force applied is, the greater the reduction rate.

This chapter considered the failure of the unconstrained plug out of the socket. However, when two sides of the plug interfere with the socket and the other two sides are constrained, the failure of this kind of constrained plug should be investigated.

5 Robotised Unplugging of a Cuboid Plug Press-Fitted into a Cuboid Socket with a Disassembly Strategy—Constrained Wiggling

This chapter introduces another unplugging technique, constrained wiggling, for cuboid plug-socket connections to reduce axial friction. In Section 5.1, an introduction to a disassembly strategy, constrained wiggling, is provided. In addition, a theoretical model of the stress distribution caused by constrained wiggling is established. In Section 5.2, the FEM is used to verify the effect of the application of lateral forces on the stress distribution. In Section 5.3, the experimental procedures for constrained wiggling and unplugging are presented. Six groups of experiments are conducted with different sizes of plugs and sockets. In Section 5.4, a summary of this chapter is provided, including the error analysis and conclusion.

5.1 Constrained wiggling

The introduction of unplugging in robotic disassembly is addressed in Section 3.1, Chapter 3. The theoretical model of the interference-fit plug socket is built and analysed in Section 4.1, Chapter 4. Based on the introduction and theoretical model in the previous chapters, another disassembly strategy, constrained wiggling, is considered in this chapter.

The unconstrained wiggling method can be used on the premise that there is enough space for a small amount of displacement between the two sides of the cuboid plug and the socket. However, considering that some plugs and sockets are closely connected and that there is no space for lateral displacement [115], it is necessary to discuss the use of the constrained wiggling method.

Constrained wiggling refers to an unplugging method in which a periodic lateral force is applied perpendicular to the interference contact surface while maintaining an upwards pulling force (Figure 5.1) so that the pressure distribution of the contact surface changes during plug removal.

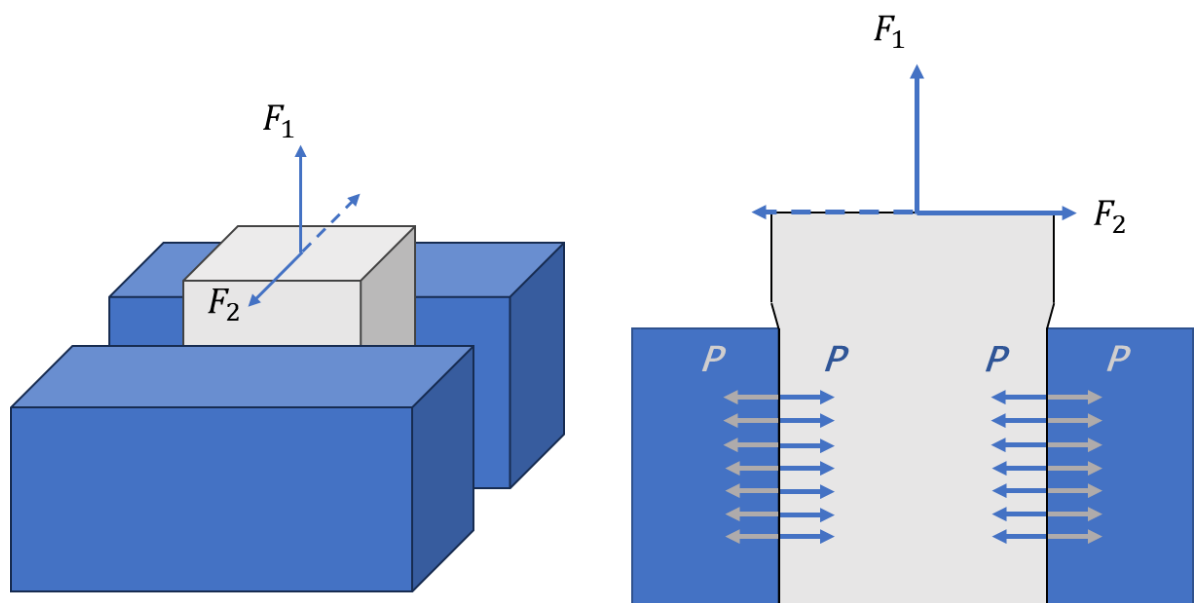


Figure 5.1: Schematic diagram of constrained wiggling and force application.

From Equations (4.5) and (4.7), it can be concluded that the maximum axial friction force that needs to be overcome to unplug the plug is related to the motion state of the plug and the stress on the contact surface. The former is related to the use of different friction coefficients, while the latter determines the total contact pressure. To analyse whether this constrained wiggling method can reduce axial friction, first, it is necessary to consider the influence of lateral force on the contact stress distribution. Based on this, a theoretical model was built to perform mechanical analysis.

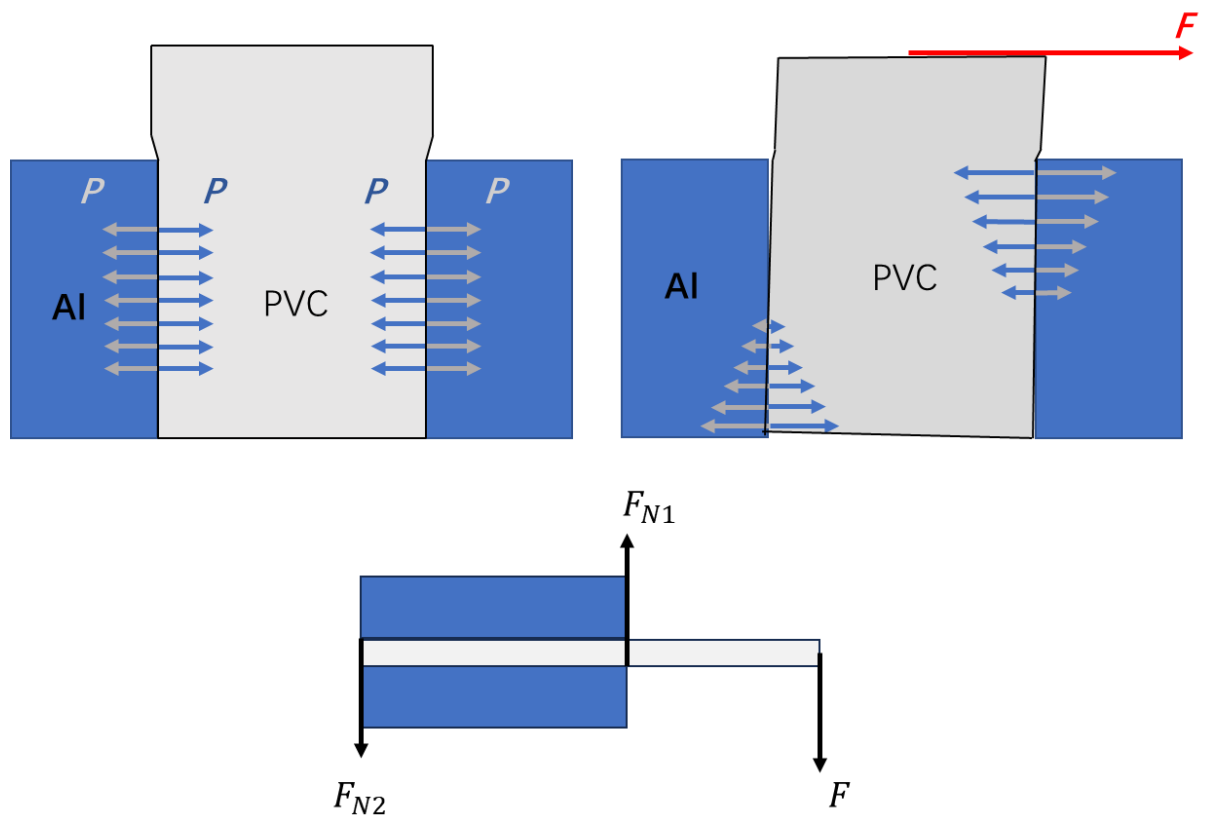


Figure 5.2: Schematic diagram of the change in contact surface stress with increasing lateral force.

The plug-socket model can be regarded as a cantilever beam [114] inserted into the wall; the difference is that the plug socket has an interference fit contact. Therefore, when a lateral force is applied on a plug, it is equivalent to applying a downwards force at the end of the cantilever beam. The mechanical analysis of this shows that when the cantilever beam is in contact with the wall, it will be supported by two opposite forces distributed at two ends of the contact. However, unlike the cantilever beam, the plug socket itself has a uniformly distributed pressure formed by elastic deformation of the plug. Based on this, the support force applied at both ends will be transformed into a pressure distribution with a certain linear law, as shown in Figure 5.2.

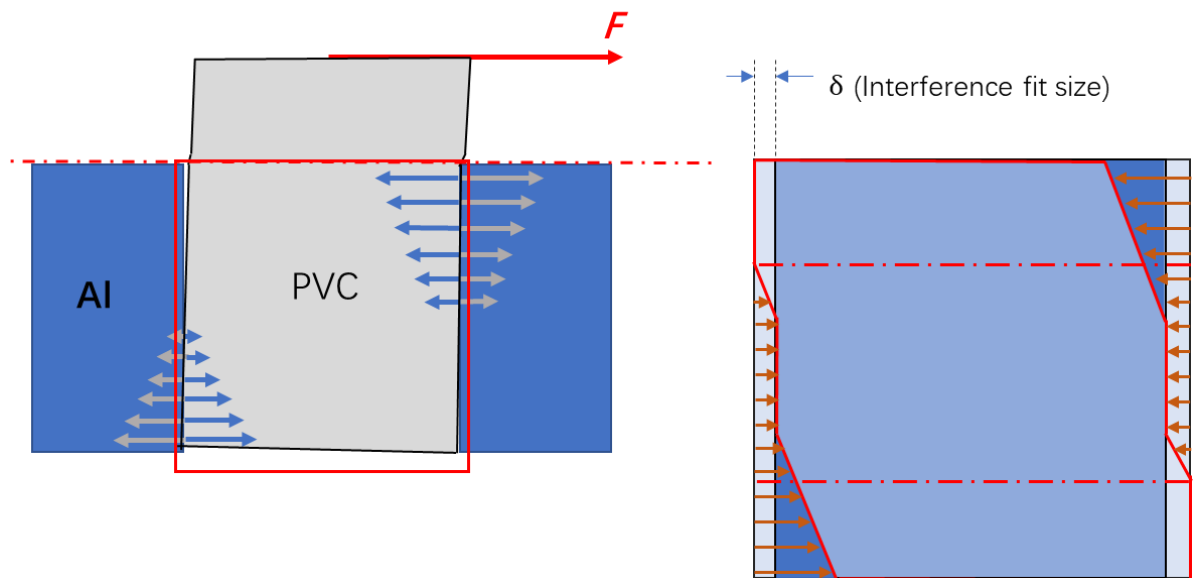


Figure 5.3: Schematic diagram of the contact surface stress distribution.

To further study the stress analysis, the part of the plug that is in contact with the socket is separated for mechanical analysis. When the deformation of one side of the plug is greater than twice the interference fit size, the other side will return to its original size without elastic

deformation. Hence, in Figure 5.3, two dash-dotted lines divide this part of the plug into three areas. In the top and bottom regions, since the deformation of one side exceeds twice the amount of interference and the other side returns to its original size due to elasticity, no stress occurs. In the middle part, due to the influence of lateral force, the deformation on one side is greater than the interference but less than twice the interference, so there will still be a small amount of deformation on the other side, forming a transition area.

To determine the relationship between both sides' stress distributions and the applied lateral force, a plane coordinate system was established. The baseline, 0 of the x-axis, was set at the top of the model, and the y-axis was used to reflect the magnitude of the stress. Furthermore, Δl_1 and h_1 were used to represent the deformation of the upper right side, while the other two symbols, Δl_2 and h_2 , indicated the left side's deformation (Figure 5.4).

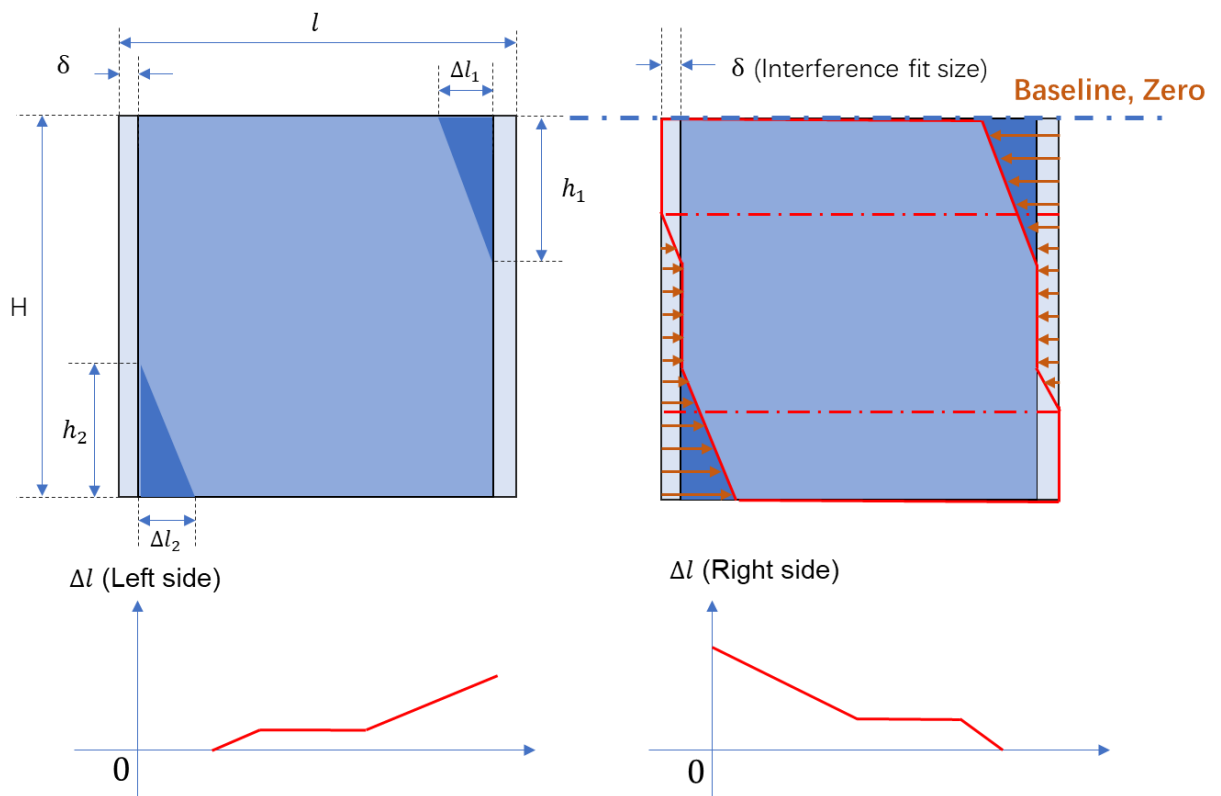


Figure 5.4: Deformation diagram and function on both sides of the plug.

Based on the function graphs in Figure 5.4, the deformations of both sides can be expressed as follows:

$$\Delta l(\text{right side}) = \begin{cases} -\frac{\Delta l_1}{h_1}x + \Delta l_1 + \delta & (0, h_1) \\ \delta & (h_1, H - h_2) \\ -\frac{\Delta l_2}{h_2}x + \delta + \frac{\Delta l_2 H}{h_2} - \Delta l_2 & \left(H - h_2, H - h_2 + \frac{\delta h_2}{\Delta l_2}\right) \end{cases} \quad (5.1)$$

$$\Delta l(\text{left side}) = \begin{cases} \frac{\Delta l_1}{h_1}x - \Delta l_1 + \delta & \left(h_1 - \frac{\delta h_1}{\Delta l_1}, h_1\right) \\ \delta & (h_1, H - h_2) \\ \frac{\Delta l_2}{h_2}x + \delta - \frac{\Delta l_2 H}{h_2} + \Delta l_2 & (H - h_2, H) \end{cases} \quad (5.2)$$

By using the Law of Conservation of Angular Moments [116], the following equation can be obtained:

$$\mathbf{M} + \left(\int \mathbf{P}(\text{right side}) \cdot x \, dx - \int \mathbf{P}(\text{left side}) \cdot x \, dx \right) * \mathbf{w} = \mathbf{0} \quad (5.3)$$

where \mathbf{M} is the applied external moment caused by the lateral force and \mathbf{w} is the width of the plug.

Based on Equation (4.1), Equation (5.3) can be expressed as follows:

$$M + \left(\frac{E}{l} \int \Delta l(\text{right side}) \cdot x \, dx - \frac{E}{l} \int \Delta l(\text{left side}) \cdot x \, dx \right) * w = 0 \quad (5.4)$$

Then, Equation (5.1) and Equation (5.2) are substituted into Equation (5.4). The equation is given by:

$$\begin{aligned} \frac{l}{Ew} M + \frac{1}{6} \Delta l_1 h_1^2 + \frac{1}{2} \delta h_1^2 + \frac{1}{6} \delta^3 \left(\frac{h_2}{\Delta l_2} \right)^2 + \frac{1}{2} H \delta^2 \left(\frac{h_2}{\Delta l_2} \right) - \frac{1}{2} h_2 \delta^2 \left(\frac{h_2}{\Delta l_2} \right) = \\ - \frac{1}{6} \delta^3 \left(\frac{h_1}{\Delta l_1} \right)^2 + \frac{1}{2} h_1 \delta^2 \left(\frac{h_1}{\Delta l_1} \right) - \frac{1}{6} \Delta l_2 h_2^2 + H h_2 \delta - \frac{1}{2} \delta h_2^2 + \frac{1}{2} \Delta l_2 h_2 H \end{aligned} \quad (5.5)$$

Because the tilt angle of the plug remains constant after lateral force is applied, the slopes of the deformation on both sides are the same and determined as follows:

$$k = \frac{\Delta l_1}{h_1} = \frac{\Delta l_2}{h_2} \quad (5.6)$$

Hence, Equation (5.5) can be simplified as follows:

$$\begin{aligned} \frac{l}{Ew} M + \frac{1}{6} k h_1^3 + \frac{1}{6} k h_2^3 + \frac{1}{2} \delta h_1^2 + \frac{1}{2} \delta h_2^2 + \frac{1}{3} \delta^3 \left(\frac{1}{k} \right)^2 + \frac{1}{2} H \delta^2 \left(\frac{1}{k} \right) \\ = \frac{1}{2} h_2 \delta^2 \left(\frac{1}{k} \right) + \frac{1}{2} h_1 \delta^2 \left(\frac{1}{k} \right) + H h_2 \delta + \frac{1}{2} k h_2^2 H \end{aligned} \quad (5.7)$$

According to Newton's first law [117], the sum of the forces on the plug is 0, which can be expressed as follows:

$$\mathbf{F} - \left(\int \mathbf{P}(\textit{right side}) dx - \int \mathbf{P}(\textit{left side}) dx \right) * \mathbf{w} = \mathbf{0} \quad (5.8)$$

where \mathbf{F} is the applied lateral force.

Substituting Equation (5.1), Equation (5.2) and Equation (5.6) into Equation (5.8), the following equation can be obtained:

$$\frac{l}{Ew} \mathbf{F} = \frac{1}{2} k h_1^2 - \frac{1}{2} k h_2^2 + \delta(h_1 - h_2) \quad (5.9)$$

According to the geometric model of the plug, when the plug is inclined at a certain angle, since the hardness of the socket is much greater than that of the plug, the deformation of the socket is negligible. Therefore, the distance between the inclined lines formed by deformation at both ends of the plug is equal to the inner diameter of the socket (Figure 5.5).

Hence, the distance can be calculated as follows:

$$d = \frac{H - h_1}{\sqrt{1 + k^2}} k + \frac{l - 2\delta - k h_2}{\sqrt{1 + k^2}} = l - 2\delta \quad (5.10)$$

Equation (5.10) can be simplified as follows:

$$k(H - h_1 - h_2)^2 + 2(l - 2\delta)(H - h_1 - h_2) = k(l - 2\delta)^2 \quad (5.11)$$

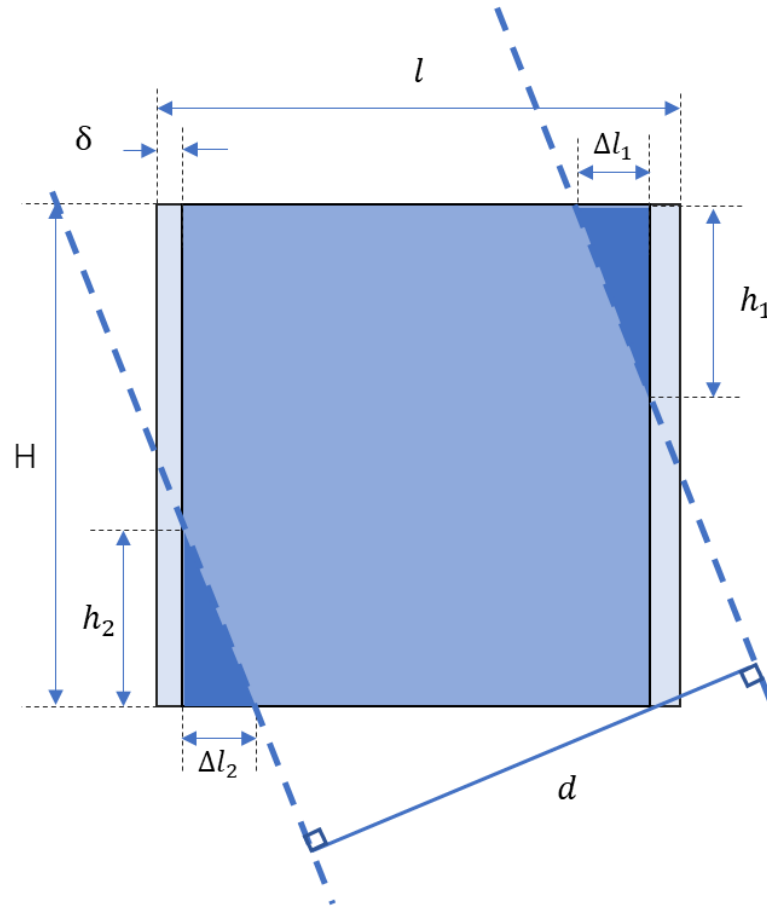


Figure 5.5: Geometry of the distance between two sides' deformation tilt lines.

By combining the above three formulas, Equation (5.7) is obtained from the Law of Conservation of Angular Momentum, Equation (5.9) is based on Newton's first law, and Equation (5.11) is generated from the geometric analysis. A system of equations with three variables k , h_1 , and h_2 can be obtained. When the size of the model and the magnitude of the applied lateral force are determined, the solutions of these three variables can be obtained according to this equation system.

5.2 FEM of cuboid unplugging

Finite element modelling (FEM) was used to verify whether the effect of the application of lateral forces on the stress distribution on both sides of the plug matches the stress distribution described by the theoretical model in Section 5.1.

The 3D plug-socket model with interference fit for FE simulation was established and demonstrated in Section 4.3, including the dimensions of the model, parameters of the material, mesh of the components and contact model between the plug and the socket.

To understand the influence of the application of lateral force on the stress distribution of the plug, a new analysis step was added based on the original analysis model. In this new step, the boundary conditions applied to the socket remained the same as those in the initial step, and a reference point was created in the centre of the top surface of the plug. In the 'Interaction' function module, the reference point was coupled to the top surface of the plug, constraining the motion of this surface with the movement of a constraint control point, that is, the reference point. After that, a concentrated force (2 N) in the +x direction was applied to this reference point, which is equivalent to applying a lateral force to the plug (Figure 5.6). The reason for using the reference point to apply lateral force to replace the added concentrate force directly on the plug is that the latter causes the local deformation of the plug stress point and its surroundings to be significant [118], thus affecting the overall stress distribution of the plug.

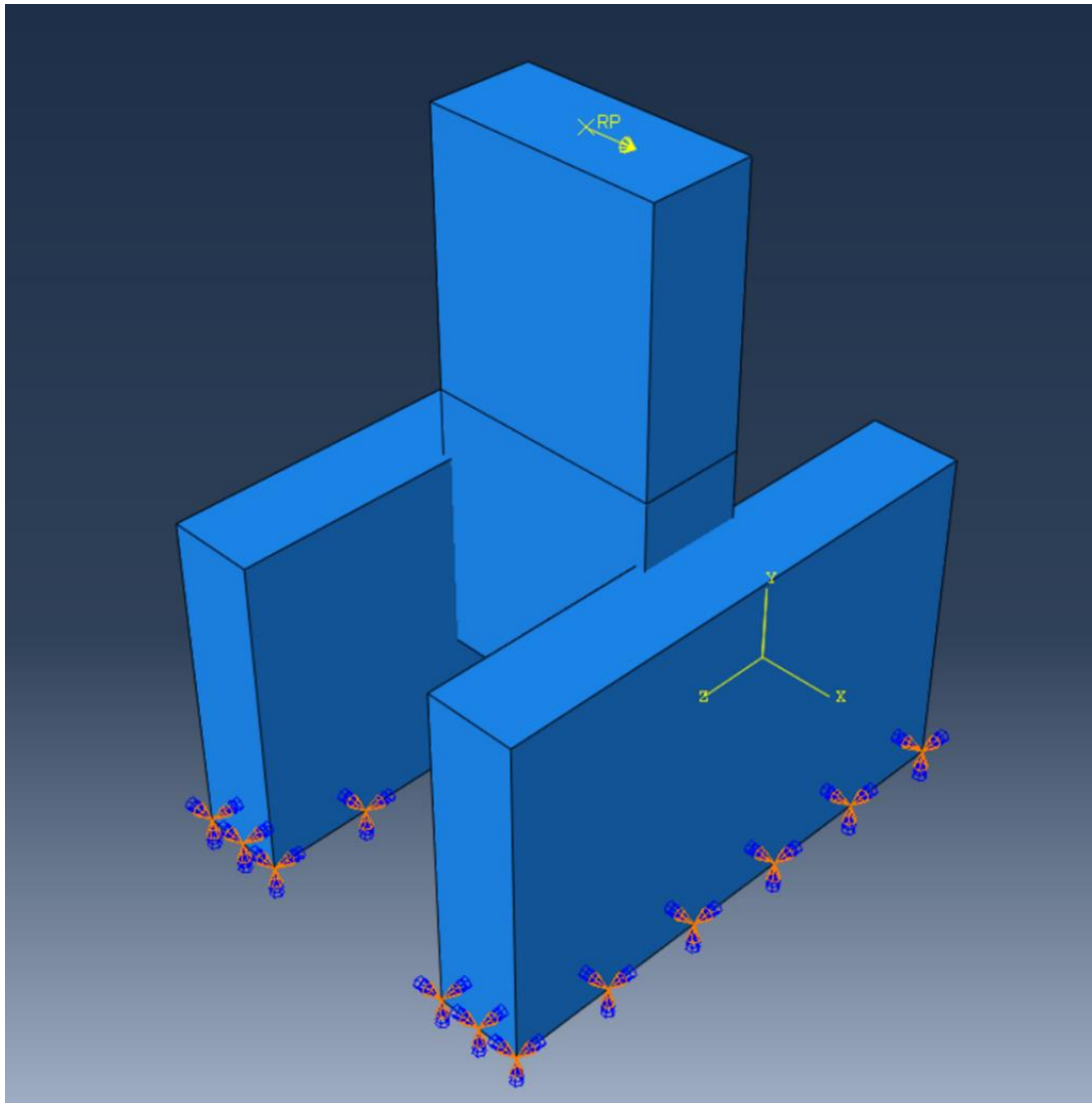


Figure 5.6: Boundary conditions applied to the plug-socket model.

Figure 5.7 shows the stress distribution of the whole model with a 2 N lateral force from the simulation. The explanation of why the stress at the bottom of the socket is much greater than the stress on the plug is provided in Section 4.3.

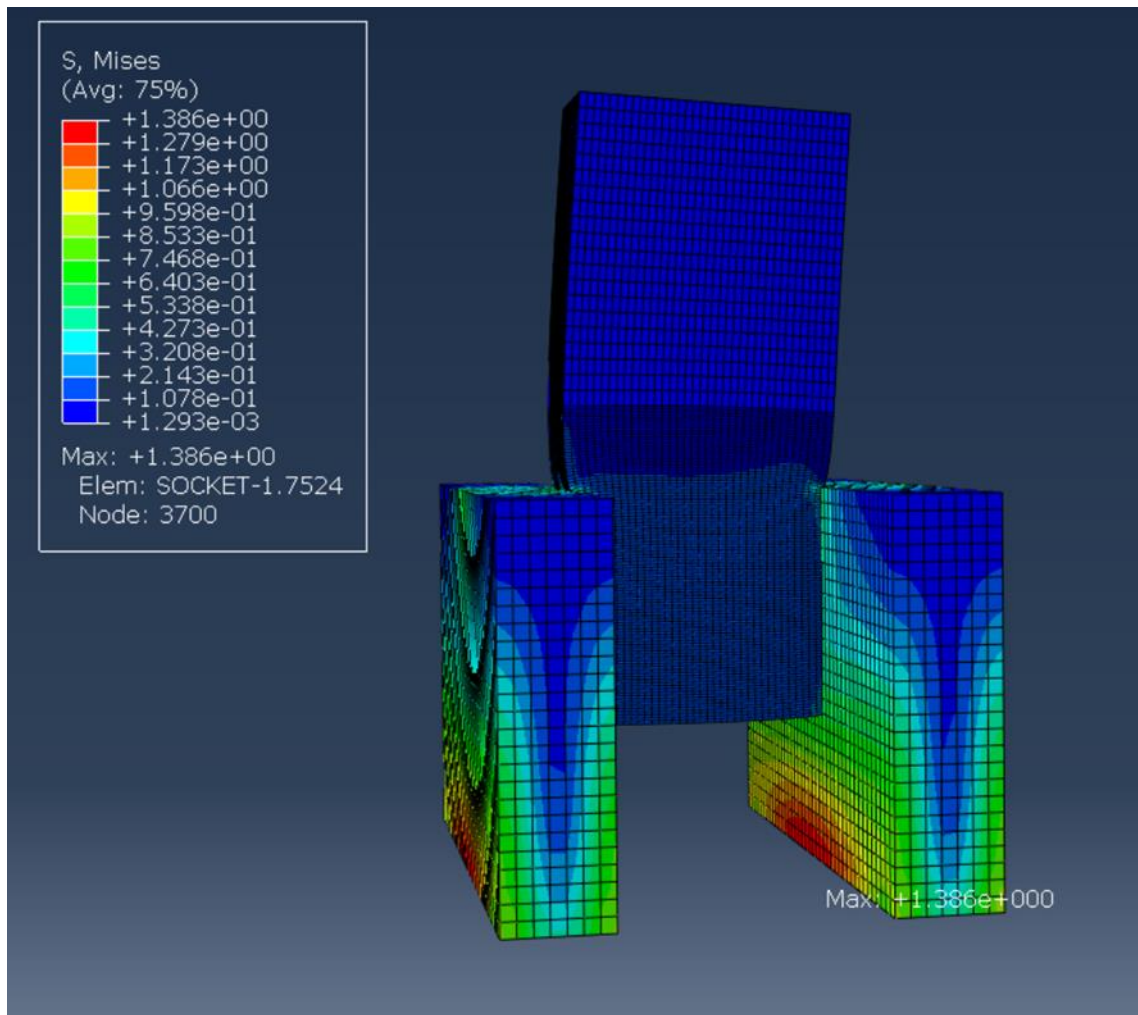


Figure 5.7: Stress distribution of the plug-socket model with a 2 N lateral force.

Figure 5.8(d) shows the stress distribution of the plug with a 2 N lateral force. Like in Section 4.3, the socket is momentarily hidden to better display the stress distribution of the plug, and the limitation of the stress in the legend, which was previously indicated in red, is adjusted to 0.3. Figure 5.8(a), Figure 5.8(b), and Figure 5.8(c), respectively describe the initial stress distribution of the plug exerted by the lateral force, the stress distribution in the middle stage and the final stress distribution. As the lateral force was gradually applied to the plug according to the increase in strength in the simulation, the maximum stress at the contact

edge gradually increased to 0.5 MPa, but the contact pressure on the left side decreased, which is also consistent with the stress distribution of the theoretical model.

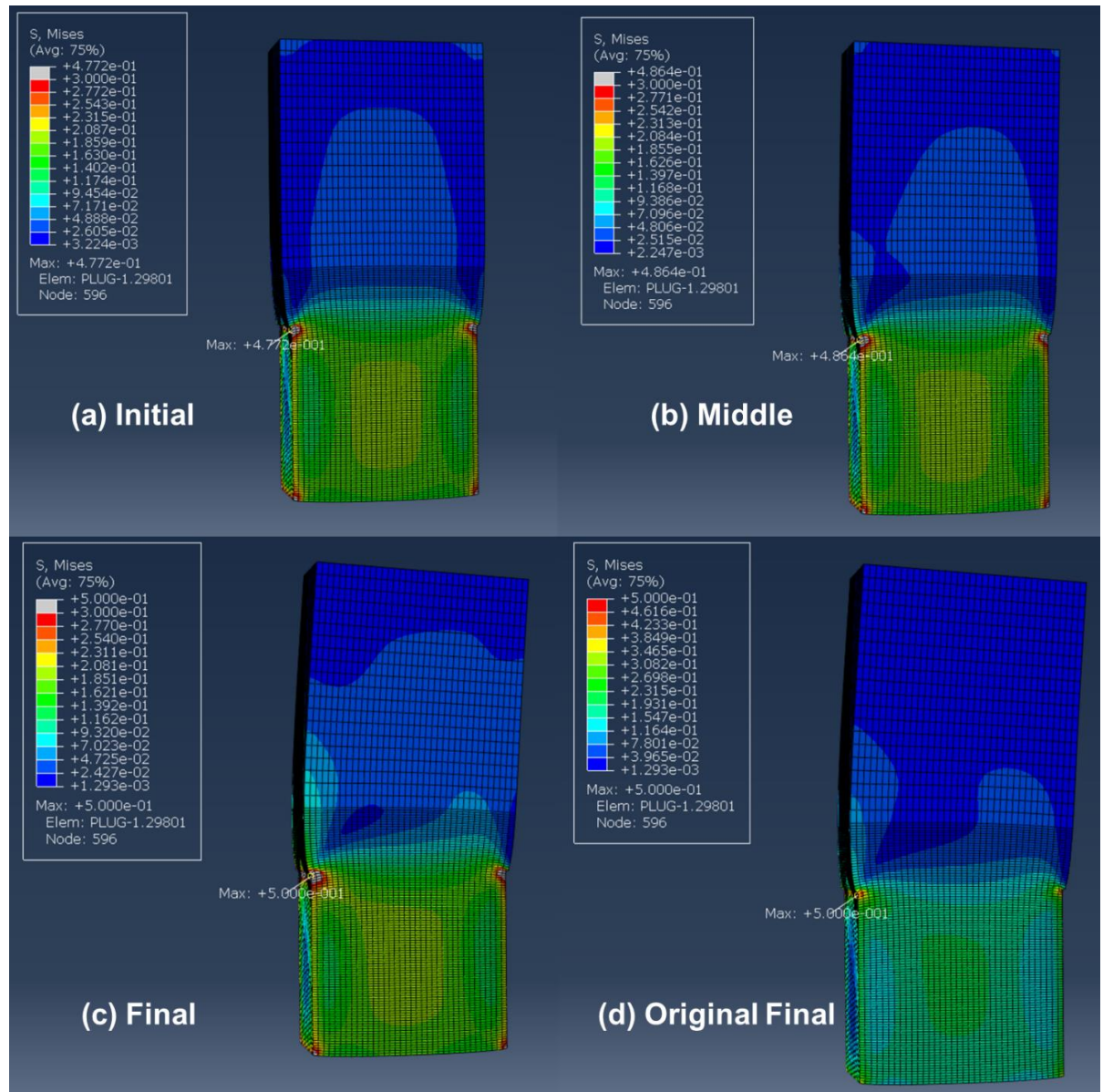


Figure 5.8: Stress distribution of the plug with a 2 N lateral force.

5.3 Experiments

To verify whether the unplugging strategy, constrained wiggling, can reduce axial friction, experiments involving direct pulling and wiggling unplugging the interference-fit plug out of the socket were performed.

5.3.1 Experimental setup

The experimental setup for cuboid unplugging is described in Section 4.4 and includes the equipment used in the experiment, the dimensions of the plugs and the aluminium plates and the material properties of the plugs and the sockets. The experimental procedures for directly pulling the plug out of the socket are detailed in Section 4.4.1. The analysis of residual forces occurring in experiments is conducted in Section 4.4.2.

5.3.2 Constrained wiggling

Based on Section 5.1, the constrained wiggling method is applied to unplugging where two of the four surfaces of contact between the plug and the socket are an interference fit and the other two sides are in tight contact. Since the direction of the applied lateral force has changed, a new gripping direction and new 3D coordinates are used and established (Figure 5.9).

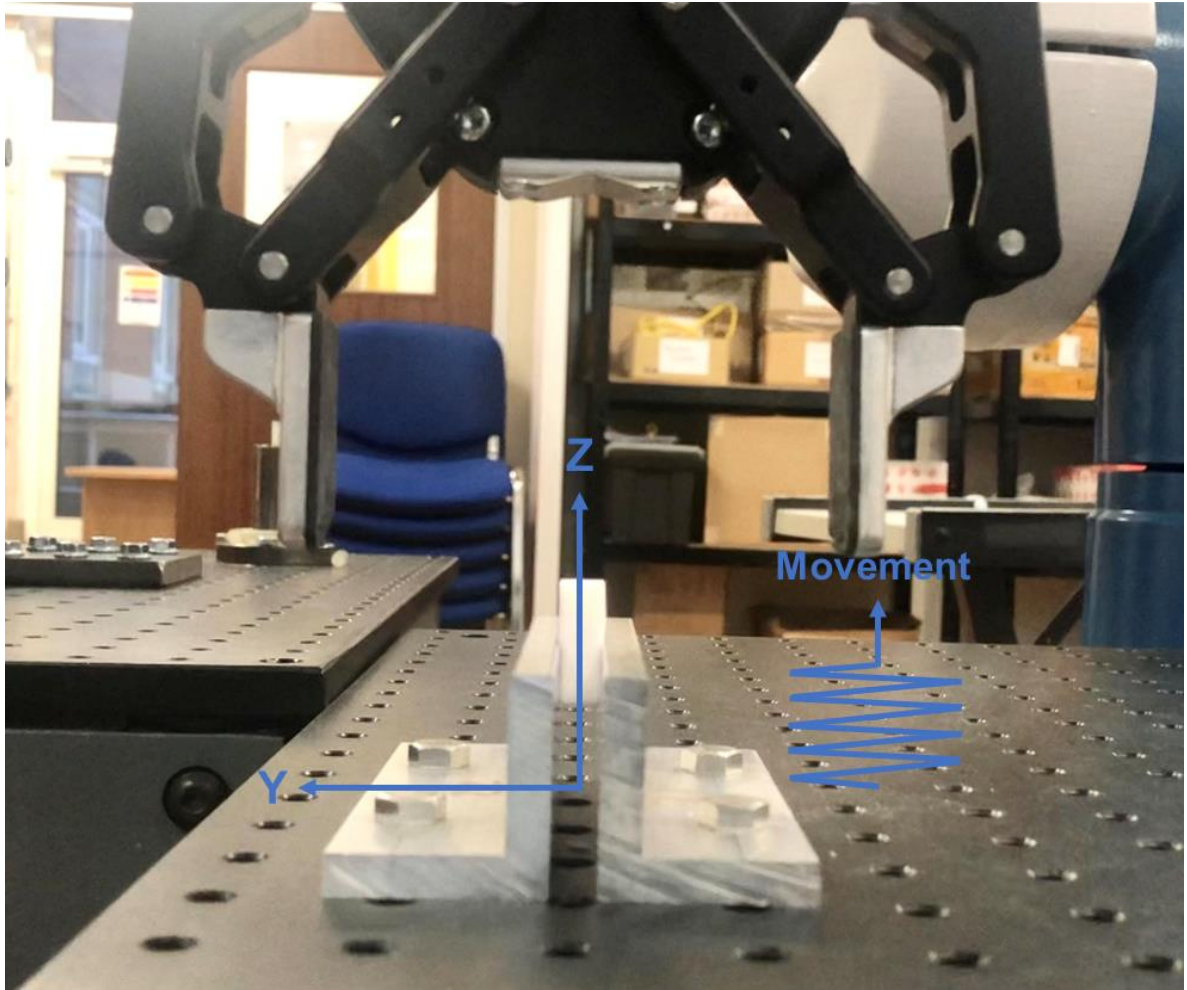


Figure 5.9: Coordinates and gripping direction for constrained wiggling.

After determining the gripping direction and the three-dimensional coordinate system, it is necessary to consider how to apply an upwards force and periodic lateral force to the PVC block at the same time through the robot and gripper.

Based on robot programming and sensor data transmission, the whole process of constrained wiggling without plugging is divided into many small displacements. Figure 5.10 describes the logic of robot programming for constrained wiggling. First, the appropriate method for adding lateral force to the PVC block should be determined. Since the robot cannot be programmed to directly apply a constant lateral force, a force limitation was set according

to the size of the PVC block used in the experiment. After grabbing the PVC block, the robot moves 0.1 mm and 0.05 mm in the +z and +y directions, respectively, simultaneously. Then, the force in the y direction of the sensor is read, F_y , and compared with the set force value of the limitation. If it is less than the set value, repeat the above moves and comparisons until the sensor's F_y readings are equal to or greater than the setting value. At this point, the robot's direction of movement is changed to 0.1 mm and 0.05 mm in the +z and -y directions, respectively, and the comparison relationship is changed to determine whether the force in the y direction is greater than the negative value of the set force limitation. If the above inequality is established, repeat the above moves and comparisons until F_y is less than or equal to the negative value. After that, the program leads the robot back to the first step of movement and forms a complete loop. In the parallel program, when the gripper grabs the PVC block and the robot starts recording force and torque data in real time, the robot's displacement in the z direction is also checked in real time and compared with the initial contact depth between the PVC block and the aluminum plate. Of course, to ensure that the program can be stopped after the PVC block is completely pulled out, the generally set displacement will be slightly greater than the depth. Once the displacement is greater than this set value, the robot will stop moving, the gripper will be released, and the program will be closed.

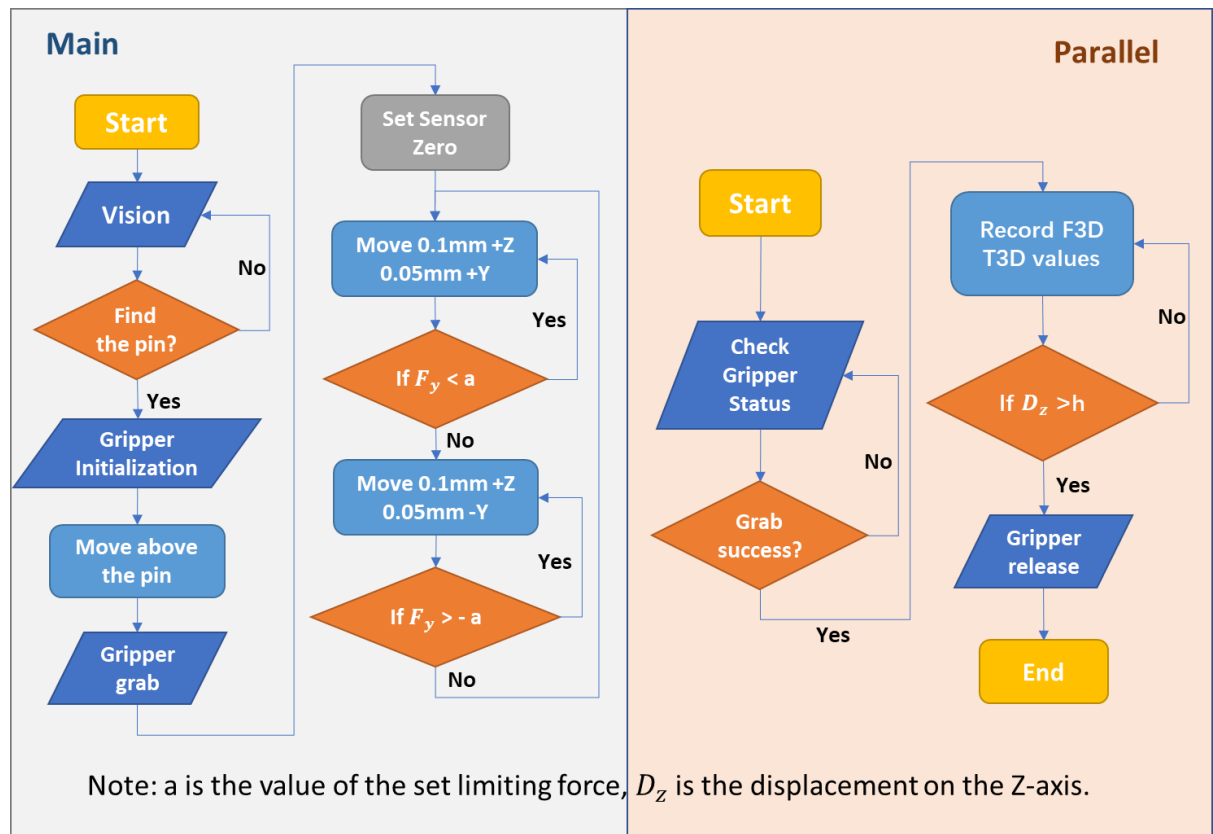


Figure 5.10: Flow charts of the robot programs for constrained wiggling unplugging.

5.3.2.1 7.5 mm-7 mm unplugging experiment

As mentioned above, different sizes of aluminium can be used to form gaps of different sizes (Section 4.4). Aluminium angles of 22 mm and 21 mm were first chosen to create a 7 mm wide ‘socket’ in the first series of experiments. Three 7.5-mm-long, 20-mm-long PVC blocks were selected—one for direct pulling out and the other two for 3 N and 4 N lateral forces. Similarly, before the experiment, the gap distances at different positions were measured with a Vernier calliper, and the average value was taken. The dimensions of the PVC blocks used were subsequently measured. The dimensions and measurements of the experiments are detailed in Table 5.1. The depth of the contact was determined to be 10 mm.

Table 5.1: Dimensions and measurements for the 7.5 mm-7 mm unplugging experiments.

	Standard size	Measurement	Note
Gap	7 mm	7.0025 mm	Average value
Block 1	7.5 mm	7.47 mm	Direct pulling
Block 2	7.5 mm	7.48 mm	3 N lateral
Block 3	7.5 mm	7.52 mm	4 N lateral

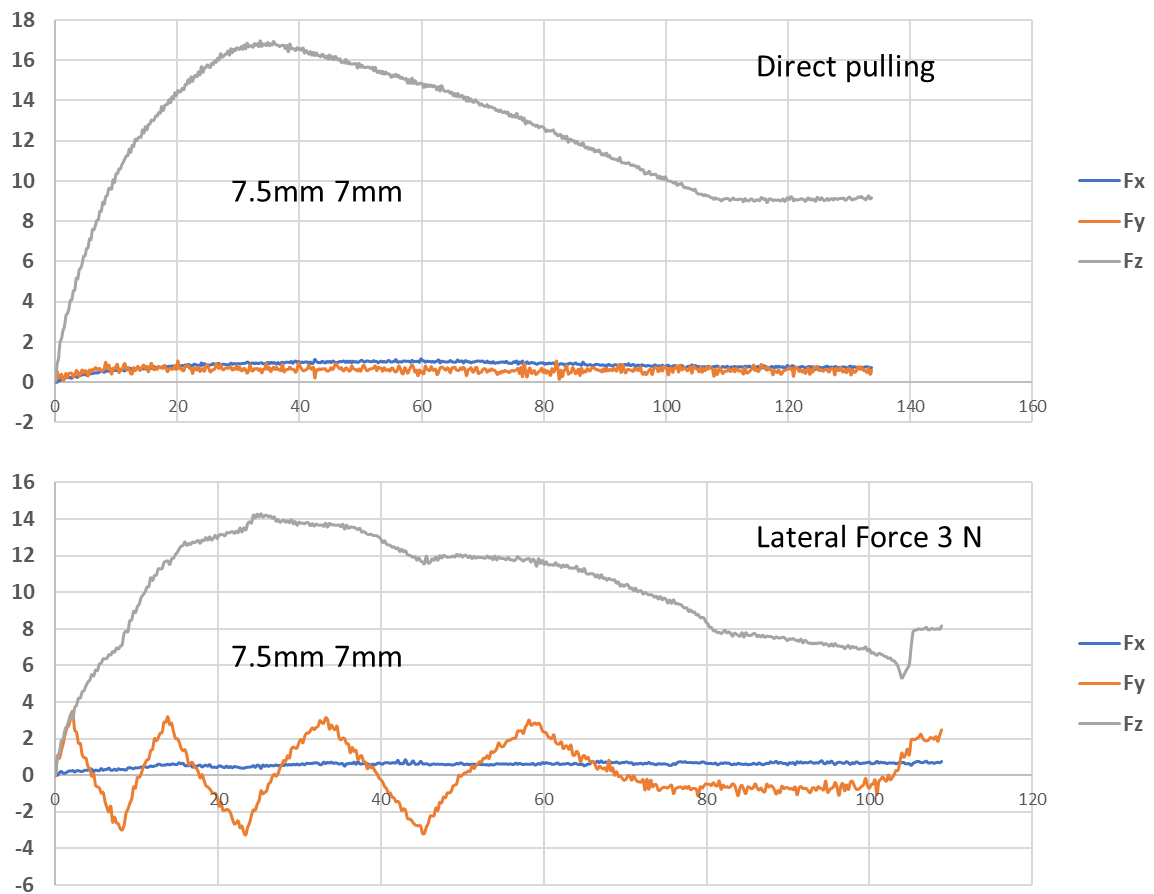


Figure 5.11: Variation curves of the force for the 7.5 mm-7 mm constrained unplugging experiments.

Figure 5.11 shows the force changes in the three axes during the two sets of experiments. The reason for not showing the force curve of the wiggling pulling process under the action of a horizontal force of 4 N is that in the experiment, the PVC block was unable to withstand lateral stress and broke, as shown in Figure 5.12. The experimental results are listed in Table 5.2.

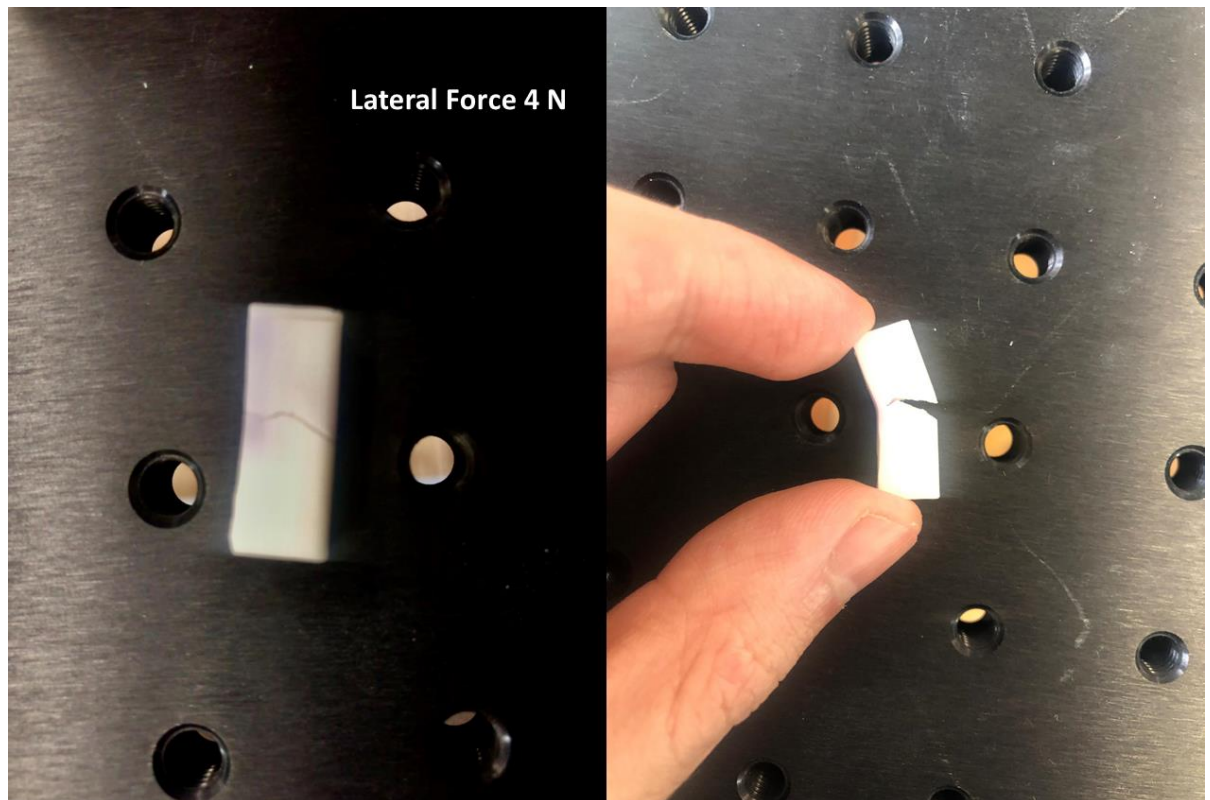


Figure 5.12: PVC block that broke after applying 4 N of lateral force.

Table 5.2: Results of the 7.5 mm-7 mm constrained unplugging experiments.

Set	Direct pulling	Lateral Force 3 N	Lateral Force 4 N
Max Fz	16.94991	14.32154	Failed
Residual Fz	9.05737	8.00875	Failed
Actual fz	7.89254	6.31279	Failed
Unit: N			

By comparing the three-dimensional force curves of direct pulling and applying lateral force, it can be found that when there was a horizontal force applied on the block, the value of Fz fluctuated with the change in the horizontal force, but in the overall numerical value compared with that of the direct pull, there was a relatively large reduction. During the final period of the extraction process, in the set of experiments in which the horizontal force was applied, the Fz value noticeably increased, which was caused by the bending of the PVC and the instantaneous restoration of exactly the complete pull-out, as shown in Figure 5.13.

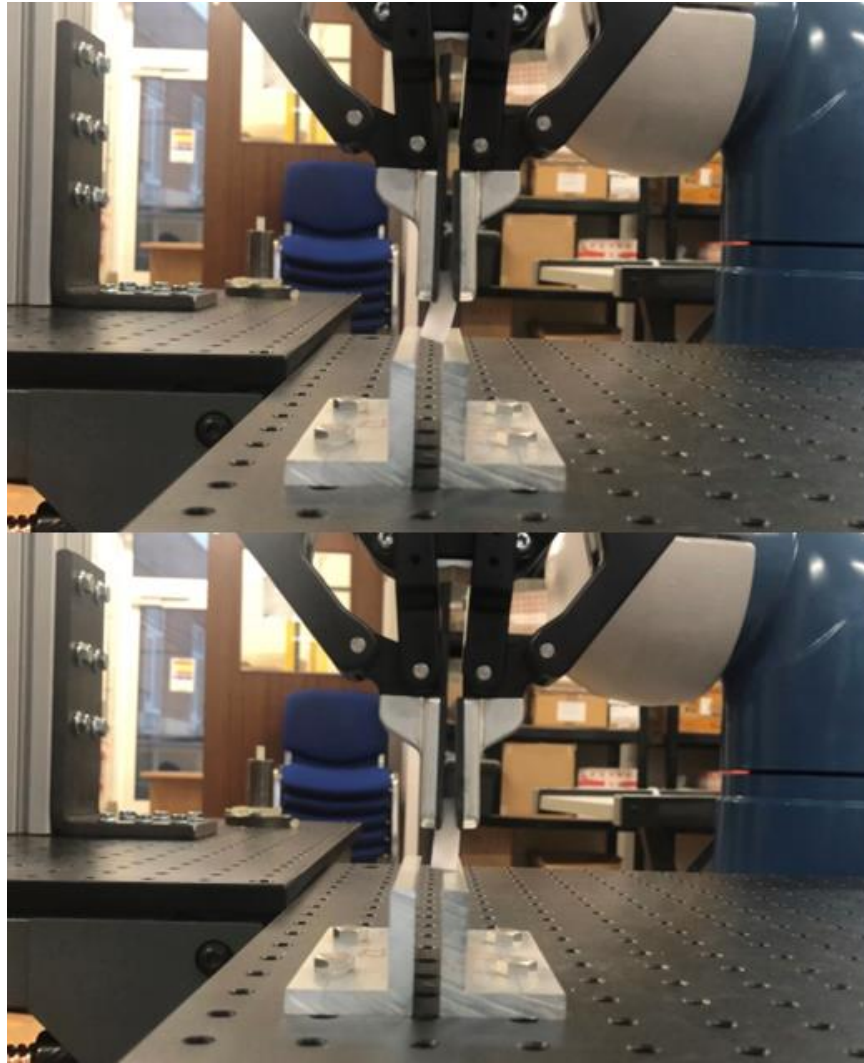


Figure 5.13: The bending and recovery of the PVC block at the moment of pulling out.

5.3.2.2 7.6 mm-7 mm unplugging experiment

To explore the influence of the size of the interference on the experimental results, several sets of experiments were performed using 7.6 mm PVC blocks while keeping the socket width at 7 mm. The dimensions and measurements of the 7.6 mm-7 mm unplugging experiments are shown in Table 5.3.

Table 5.3: Dimensions and measurements for the 7.6 mm-7 mm unplugging experiments.

	Standard size	Measurement	Note
Gap	7 mm	7.0025 mm	Average value
Block 1	7.6 mm	7.57 mm	Direct pulling
Block 2	7.6 mm	7.60 mm	3 N lateral
Block 3	7.6 mm	7.58 mm	4 N lateral

Figure 5.14 illustrates the force and torque changes in three sets of experiments, including direct pulling, applying 3 N of lateral force, and applying 4 N of lateral force. The results of these experiments are presented in Table 5.4.

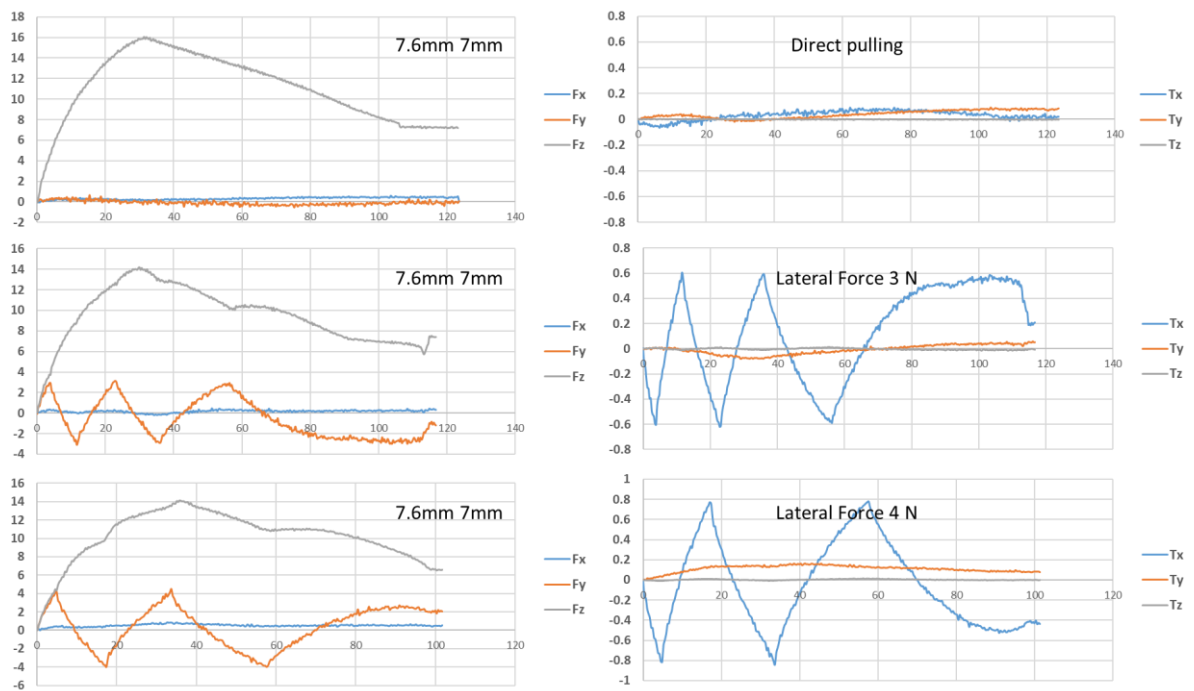


Figure 5.14: Variation curves of the force and torque for the 7.6 mm-7 mm constrained unplugging experiments.

Table 5.4: Results of the 7.6 mm-7 mm constrained unplugging experiments.

Set	Direct pulling	Lateral Force 3 N	Lateral Force 4 N
Max Fz	16.04655	14.19160	14.14596
Residual Fz	7.26728	7.42973	6.62380
Actual fz	8.77927	6.76187	7.52216
Unit: N			

5.3.2.3 9 mm-8 mm unplugging experiment

A slightly larger model with 9 mm PVC blocks and an 8 mm gap was used to study the impact of greater interference (1 mm) on extraction and wiggling. The contact depth of the model was still set to 10 mm. Similarly, although the standard values of the model were determined, the actual size of the model still needs to be accurately measured to reduce experimental and theoretical errors. The measurement results are shown in Table 5.5.

Table 5.5: Dimensions and measurements for the 9 mm-8 mm unplugging experiments.

	Standard size	Measurement	Note
Gap	8 mm	8.0050 mm	Average value
Block 1	9 mm	8.98 mm	Direct pulling
Block 2	9 mm	9.01 mm	4 N lateral
Block 3	9 mm	8.95 mm	5 N lateral

As the size of the model increased, the interference increased to 1 mm, and the applied horizontal force also increased. Therefore, 4 N and 5 N horizontal forces were used in this series of experiments. The following graphs indicate the force and torque changes for the three sets of experiments (Figure 5.15). The results obtained from these graphs are shown in Table 5.6.

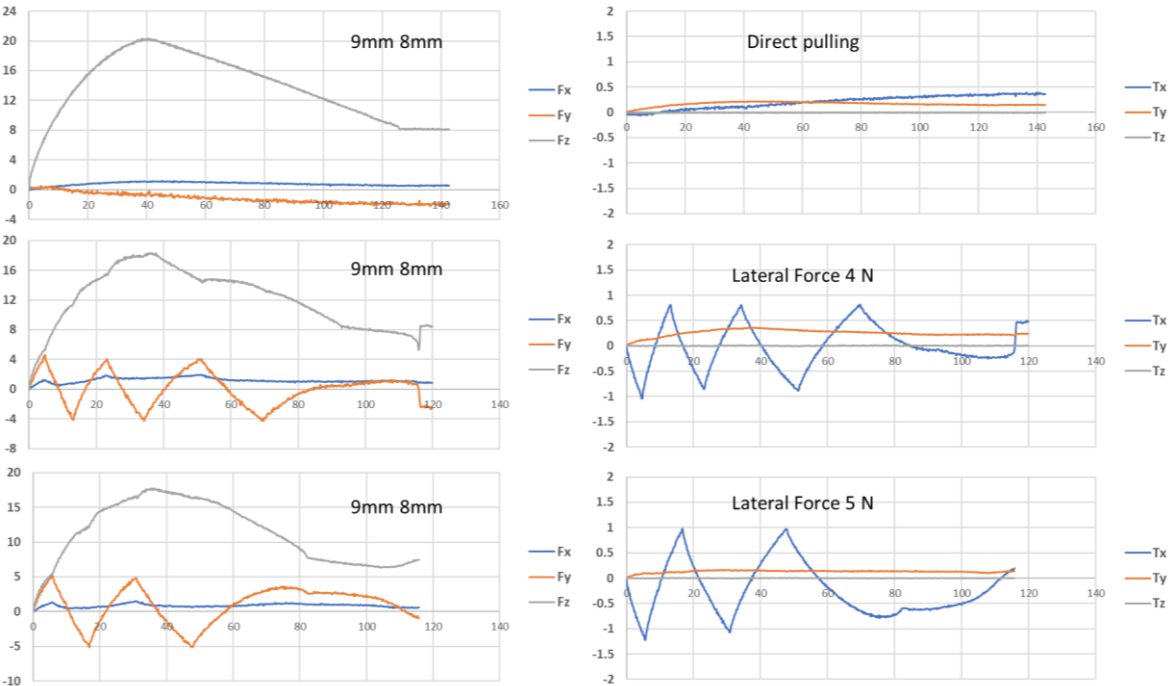


Figure 5.15: Variation curves of the force and torque for the 9 mm-8 mm constrained unplugging experiments.

Table 5.6: Results of the 9 mm-8 mm constrained unplugging experiments.

Set	Direct pulling	Lateral Force 4 N	Lateral Force 5 N
Max Fz	20.33185	18.34689	17.80859
Residual Fz	8.18284	8.51117	7.43680
Actual fz	12.14901	9.83572	10.37179
Unit: N			

5.3.2.4 11 mm-10 mm unplugging experiment

To understand the influence of the size of the model on the pull-out force and the wiggling method for the same interference, a group of experiments with 11-mm PVC blocks and a 10-mm gap were conducted. The arrangement of the experiment was the same as that of the previous group. The measurements of the model and PVC blocks are detailed in Table 5.7.

Table 5.7: Dimensions and measurements for the 11 mm-10 mm unplugging experiments.

	Standard size	Measurement	Note
Gap	10 mm	10.0075 mm	Average value
Block 1	11 mm	10.98 mm	Direct pulling
Block 2	11 mm	10.95 mm	4 N lateral
Block 3	11 mm	10.97 mm	5 N lateral

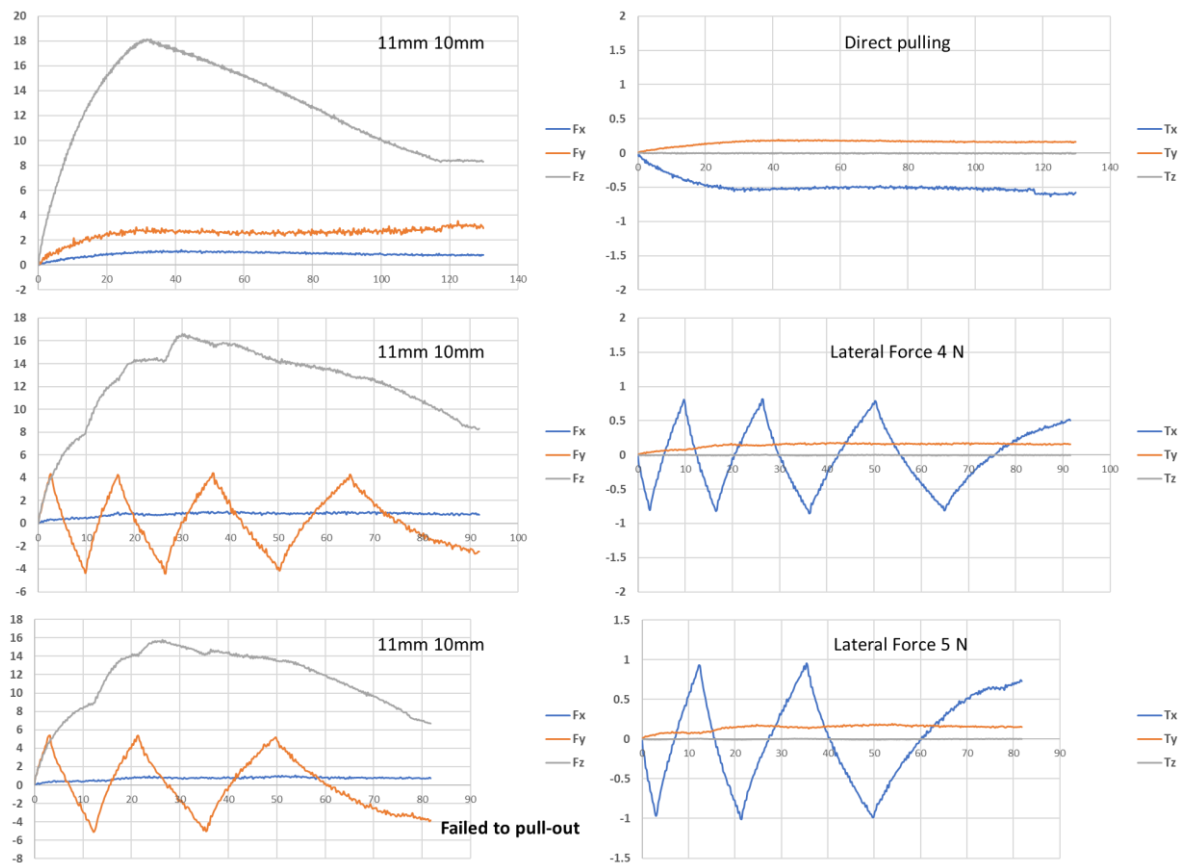


Figure 5.16: Variation curves of the force and torque for the 11 mm-10 mm constrained unplugging experiments.

Figure 5.16 shows the force and torque changes in three sets of 11 mm-10 mm constrained unplugging experiments. The first two sets of experiments were completed completely. However, the PVC block in the last set of experiments with 5 N of lateral force failed to pull out. The reason for this failure was that the bending of the block was uncontrollable, and the block was damaged by hitting the AI angle. Therefore, the program was stopped, and the residual force in the Z direction could not be calculated. The rest of the force graph results are displayed in Table 5.8.

Table 5.8: Results of the 11 mm-10 mm constrained unplugging experiments.

Set	Direct pulling	Lateral Force 4 N	Lateral Force 5 N
Max Fz	18.13648	16.61348	15.81363
Residual Fz	8.38124	8.38992	Failed
Actual fz	9.75524	8.22356	Failed
Unit: N			

5.3.2.5 18 mm-16.5 mm unplugging experiment

To test larger model sizes and different contact depths, this group of experiments used 18 mm standard PVC blocks and a 16.5 mm width socket, which resulted in 1.5 mm of interference and increased the contact depth to 15 mm. Because one set of experiments was directly pulled out, the conditions for the application of the other three sets were limited to 4 N, 5 N, and 6 N for the horizontal forces applied. Before the experiment started, precise measurements were still generated, and the results are presented in Table 5.9.

Table 5.9: Dimensions and measurements for the 18 mm-16.5 mm unplugging experiments.

	Standard size	Measurement	Note
Gap	16.5 mm	16.4975 mm	Average value
Block 1	18 mm	18.05 mm	Direct pulling
Block 2	18 mm	18.20 mm	4 N lateral
Block 3	18 mm	18.17 mm	5 N lateral

Figure 5.17 illustrates the force and torque changes of the four sets of experiments during the unplugging process. The experimental data can be found in Table 5.10.

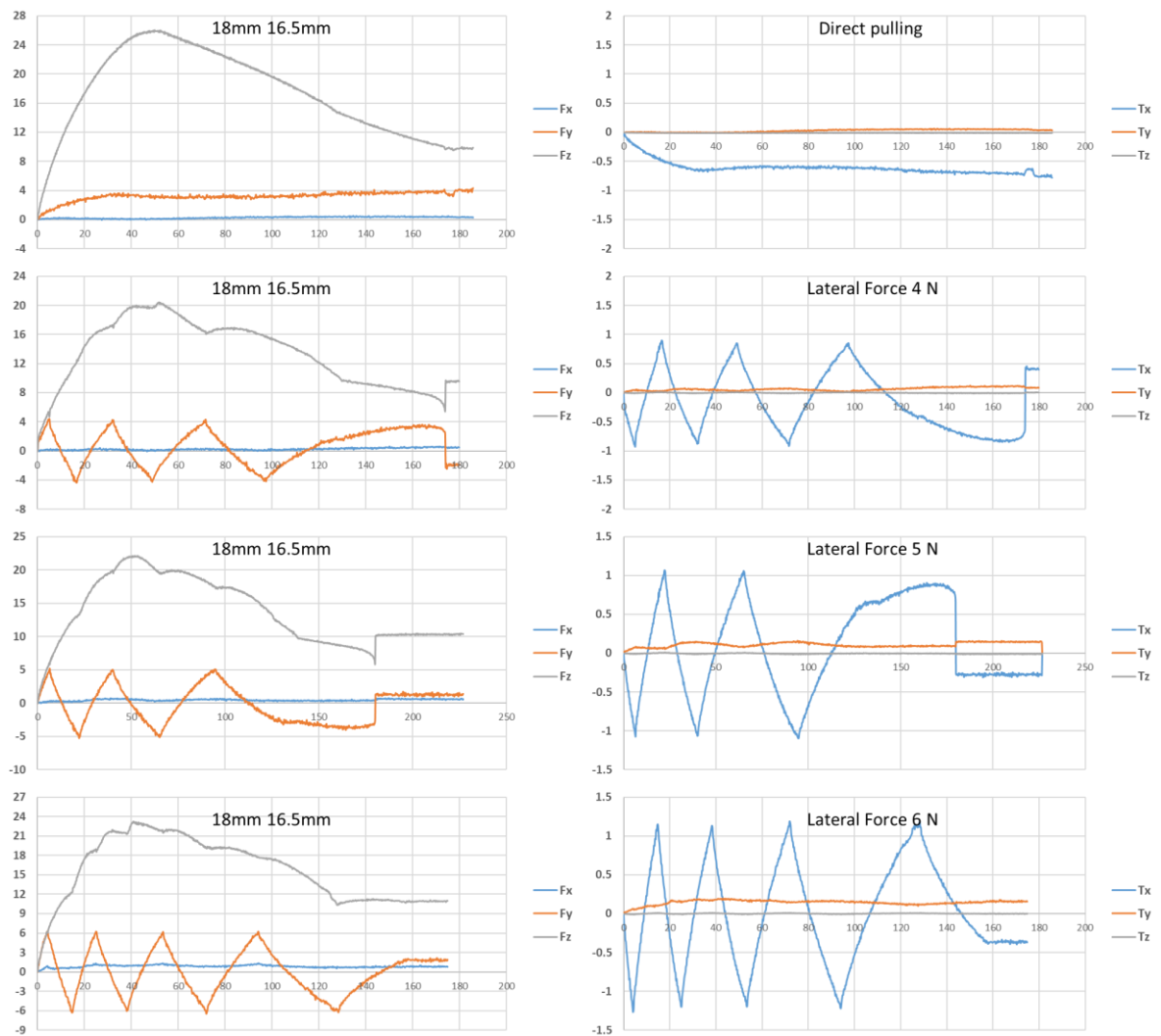


Figure 5.17: Variation curves of the force and torque for the 18 mm-16.5 mm constrained unplugging experiments.

Table 5.10: Results of the 18 mm-16.5 mm constrained unplugging experiments.

Set	Direct pulling	Lateral Force 4 N	Lateral Force 5 N	Lateral Force 6 N
Max Fz	25.98643	20.39862	22.18261	23.24588
Residual Fz	9.80582	9.53502	10.34615	10.92338
Actual fz	16.18061	10.86360	11.83646	12.32250
Unit: N				

5.3.2.6 18 mm-17 mm unplugging experiment

To analyse the impact of the width of the socket on the unplugging force and wiggling method friction reduction, the same standard-size (18 mm) PVC blocks and a 17-mm gap were chosen for the unplugging experiments. The initial contact depth remained unchanged at 15 mm. Two sets of experiments were arranged, one for direct pulling and the other for applying 5 N of lateral force.

The measurement results for this group of experiments are provided in Table 5.11.

Table 5.11: Dimensions and measurements for the 18 mm-17 mm unplugging experiments.

	Standard size	Measurement	Note
Gap	17 mm	17.0025 mm	Average value
Block 1	18 mm	18.05 mm	Direct pulling
Block 2	18 mm	18.01 mm	5 N lateral

Figure 5.18 depicts the force and torque variations during the unplugging procedure in two sets of experiments. Table 5.12 displays the experimental results.

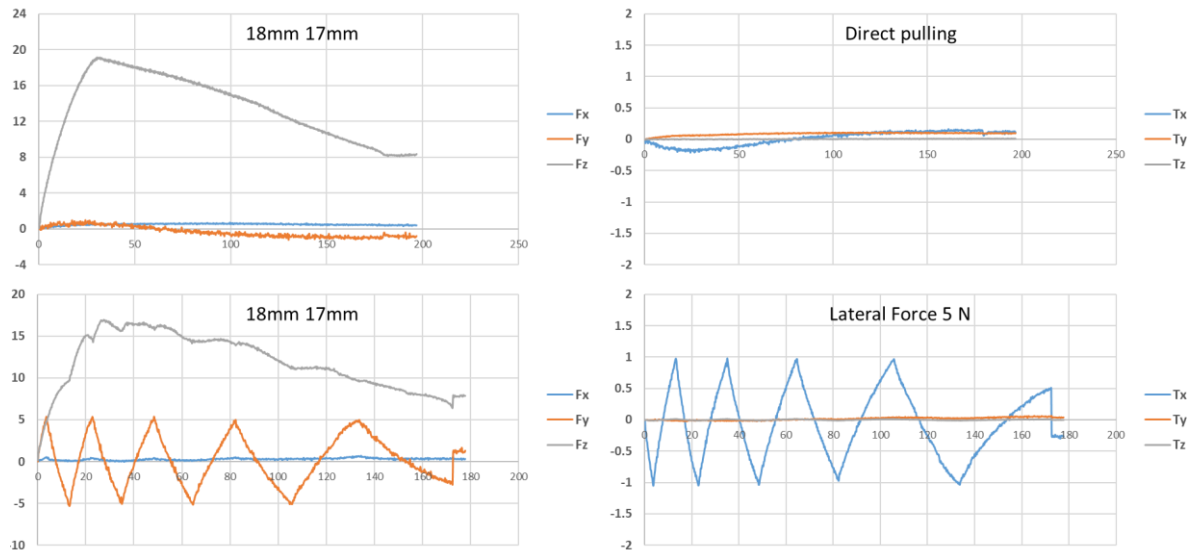


Figure 5.18: Variation curves of the force and torque for the 18 mm-17 mm constrained unplugging experiments.

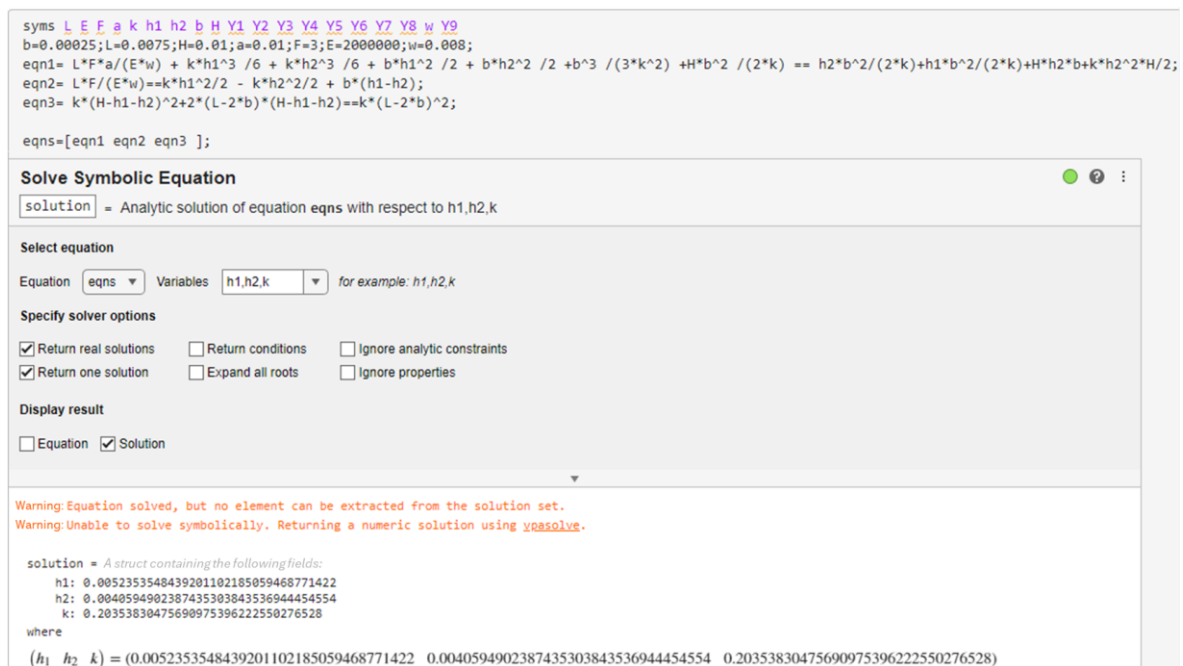
Table 5.12: Results of the 18 mm-17 mm constrained unplugging experiments.

Set	Direct pulling	Lateral Force 5 N
Max Fz	19.12360	16.98027
Residual Fz	8.20672	7.83551
Actual fz	10.91688	9.14476
Unit: N		

5.4 Summary

Based on the study of the abovementioned theoretical model, the resulting system of equations contains three formulas, Equations (5.7), (5.9) and (5.11), as well as three variables, k , h_1 and h_2 . Using MATLAB [119] to bring the dimensions of the experimental model into the equation system, the values of three variables can be obtained. Then, the maximum static friction of the theory and the maximum dynamic friction after the application of lateral force (LF) could be calculated by using Equations (4.5) and (4.7).

Figure 5.19 shows an example of using MATLAB to calculate three variables. The model size used in the example is a 7.5 mm-7 mm unplugging experiment, and the lateral force applied is 3 N.



```
syms L E F a k h1 h2 b H Y1 Y2 Y3 Y4 Y5 Y6 Y7 Y8 w Y9
b=0.00025;L=0.0075;H=0.01;a=0.01;F=3;E=2000000;w=0.008;
eqn1= L*F*a/(E*w) + k*h1^3 /6 + k*h2^3 /6 + b*h1^2 /2 + b*h2^2 /2 +b^3 /(3*k^2) +H*b^2 /(2*k) == h2*b^2/(2*k)+h1*b^2/(2*k)+H*h2*b+k*h2^2*H/2;
eqn2= L*F/(E*w)==k*h1^2/2 - k*h2^2/2 + b*(h1-h2);
eqn3= k*(H-h1-h2)^2+2*(L-2*b)*(H-h1-h2)==k*(L-2*b)^2;

eqns=[eqn1 eqn2 eqn3];
```

Solve Symbolic Equation

Equation eqns **Variables** h1,h2,k for example: h1,h2,k

Select equation

Specify solver options

☒ Return real solutions ☐ Return conditions ☐ Ignore analytic constraints

☒ Return one solution ☐ Expand all roots ☐ Ignore properties

Display result

☐ Equation ☒ Solution

Warning: Equation solved, but no element can be extracted from the solution set.
Warning: Unable to solve symbolically. Returning a numeric solution using `vpasolve`.

solution = A struct containing the following fields:

```
h1: 0.0052353548439201102185059468771422
h2: 0.0040594902387435303843536944454554
k: 0.20353830475690975396222550276528
```

where

$(h_1 \ h_2 \ k) = (0.0052353548439201102185059468771422 \ 0.0040594902387435303843536944454554 \ 0.20353830475690975396222550276528)$

Figure 5.19: Example of using MATLAB to calculate the variables.

Table 5.13 and Figure 5.20 summary the theoretical and experimental results for all the model sizes. The average error for all experiments is 9.24%. The theoretical value is the theoretical maximum axial friction obtained by substituting the default value of the model into the MATLAB code. The actual value is obtained by bringing exact measurements of model dimensions into the programme. The experimental value is given by reducing the residual force of the z-axis by the maximum force on the z-axis in the experiment. Error1 is the error between the theoretical value and the experimental value, while Error2 compares the actual value with the experimental value.

Table 5.13: Summary of the theoretical, actual, and experimental results for all the sets of experiments.

7.5 mm-7 mm	Theoretical	Actual	Experimental	Error1	Error2
Direct	8.53333	8.01071	7.89254	7.51%	1.48%
LF 3 N	7.31078	7.23643	6.31279	13.65%	12.76%
7.6 mm-7 mm	Theoretical	Actual	Experimental	Error1	Error2
Direct	10.10526	9.59577	8.77927	13.12%	8.51%
LF 3 N	7.66577	7.65554	6.76187	11.79%	11.67%
LF 4 N	9.49477	9.42450	7.52216	20.78%	20.19%
9 mm-8 mm	Theoretical	Actual	Experimental	Error1	Error2
Direct	14.22222	13.89755	12.14901	14.58%	12.58%
LF 4 N	10.48756	10.50275	9.83572	6.22%	6.35%

LF 5 N	12.28724	12.11844	10.37179	15.59%	14.41%
11 mm-10 mm	Theoretical	Actual	Experimental	Error1	Error2
Direct	11.63636	11.33698	9.75524	16.17%	13.95%
LF 4 N	10.00912	9.85067	8.22356	17.84%	16.52%
18 mm-16.5 mm	Theoretical	Actual	Experimental	Error1	Error2
Direct	16.00000	16.51413	16.18061	1.13%	2.02%
LF 4 N	9.84271	10.69257	10.86360	10.37%	1.60%
LF 5 N	10.94599	11.49646	11.83646	8.14%	2.96%
LF 6 N	12.32367	12.41121	12.32250	0.01%	0.71%
18 mm-17 mm	Theoretical	Actual	Experimental	Error1	Error2
Direct	10.66667	11.14238	10.91688	2.35%	2.02%
LF 5 N	9.52855	9.54632	9.14476	4.03%	4.55%

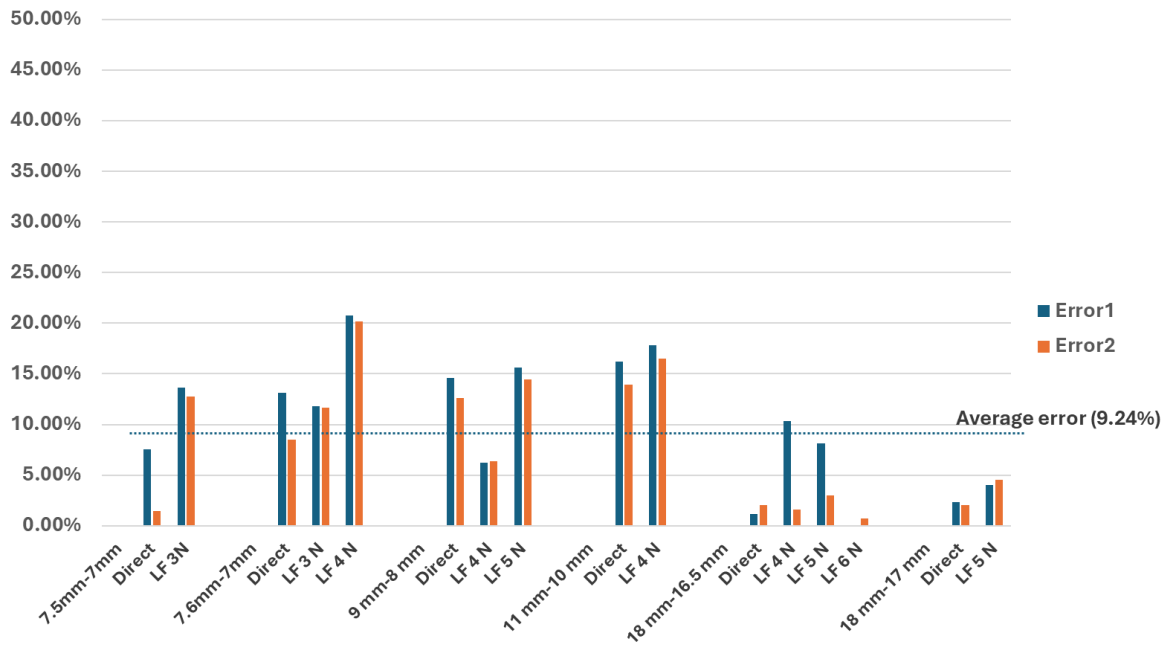


Figure 5.20: Error distribution and average error of these sets of experiments.

These data indicate that the error between the actual value and the experimental value is always smaller than that between the theoretical and experimental values and prove that the precise measurement of the PVC blocks and the difference between two aluminium angles before the experiment are necessary and crucial steps in reducing the error.

In addition, when the standard value of the PVC block used is 18 mm, the error between the experimental value, the theoretical value, and the actual value is always less than 5%. In contrast, when the size of the PVC block used is less than 18 mm, the error is larger than that of the other blocks, and the experimental values are always smaller than the theoretical and actual values. Multiple inspections and comparisons of the PVC blocks after the experiment revealed that the small size of the PVC blocks made them susceptible to significant deformation during the unplugging process and produced plastic deformation because the stress exceeded the yield strength, reducing the actual contact interference.

Comparing the data of the 7.5 mm-7 mm group and the 7.6 mm-7 mm group, it can be seen that for a constant width of socket, the greater the interference is, the greater the required pulling force. When the same lateral force is applied, the greater the interference is, the greater the reduction in the maximum axial friction.

By comparing the results of the 8 mm-9 mm experimental group and the 11 mm-10 mm experimental group, it can be concluded that for the same interference, the larger the size of the model is, the smaller the strain and the smaller the required pullout force. For the same applied lateral force, the larger the model size is, the smaller the axial friction reduction.

The experimental results for 18 mm-16.5 mm and 18 mm-17 mm demonstrate that for PVC blocks of the same dimension, the larger the gap is, the smaller the interference, and the smaller the friction force to be overcome. The more widely the socket is applied to the same horizontal force, the less the reduction in axial friction.

According to the results of all the experimental groups, it can also be concluded that for the same model size, the greater the lateral force applied is, the smaller the reduction in axial friction.

6 Conclusion

6.1 Conclusions

This thesis addressed three different unplugging strategies for two different shapes of plug-socket connections. The three strategies are a) twisting and pulling a cylindrical plug out of a cylindrical socket; b) wiggling and pulling a cuboid plug out of a cuboid socket while the plug is unconstrained; and c) wiggling and pulling a cuboid plug out of a cuboid socket while the plug is constrained. The purpose of this thesis is to investigate unplugging as a robotic disassembly operation and demonstrate disassembly strategies for unplugging so that a robot can complete it more easily.

In the first section of this thesis, the unplugging problem in robotic disassembly was described, and the definition of a ‘plug-socket’ connection was implemented. A theoretical model of a cylindrical interference-fit plug socket was established to analyse the governing mechanics during the unplugging process. FEM was adopted to validate the theoretical model. A series of experiments involving plugs of different sizes were conducted. The average errors compared with the results of theory, simulation and experimentation are less than 5%, which is within the acceptable range. Theoretical, simulation and experimental results all prove that the disassembly strategy of twisting and pulling can change the direction of the total friction force experienced by the plug during the process of being pulled out, thereby reducing the maximum axial friction that needs to be overcome for pulling out.

In the second part of this thesis, the cuboid plug-socket unplugging problem was discussed. An interference-fit plug-socket model was created to analyse the stress distribution of the plug during extraction. Further mechanical analysis of unconstrained wiggling was performed. A 3D cuboid interference-fit plug-socket model was devised in ABAQUS to

predict the stress distribution of the plug due to the deformation. A set of control experiments was conducted in which the plug was directly pulled out. The reasons for the residual force generated in the direct pulling experiment were analysed through several sets of experiments with control variables. Unconstrained wiggling and unplugging experiments were conducted using the same size plugs and varying lateral forces. The results indicate that the disassembly strategy of unconstrained wiggling can reduce the maximum axial friction during the unplugging process, and the greater the applied lateral force is, the greater the reduction.

In the third section of this thesis, another disassembly strategy for cuboid plug-sockets, constrained wiggling, which is suitable when all sides of the plug are constrained, was developed. Based on the theoretical model of the cuboid plug socket built in the previous section, further mechanical analysis of the change in the stress distribution of the plug, to which the lateral force was applied, was performed. A system of equations with three variables was obtained, and MATLAB was used to solve these equations to obtain the theoretical results. ABAQUS was used as the FEA software to verify whether the influence of the applied lateral force on the stress distribution on both sides of the plug matches the stress distribution described by the theoretical model. Six sets of experiments were conducted, including the use of plugs of different sizes and sockets, different interferences, and different amounts of applied lateral force. The results demonstrate that constrained wiggling can reduce the maximum axial friction that needs to be overcome during the extraction process, thereby facilitating robotic disassembly of the cuboid plug-socket. However, as the lateral force increases, the average contact pressure also increases, which in turn increases the axial friction. The main purpose of wiggling is to alter the plug's state of motion while it is being pulled out.

6.2 Summary of Achievements

The research presented in this thesis made the following scientific contributions:

- The first proposed definition of unplugging in robotic disassembly. Improved understanding of robotised unplugging.
- Development of a theoretical model of an interference-fit cylindrical plug socket. A novel robotised disassembly strategy was proposed involving twisting and pulling to change the direction of the friction, thereby reducing the axial friction. The friction reduction of the proposed strategy was evaluated via theory, simulation and experimentation.
- Development of a theoretical model of a cuboid plug socket for contact pressure change during the extraction process. A new disassembly approach was studied, involving unconstrained wiggling of the plug, which is not constrained to reduce axial friction.
- Proposal of a disassembly strategy for constrained cuboid extraction. A detailed mechanical analysis was conducted of the change in the stress distribution of the plug, to which the lateral force was applied.

6.3 Future Work

This thesis investigated disassembly strategies for unplugging different shapes of plugs out of sockets. Possible future work related to the different chapters is described below.

Chapter 3 proposes the twist-and-pull method of unplugging a cylindrical peg press-fitted into a cylindrical hole. The theoretical model created in this chapter is a simplified linear-elastic model. In the future, a theoretical model that includes both elastic and plastic deformation could be developed to adapt to situations where local stresses exceed plastic thresholds. Considering that the material of the plug used in the experiment, ethylene vinyl acetate (EVA), is much softer than that used in the socket or steel, repeated tests could not be performed on the same plug to determine the effect of the twist-and-pull operation on surface wear. Different materials should be investigated to verify the applicability of this twisting method. Wear analysis of unplugging is necessary to determine the extent of the damage to the plug when it is twisted and pulled out. In addition, the twisting-pulling method is applicable only to single-cylinder unplugging. The development of a disassembly method that can be adapted for multiple cylinders should be considered in future work.

Chapter 4 addresses the unconstrained wiggling method of unplugging an unconstrained cuboid plug out of a socket. The theoretical model of the stress distribution built in this chapter is a simplified elastic model. The stress at the edge of the contact between the plug and the socket can be further analysed, and plastic deformation can be considered to develop the theoretical model. The current model is based on a hard socket with a soft plug. Other material combinations that might be researched include a hard plug with a soft socket, a socket and a plug made of hard materials, and a socket and a plug made of soft materials.

Chapter 5 proposes the constrained wiggling method of unplugging a constrained cuboid plug out of a socket. The analysis of the change in the stress distribution of the plug in the theoretical model is static. A dynamic analysis of the wiggling process is worth pursuing to make the theoretical results more relevant to real-life applications.

Appendix A. Experimental data for Chapter 3

This appendix presents the data for all the experiments in Chapter 3, including pins of different sizes that were directly pulled out or twisted out of the socket.

A.1 Experimental data on directly pulling pins out of the socket

Table A.1: Experimental data for the force along the Z-axis changing throughout direct pulling.

Time	7.02	7.04	7.06	7.08(Failed)	7.08
0	0.145702	0.006273	-0.019533	-0.042509	0.158024
0.5	0.333302	0.193670	-0.492930	0.003474	-0.252667
1	0.203733	-0.587238	0.274731	-0.129135	0.397339
1.5	-0.803862	-1.122705	1.051586	0.220796	-0.704498
2	0.375525	0.256867	1.241302	1.329813	1.017014
2.5	0.196440	0.301653	0.164427	0.133474	-0.306114
3	0.148686	0.400023	0.207537	0.181461	10.399582
3.5	7.913421	15.885964	23.992453	29.918902	32.150782
4	5.917057	13.759536	21.466788		26.743485
4.5	4.795776	11.120662	18.508111		22.958015
5	4.292802	9.507178	16.726525		20.945990
5.5	3.766329	8.056572	14.402168		19.095525
6	3.522024	6.849318	13.132061		16.865035
6.5	3.067290	5.641719	11.806880		15.660480
7	2.995904	5.096017	10.796530		13.977245
7.5	2.865654	4.912887	10.497180		13.096245
8	2.679098	4.971675	10.330825		13.244245
8.5	2.480233	4.800572	8.970593		12.866755

9	2.314620	5.299552	9.253138	13.642000
9.5	2.401178	5.307297	9.285069	12.436500
10	2.475461	5.529184	9.231756	12.364010
10.5	2.118006	5.302644	9.190449	12.087753
11	2.035201	5.598863	9.343228	12.048755
11.5	1.828768	5.431156	9.457802	11.300239
12	1.735294	5.429225	9.040619	12.364748
12.5	1.755516	5.515552	9.037061	11.304739
13	1.248871	5.302948	8.867567	11.853996
13.5	1.461573	5.262603	8.283978	11.716488
14	1.617315	5.410717	8.266233	11.084500
14.5	1.293817	5.580747	7.939796	11.194262
15	1.650933	5.337140	7.282061	10.479751
15.5	1.422068	5.251125	5.956880	10.044757
16	1.376759	5.221394	4.946530	8.799262
16.5	1.140663	4.772363	4.647180	8.398510
17	1.104655	5.031379	4.480825	7.758744
17.5	1.097553	4.653469	5.070593	7.217742
18	0.997110	4.358148	5.353138	7.429518
18.5	0.864234	3.952635	5.385069	7.553257
19	0.728529	4.070300	5.331756	6.367750
19.5	0.177391	3.866321	5.290449	6.403990
20	0.400173	3.574474	5.443228	5.952745
20.5	0.174559	3.447979	5.557802	5.225375
21	0.256404	2.918465	5.140619	5.508750
21.5	0.274923	2.615808	5.137061	5.123883
22	0.295824	2.564025	4.967567	4.906997
22.5	0.276924	2.483030	4.383978	5.354121
23	0.550745	1.827825	4.366233	4.835873
23.5	0.347570	2.067660	4.039796	5.208879
24	0.316022	1.877763	3.825937	4.861369
24.5	0.429974	1.336039	3.437918	4.535496
25	-0.012586	1.315933	3.357514	5.187630
25.5	0.119277	1.399063	3.249113	4.343748

26	0.001586	1.422018	3.012013	4.412621
26.5	0.282812	0.712761	2.550918	4.740133
27	0.266758	1.462280	2.657856	4.313751
27.5	0.253197	1.344352	2.516440	3.672883
28	-0.064033	1.112582	2.125984	4.707753
28.5	0.116527	1.252728	1.795376	3.740131
29	-0.085604	1.003225	1.629066	3.660008
29.5	-0.019617	1.054345	1.389519	3.220873
30	0.612254	1.049525	1.474926	2.889248
30.5	0.231410	1.293718	1.200536	2.501005
31	0.125859	1.054863	0.922814	2.220000
31.5	0.389036	1.031666	1.197390	2.188498
32	0.402827	1.359149	1.401462	1.483995
32.5	0.145905	1.120942	0.774085	1.183126
33	0.061908	0.976223	0.746492	1.537371
33.5	0.293568	1.280556	1.030288	1.158121
34	0.432312	0.581577	1.263520	0.812745
34.5	0.112088	-0.088388	1.158106	0.136009
35	0.379581	0.144524	0.444051	0.553256
35.5	0.186871	0.401466	0.241236	0.196999
36	0.219603	0.166025	1.375427	0.514006
36.5	0.343271	0.348835	0.834045	0.005131
37	0.769829	0.694029	0.852388	0.194123
37.5	0.115089	0.600404	0.733861	0.160879
38	-0.215600	0.578247	0.563010	-0.124881
38.5		-0.502288	0.720602	0.259123
39		0.045397	0.516440	-0.017369
39.5			0.368359	0.438503
40			-0.367857	-0.011125
40.5			0.118464	0.142371
41			0.145575	-0.418628
41.5			0.241407	0.293753
42			0.133360	-0.072995

A.2 Experimental data on twisting pulling pins out of the socket

Table A.2: Experimental data for the force change along the Z-axis for different pin sizes in the case of twisting-pulling.

Time	7.02	7.04	7.06	7.08
0	-0.011255	-0.042509	0.081867	-0.270865
0.5	0.054568	-0.129135	-0.041851	0.339801
1	0.774906	0.729813	0.262627	1.719544
1.5	0.300731	0.181461	1.388035	0.018660
2	0.053898	-0.087795	0.270395	0.618044
2.5	0.094468	0.106894	0.013676	0.102043
3	1.893982	4.475615	8.459457	10.061186
3.5	5.054250	11.147091	15.922423	22.344792
4	4.108519	8.861859	14.606085	19.152024
4.5	3.440984	8.747916	13.547267	18.060910
5	3.301249	8.031875	13.039446	16.737496
5.5	3.350668	7.943818	12.176353	15.918590
6	3.483059	7.549439	11.557658	15.303574
6.5	3.652138	7.717577	11.446242	14.039184
7	3.554861	8.031274	10.692027	14.683464
7.5	3.692405	8.081693	10.366416	13.981076
8	3.885512	8.317505	10.057731	13.664498
8.5	3.988906	8.175461	9.849935	13.051116
9	3.926625	8.339937	9.630252	12.737495
9.5	3.998742	8.478559	9.365043	12.199329
10	4.059522	8.350444	9.194291	11.393921
10.5	4.003349	8.336771	8.784143	11.767479
11	3.997353	8.374548	8.958187	10.961960
11.5	4.013917	8.521373	9.385366	10.961479
12	3.941494	8.525531	9.066808	10.941208
12.5	4.080117	8.401674	9.377814	10.869047
13	4.025811	8.144156	8.950634	10.519487
13.5	3.912899	8.438785	8.070319	10.335615

14	4.042083	8.512676	8.106262	10.169088
14.5	4.074481	7.941841	8.311546	9.955358
15	3.824192	7.568361	8.080654	9.670824
15.5	3.660435	8.371137	8.505177	9.820104
16	4.012422	7.834833	8.536241	9.705099
16.5	3.777273	7.502760	8.276926	9.881273
17	3.631671	7.552253	8.505883	9.799146
17.5	3.653372	7.279697	8.492267	8.490318
18	3.533867	7.072102	8.643394	8.668518
18.5	3.442845	6.852926	8.560551	8.309452
19	3.346744	6.958284	8.810845	8.322567
19.5	3.392940	7.125201	8.034461	8.934010
20	3.466126	7.143353	7.998807	9.037728
20.5	3.474086	6.805020	7.590017	8.563023
21	3.325740	6.488075	7.451972	8.882881
21.5	3.272271	6.763339	7.227841	8.454075
22	3.392964	6.422931	7.459826	8.587318
22.5	3.243708	6.364921	7.149359	8.500927
23	3.218273	6.375993	6.437405	8.275433
23.5	3.223128	6.655481	6.574984	8.709351
24	3.174672	6.152504	6.849415	8.584641
24.5	3.125136	5.734566	6.277286	8.817459
25	2.941887	5.726725	6.283407	8.651276
25.5	2.938449	5.529299	5.798540	8.585381
26	2.851885	5.669871	5.855397	8.726906
26.5	2.913520	5.240988	5.623659	8.851288
27	2.639972	5.576415	5.429427	8.729652
27.5	2.787044	5.209850	5.607317	8.661510
28	2.711819	4.508303	5.222584	8.316929
28.5	2.489717	4.854478	5.170103	8.267273
29	2.556002	4.672541	5.138345	8.408470
29.5	2.561730	4.316828	4.593311	8.363182
30	2.320263	4.184127	4.605293	8.127270
30.5	2.347579	4.012613	4.501175	8.031864

31	2.186876	4.088709	4.955669	8.036530
31.5	2.220242	4.651511	4.334514	7.739857
32	2.381508	4.059054	3.982533	7.871525
32.5	1.950739	3.906657	4.515700	7.972946
33	1.883919	3.679529	4.170103	7.938190
33.5	1.784332	3.959465	4.108416	7.508411
34	1.907073	3.295260	3.778372	7.754162
34.5	1.615845	3.206093	3.402814	7.067463
35	1.576748	3.119421	3.810465	7.380543
35.5	1.538746	3.301463	3.565974	7.569687
36	1.618565	2.675523	3.630423	7.106667
36.5	1.344114	2.530989	3.443759	7.273006
37	1.280741	2.372561	3.160664	7.337513
37.5	1.211277	2.074818	3.470166	7.233231
38	1.080728	1.884689	3.294047	7.332054
38.5	0.997363	1.906599	3.472157	7.240120
39	1.006970	1.625150	2.947997	7.232063
39.5	0.883566	1.778963	2.753714	6.914749
40	0.951007	2.146107	3.020321	6.569206
40.5	1.026485	1.602383	2.680853	6.923611
41	0.959083	1.949746	3.224160	5.879524
41.5	1.111389	1.512082	3.437484	5.397211
42	0.919490	1.414182	2.656829	5.010394
42.5	0.876564	1.776724	2.839893	5.400158
43	0.693525	1.136246	2.942470	5.148472
43.5	0.669200	1.360623	2.509608	5.035590
44	0.853081	1.203404	1.663953	5.139263
44.5	0.442146	1.079695	2.251775	4.889606
45	0.387905	1.104889	2.437960	4.690422
45.5	0.373301	1.025587	2.145839	4.754185
46	0.306283	1.135448	1.311770	4.802055
46.5	0.147943	1.087264	2.719221	4.800735
47	0.214639	1.327057	2.497287	4.568039
47.5	0.334143	0.544054	2.430465	4.730576

48	0.398738	0.308632	2.571532	4.578411
48.5	0.303350	0.209136	2.276063	4.628368
49	0.204251	1.427112	2.323918	4.502216
49.5	0.285614	-0.208712	1.461029	4.758049
50	0.248227	0.423540	1.540261	4.462914
50.5	0.197017	0.620910	2.074957	4.404369
51	0.117184	-0.043611	2.327266	4.418518
51.5	0.132333	0.668856	2.173591	4.350513
52	0.179414	0.854246	2.157584	4.457233
52.5	0.211661	0.562565	1.930292	4.542515
53	0.046659	0.523936	2.004230	4.516632
53.5	0.107643	0.686214	2.179085	3.999233
54	0.160376	0.427583	1.252181	4.107727
54.5	0.013661	0.614011	1.389006	4.112080
55	0.167793	0.354093	1.539671	3.899696
55.5	-0.248790	0.734474	1.570116	4.182129
56	-0.272185	0.360986	1.084207	4.052807
56.5	0.021042	0.440156	0.847133	3.900917
57	0.053250	0.532161	1.307744	4.212040
57.5	0.122164	-0.030450	0.898325	3.987320
58	-0.241462	0.307276	0.847053	4.060009
58.5	0.020481	0.075573	1.018622	3.600700
59	-0.115040	0.536361	0.653754	3.720318
59.5	0.142800	0.322168	0.918114	3.563406
60	-0.255294	0.094002	0.220152	3.368770
60.5	-0.041557	0.122165	1.491258	3.394018
61	-0.084267	0.200044	0.969776	3.231622
61.5	-0.282668	0.303445	1.063548	3.318198
62	-0.059375	0.272255	0.709802	3.155305
62.5	0.062190	-0.069697	0.653692	3.009039
63	0.100174	0.145325	0.744593	3.078111
63.5	-0.240529	0.319275	0.672505	2.985304
64	-0.035862	0.080672	0.922169	2.793903
64.5	-0.087728	0.298878	0.925626	2.926727

65	-0.095135	0.313748	0.461853	2.608470
65.5	-0.075771	-0.164543	0.724771	2.336318
66	-0.284240	0.066606	0.554896	2.527270
66.5	-0.147153	0.083071	0.599334	2.303186
67	-0.212378	0.257445	0.220335	1.636530
67.5	-0.168011	0.262005	0.180243	1.339857
68	-0.271292	0.216164	0.221322	0.871525
68.5	-0.074518	-0.089100	0.428381	0.972946
69	-0.170666	-0.207345	-0.099163	0.938190
69.5	0.166960	0.247335	0.059768	0.508411
70	-0.074895	0.026991	0.044134	0.754162
70.5	0.356039	-0.092872	0.059768	0.067463
71	-0.111324	0.063608	-0.075316	0.380543
71.5	0.091431	0.190393	-0.183292	0.569687
72	0.056706	-0.085407	-0.211879	0.106667
72.5	-0.049621	0.406010	-0.180436	0.273006
73	0.032035	0.126948	0.064923	0.337513
73.5	0.017814	0.104264	-0.153299	0.233231
74	0.052234	0.064664	0.008754	0.332054
74.5	-0.018747	0.056586	-0.006777	0.240120
75	0.038389	0.036531	-0.010262	0.116032

Table A.3: Experimental data for the torque change along the Z-axis for different pin sizes in the case of twisting-pulling.

Time	7.02	7.04	7.06	7.08
0	-0.000217	-0.001558	0.001737	-0.002558
0.5	-0.000006	0.003605	-0.001040	0.002605
1	0.001901	-0.000270	0.006674	0.002730
1.5	0.003840	0.007707	0.004510	0.007707

2	0.000920	0.003690	0.004751	0.004690
2.5	0.000993	0.002649	0.006231	0.007649
3	0.006149	0.023312	0.028870	0.048568
3.5	0.021560	0.043219	0.065224	0.086595
4	0.014481	0.030038	0.039823	0.064425
4.5	0.011064	0.028918	0.044475	0.054114
5	0.009105	0.030384	0.042349	0.048919
5.5	0.008975	0.025840	0.037747	0.051586
6	0.009878	0.030622	0.037473	0.054776
6.5	0.009526	0.028182	0.039125	0.052259
7	0.010562	0.025590	0.033569	0.053060
7.5	0.012016	0.029502	0.043361	0.048794
8	0.012387	0.027352	0.029262	0.045297
8.5	0.012067	0.026790	0.032426	0.044998
9	0.011854	0.027423	0.034074	0.039455
9.5	0.012804	0.031151	0.037215	0.045768
10	0.014145	0.025994	0.041250	0.045343
10.5	0.013324	0.027637	0.033829	0.042517
11	0.014464	0.025597	0.039832	0.043786
11.5	0.013879	0.028648	0.039941	0.045317
12	0.014079	0.026248	0.037963	0.048254
12.5	0.015042	0.026042	0.039281	0.046204
13	0.015042	0.030364	0.038543	0.052223
13.5	0.015882	0.026351	0.048724	0.051055
14	0.015571	0.024492	0.038798	0.046672
14.5	0.015832	0.025469	0.047134	0.050490
15	0.016594	0.028402	0.044984	0.051818
15.5	0.016819	0.027352	0.055365	0.047125
16	0.016739	0.026887	0.053236	0.049179
16.5	0.017276	0.030009	0.050785	0.052922
17	0.016866	0.031893	0.049994	0.047661
17.5	0.016538	0.029730	0.051638	0.052017
18	0.016880	0.028687	0.051244	0.049222
18.5	0.016299	0.027001	0.049370	0.055961

19	0.016093	0.025068	0.049775	0.049908
19.5	0.018135	0.027055	0.054172	0.046231
20	0.018380	0.027523	0.053250	0.051569
20.5	0.017542	0.024011	0.051517	0.058506
21	0.018285	0.026159	0.056425	0.054138
21.5	0.017864	0.025412	0.053924	0.058049
22	0.017916	0.025553	0.050469	0.056410
22.5	0.018477	0.022391	0.054667	0.056419
23	0.018115	0.026526	0.055240	0.056965
23.5	0.018161	0.022478	0.054504	0.055092
24	0.017835	0.023483	0.049631	0.055911
24.5	0.018256	0.023039	0.058162	0.052884
25	0.017581	0.023608	0.055729	0.053860
25.5	0.017385	0.026065	0.057399	0.048005
26	0.018964	0.021823	0.057385	0.050772
26.5	0.018524	0.022883	0.055966	0.053893
27	0.018707	0.023465	0.052313	0.048974
27.5	0.019241	0.023165	0.056499	0.050245
28	0.018039	0.022861	0.055871	0.046983
28.5	0.018816	0.020995	0.054245	0.049068
29	0.018876	0.022631	0.056736	0.044726
29.5	0.018165	0.020037	0.057879	0.047831
30	0.019409	0.020803	0.053216	0.045859
30.5	0.018362	0.018197	0.058489	0.050541
31	0.018177	0.021713	0.049804	0.051578
31.5	0.018528	0.018279	0.055734	0.044541
32	0.017825	0.021692	0.052961	0.041222
32.5	0.018303	0.020021	0.048908	0.047397
33	0.018147	0.020275	0.052024	0.042435
33.5	0.017974	0.018445	0.057341	0.048112
34	0.017828	0.019109	0.050434	0.048977
34.5	0.017902	0.017927	0.053054	0.047404
35	0.018940	0.019376	0.054361	0.042384
35.5	0.017708	0.018465	0.048079	0.045708

36	0.018212	0.021261	0.049032	0.043462
36.5	0.017527	0.019741	0.047191	0.037344
37	0.017445	0.017371	0.051884	0.043299
37.5	0.016766	0.015878	0.048305	0.034547
38	0.017969	0.019208	0.049900	0.038276
38.5	0.016880	0.017009	0.043624	0.040323
39	0.016104	0.016560	0.042099	0.035787
39.5	0.015734	0.017267	0.040791	0.032549
40	0.016558	0.018648	0.036991	0.033119
40.5	0.016340	0.015320	0.040259	0.034861
41	0.015689	0.017383	0.039955	0.031703
41.5	0.016368	0.015454	0.034472	0.027900
42	0.015825	0.018537	0.036528	0.025263
42.5	0.015906	0.014645	0.035921	0.025126
43	0.015668	0.016306	0.034148	0.023579
43.5	0.014411	0.014141	0.031305	0.024834
44	0.014159	0.015747	0.032437	0.024748
44.5	0.014856	0.016899	0.028770	0.022112
45	0.015021	0.017113	0.025057	0.023092
45.5	0.014368	0.015973	0.024797	0.022311
46	0.014089	0.016193	0.028335	0.021725
46.5	0.014040	0.015698	0.021714	0.023476
47	0.013351	0.014287	0.025900	0.022631
47.5	0.013629	0.015091	0.027240	0.024247
48	0.012789	0.014434	0.027847	0.022087
48.5	0.014441	0.015907	0.024865	0.023392
49	0.012924	0.016447	0.023435	0.019189
49.5	0.011881	0.017435	0.024574	0.021125
50	0.011458	0.013928	0.024697	0.022584
50.5	0.012064	0.012289	0.023709	0.017434
51	0.011825	0.011631	0.018929	0.019004
51.5	0.011209	0.012569	0.018054	0.019910
52	0.010749	0.012117	0.018561	0.019145
52.5	0.011611	0.010721	0.021139	0.020882

53	0.010853	0.013563	0.022234	0.021301
53.5	0.009784	0.010892	0.015578	0.017636
54	0.010224	0.011134	0.020126	0.019406
54.5	0.010063	0.010424	0.017541	0.018784
55	0.010496	0.011695	0.015542	0.017764
55.5	0.010141	0.012719	0.015759	0.017168
56	0.010246	0.012564	0.017291	0.020860
56.5	0.010134	0.008429	0.017937	0.017779
57	0.009604	0.011336	0.018963	0.018072
57.5	0.009671	0.012288	0.015419	0.018855
58	0.009070	0.014242	0.017762	0.017054
58.5	0.008865	0.011759	0.017634	0.015168
59	0.007922	0.012981	0.015360	0.015196
59.5	0.007876	0.012849	0.019415	0.014363
60	0.009579	0.010569	0.018627	0.014622
60.5	0.009087	0.010306	0.016041	0.014046
61	0.009028	0.010211	0.018107	0.015035
61.5	0.009140	0.012297	0.018128	0.013100
62	0.006354	0.010259	0.021032	0.012208
62.5	0.008037	0.010591	0.018535	0.012148
63	0.007643	0.009133	0.017328	0.011216
63.5	0.006272	0.010216	0.017192	0.010765
64	0.005281	0.008302	0.016490	0.012094
64.5	0.005125	0.010023	0.015998	0.011116
65	0.004583	0.009975	0.010180	0.010151
65.5	0.004818	0.009295	0.008665	0.010193
66	0.003508	0.007651	0.008378	0.010936
66.5	0.001751	0.004605	0.008989	0.010296
67	0.002258	0.005603	0.009025	0.009744
67.5	0.001636	0.004525	0.008403	0.010094
68	0.000689	0.003279	0.008364	0.007690
68.5	0.000147	0.003868	0.008471	0.007264
69	0.000431	0.003643	0.012322	0.006834
69.5	0.000437	0.000700	0.008883	0.007600

70	0.000487	0.005529	0.008797	0.006574
70.5	0.000455	0.003332	0.007420	0.006058
71	-0.000291	0.002520	0.005039	0.006483
71.5	0.001056	0.002333	0.005784	0.004899
72	-0.000288	0.004021	0.005103	0.005347
72.5	-0.000620	0.002413	0.004782	0.004195
73	0.001148	-0.002029	0.005068	0.003728
73.5	-0.000246	0.000148	0.002890	0.002999
74	-0.000645	-0.002020	0.001714	0.003107
74.5	-0.000696	-0.002073	0.001335	0.002263
75	-0.001291	-0.001455	0.000976	0.001061

Appendix B. Experimental data for Chapter 4 and Chapter 5

This appendix provides the data for the experiments described in Chapter 4 and Chapter 5.

All the experimental data for Chapter 4 and Chapter 5 are available at the following link:

<https://doi.org/10.25500/edata.bham.00001011>

The following experimental data are examples for each subsection.

B.1 Experimental data for residual force analysis

Table B.1: Experimental data for the force change in the 3-axis test during contactless grasping.

Time	F_x	F_y	F_z
0	0.022807	0.024484	-0.002296
0.239	0.060513	0.057069	0.078362
0.478	-0.014741	0.002994	0.405676
0.717	0.005391	0.289762	0.126526
0.956	0.027393	0.009118	0.198704
1.195	0.017913	-0.208424	0.399168
1.434	0.046887	-0.100456	0.412426
1.673	0.020617	-0.139782	0.581471
1.912	0.004294	0.064106	0.735954
2.151	0.012993	-0.184223	0.815094
2.39	0.035385	0.071004	0.953419
2.629	0.070368	0.078267	1.085732
2.868	0.057091	-0.044051	1.199835
3.107	0.073527	-0.215172	1.262184
3.346	0.163622	-0.103314	1.372292
3.585	0.135882	-0.115040	1.538719

3.824	0.111843	0.062123	1.620642
4.063	0.086124	-0.079666	1.729723
4.302	-0.005228	-0.024257	1.780020
4.541	0.048761	-0.028307	1.921459
4.78	0.124023	0.042619	1.998573
5.019	0.084850	-0.019049	2.103197
5.258	0.103742	0.078419	2.201817
5.497	0.105779	0.097745	2.384335
5.736	0.115224	0.016347	2.346643
5.975	0.091878	0.149908	2.512693
6.214	0.081238	0.158358	2.520748
6.453	0.091614	0.037156	2.655375
6.692	0.157009	-0.041521	2.775667
6.931	0.160050	0.148685	2.884272
7.17	0.191423	0.039545	2.816948
7.409	0.195735	0.186725	3.019680
7.648	0.109478	0.134415	3.056158
7.887	0.134883	-0.072252	3.163189
8.126	0.209382	0.076190	3.217031
8.365	0.146887	0.097301	3.321028
8.604	0.214014	-0.087045	3.368561
8.843	0.185649	-0.015361	3.427456
9.082	0.224063	0.089447	3.593538
9.321	0.238726	0.005767	3.694174
9.56	0.235651	0.218963	3.737368
9.799	0.249216	-0.025998	3.798676
10.038	0.280780	0.107224	3.895792
10.277	0.220626	0.129320	3.971508
10.516	0.093037	0.045091	3.924631
10.755	0.249583	0.082459	4.085440
10.994	0.261664	0.086355	4.183056
11.233	0.286855	0.211532	4.301783
11.472	0.367801	0.309836	4.436922
11.711	0.345299	0.009719	4.361704
11.95	0.401968	-0.007315	4.421392
12.189	0.418450	-0.009062	4.387291
12.428	0.373823	-0.047275	4.328896
12.667	0.425736	0.206197	4.498367
12.906	0.406246	0.033492	4.467684

13.145	0.469056	-0.050322	4.344048
13.384	0.532998	-0.088746	4.517052
13.623	0.417500	0.032196	4.471981
13.862	0.406943	0.182610	4.494343
14.101	0.401762	0.066372	4.441141
14.34	0.428803	0.023926	4.486645
14.579	0.405896	0.133071	4.503654
14.818	0.459254	0.034462	4.441059
15.057	0.342732	-0.075127	4.299446
15.296	0.385208	-0.082800	4.386927
15.535	0.429513	0.062049	4.481003
15.774	0.356510	0.147275	4.369364
16.013	0.428081	0.172377	4.447300
16.252	0.370468	-0.039329	4.407665
16.491	0.417196	0.141103	4.403614
16.73	0.324501	0.169292	4.398317
16.969	0.339530	0.012829	4.409916
17.208	0.419372	0.188487	4.484013
17.447	0.415423	-0.015891	4.390495
17.686	0.405329	-0.029209	4.473068
17.925	0.382084	0.029766	4.430149
18.164	0.438135	0.002984	4.340919
18.403	0.383814	-0.051786	4.383259
18.642	0.438990	0.017204	4.468924
18.881	0.399334	0.150972	4.441284
19.12	0.405538	0.042374	4.421103
19.359	0.420935	0.065009	4.376980
19.598	0.394635	-0.042997	4.354092
19.837	0.449782	0.005065	4.382498
20.076	0.466037	0.402192	4.464422
20.315	0.431156	0.109133	4.434887
20.554	0.392616	0.256895	4.499174
20.793	0.397731	-0.105226	4.318209
21.032	0.412620	0.100336	4.464285
21.271	0.406679	0.197323	4.459654
21.51	0.322896	-0.106212	4.382366
21.749	0.323526	-0.052111	4.302563
21.988	0.378391	-0.011897	4.435915
22.227	0.439762	0.064937	4.430044

22.466	0.377379	0.026299	4.415491
22.705	0.401850	-0.144600	4.341063
22.944	0.449385	0.043019	4.366776
23.183	0.388333	-0.009877	4.367479
23.422	0.347454	0.053266	4.381659
23.661	0.383974	0.074318	4.351799
23.9	0.412451	-0.137812	4.305939
24.139	0.396453	0.059532	4.345673
24.378	0.424085	0.113229	4.394571
24.617	0.406543	0.010116	4.388638
24.856	0.404870	-0.017869	4.310940
25.095	0.385542	-0.094735	4.319473
25.334	0.428433	0.024476	4.397791
25.573	0.382174	0.019945	4.274052
25.812	0.428806	-0.083855	4.380423
26.051	0.412114	0.098804	4.431091
26.29	0.402480	0.103205	4.432690
26.529	0.425985	0.018558	4.351555
26.768	0.490574	0.029706	4.425320
27.007	0.346978	0.070318	4.347824
27.246	0.349789	0.205256	4.357664
27.485	0.408817	-0.125736	4.321415
27.724	0.360776	0.058652	4.375154
27.963	0.357683	0.036152	4.382540
28.202	0.398268	-0.012865	4.455427
28.441	0.406698	-0.037132	4.388767
28.68	0.369203	0.070280	4.438280
28.919	0.404080	-0.066600	4.318851
29.158	0.415663	-0.014073	4.379578
29.397	0.434164	0.102728	4.350876
29.636	0.380541	0.041808	4.394972
29.875	0.418983	0.001636	4.348419
30.114	0.408522	0.067468	4.317924
30.353	0.376502	-0.066965	4.303238
30.592	0.379897	0.201478	4.402912
30.831	0.397025	0.046164	4.307751
31.07	0.419660	-0.118149	4.470507
31.309	0.382626	0.020874	4.431944
31.548	0.343308	-0.014636	4.335543

31.787	0.338153	-0.029815	4.286383
32.026	0.474115	0.112970	4.365667
32.265	0.343868	0.139229	4.347275
32.504	0.350827	-0.030272	4.282095
32.743	0.438686	0.132026	4.360151
32.982	0.501330	0.139202	4.524111
33.221	0.418298	-0.113639	4.290295
33.46	0.433333	0.253790	4.375731
33.699	0.474639	-0.062461	4.364803
33.938	0.408320	-0.031104	4.327448
34.177	0.436899	0.012301	4.348175
34.416	0.448535	0.203256	4.460800
34.655	0.378268	0.048913	4.340219
34.894	0.379698	0.063278	4.375336
35.133	0.390268	-0.059134	4.290979
35.372	0.342863	-0.066086	4.273932
35.611	0.413892	0.140991	4.361864
35.85	0.417025	-0.082124	4.281029
36.089	0.448603	-0.014472	4.294903
36.328	0.440708	0.014051	4.407291
36.567	0.397455	0.067735	4.403095
36.806	0.475956	0.074286	4.327398
37.045	0.366729	-0.080589	4.332815
37.284	0.425905	0.150238	4.358263
37.523	0.447901	-0.036805	4.406172
37.762	0.412366	0.090882	4.363680
38.001	0.444728	0.125895	4.365347
38.24	0.418422	-0.009349	4.357563
38.479	0.420291	0.145506	4.466908
38.718	0.454708	-0.018614	4.331656
38.957	0.477606	-0.046548	4.416025
39.196	0.402270	0.266474	4.461235
39.435	0.384072	0.109800	4.350271
39.674	0.362745	-0.171657	4.336365
39.913	0.464579	0.071365	4.423223
40.152	0.418991	0.053744	4.334003
40.391	0.393679	0.066227	4.364832
40.63	0.391317	0.020616	4.300484
40.869	0.405086	0.261168	4.378744

41.108	0.359077	0.216275	4.413551
41.347	0.409014	0.020213	4.316475
41.586	0.479235	0.365818	4.484955
41.825	0.410074	-0.161199	4.334499
42.064	0.456765	0.296566	4.438784
42.303	0.429295	0.156496	4.460009
42.542	0.438494	0.064136	4.295395
42.781	0.366837	0.230183	4.371563
43.02	0.474071	-0.045716	4.439091
43.259	0.438838	0.039032	4.395348
43.498	0.400250	0.151355	4.268204
43.737	0.412767	0.153663	4.417332
43.976	0.465780	0.123351	4.419136
44.215	0.411917	-0.084047	4.306671
44.454	0.391378	-0.007903	4.375088
44.693	0.459188	0.047630	4.379910
44.932	0.354485	0.085821	4.330439
45.171	0.482697	-0.030458	4.436098
45.41	0.427418	-0.032815	4.291431
45.649	0.424787	0.168327	4.356281
45.888	0.358062	-0.048169	4.398020
46.127	0.437043	0.059355	4.369869
46.366	0.384837	0.254179	4.427912
46.605	0.484235	0.080927	4.388386
46.844	0.402826	0.299414	4.409155
47.083	0.355524	-0.016278	4.418139
47.322	0.403948	0.078248	4.406912
47.561	0.409803	-0.042615	4.353279
47.8	0.351523	-0.036705	4.330179
48.039	0.423902	0.030485	4.395857
48.278	0.323811	0.208787	4.427086
48.517	0.326167	0.133623	4.405891
48.756	0.318532	0.002833	4.323612
48.995	0.387540	-0.091251	4.392445
49.234	0.367185	-0.062158	4.365263
49.473	0.350335	0.076340	4.362591
49.712	0.359198	0.045511	4.467051
49.951	0.287347	0.016634	4.319536
50.19	0.303089	-0.227613	4.275164

50.429	0.387801	0.225859	4.453804
50.668	0.392439	0.032803	4.359072
50.907	0.358153	-0.015055	4.301016
51.146	0.384413	0.121143	4.412619
51.385	0.424114	0.046861	4.483284
51.624	0.345080	-0.102205	4.267923
51.863	0.410271	0.073859	4.361544
52.102	0.354063	-0.031344	4.374739
52.341	0.441341	0.217921	4.516628
52.58	0.381715	0.042102	4.436987
52.819	0.334718	-0.088959	4.337456
53.058	0.395025	-0.038988	4.363272
53.297	0.322183	0.190487	4.382671
53.536	0.376203	-0.195409	4.279232
53.775	0.383487	-0.138831	4.375217
54.014	0.395157	0.248590	4.468224
54.253	0.371934	0.004317	4.374895
54.492	0.381586	-0.122095	4.388472
54.731	0.363469	0.159812	4.380302
54.97	0.382762	0.138365	4.433760
55.209	0.408234	-0.140172	4.404287
55.448	0.329630	0.107957	4.399815
55.687	0.404023	0.155826	4.381968
55.926	0.370874	-0.000273	4.394356
56.165	0.395990	0.061127	4.389200
56.404	0.362319	0.047121	4.410877
56.643	0.333397	-0.075193	4.360950
56.882	0.372186	0.205507	4.469971
57.121	0.384030	-0.094158	4.428576
57.36	0.412494	-0.067783	4.397495
57.599	0.454340	0.093165	4.404602
57.838	0.308036	0.111062	4.363123
58.077	0.377476	0.108327	4.386076
58.316	0.395376	0.210287	4.510212
58.555	0.338692	-0.110652	4.315075
58.794	0.364034	-0.059149	4.323692
59.033	0.360639	-0.123963	4.329536
59.272	0.392705	0.174213	4.383116
59.511	0.352227	-0.062580	4.294863

59.75	0.367424	0.376399	4.433596
59.989	0.371391	0.141223	4.396515
60.228	0.340513	-0.071727	4.428865
60.467	0.364176	0.088055	4.430090
60.706	0.362609	0.193454	4.427624
60.945	0.373034	-0.352140	4.324787
61.184	0.454093	0.179261	4.515947
61.423	0.364751	-0.039825	4.325523
61.662	0.280936	-0.133049	4.315748
61.901	0.384387	0.062263	4.399359
62.14	0.419158	0.037474	4.420839
62.379	0.398018	-0.030006	4.373827
62.618	0.364419	0.152352	4.379658
62.857	0.416232	-0.001486	4.410423
63.096	0.346013	-0.056731	4.261620
63.335	0.339056	0.162971	4.424850
63.574	0.447636	0.049739	4.399137
63.813	0.377544	0.216807	4.449972
64.052	0.313407	-0.088318	4.380796
64.291	0.369604	0.028118	4.322424
64.53	0.369687	0.078900	4.379431
64.769	0.405371	0.148783	4.364107
65.008	0.309271	0.063654	4.319340
65.247	0.331096	0.059361	4.379301
65.486	0.405911	-0.228064	4.383369
65.725	0.381489	-0.053215	4.386223
65.964	0.278215	-0.006224	4.366337
66.203	0.350058	-0.051612	4.224268
66.442	0.405605	-0.077578	4.405140
66.681	0.348866	0.067371	4.264305
66.92	0.382917	0.220906	4.462004
67.159	0.338949	-0.023104	4.404350
67.398	0.340622	0.055439	4.345339
67.637	0.277271	-0.145201	4.258337
67.876	0.287783	0.165060	4.357447
68.115	0.370944	0.102949	4.385979
68.354	0.366429	0.142392	4.410555
68.593	0.322825	0.159358	4.373543
68.832	0.302286	0.016912	4.322779

69.071	0.321691	-0.297650	4.319040
69.31	0.380812	-0.071054	4.251896
69.549	0.422680	0.250051	4.567560
69.788	0.314242	0.073868	4.374931
70.027	0.310681	0.107487	4.339655
70.266	0.275798	-0.049306	4.354187
70.505	0.319920	0.039934	4.399851
70.744	0.328269	0.131797	4.376677
70.983	0.328742	0.259752	4.412727
71.222	0.375473	0.035305	4.438799
71.461	0.394204	-0.058184	4.395241
71.7	0.333893	0.244716	4.374107
71.939	0.340062	0.030702	4.342323
72.178	0.450048	0.212625	4.433214
72.417	0.314603	0.161885	4.290691
72.656	0.348720	0.106396	4.297672
72.895	0.349090	0.186775	4.352327
73.134	0.383097	0.297051	4.415379
73.373	0.397182	0.028933	4.442751
73.612	0.349927	-0.134013	4.226011
73.851	0.334914	0.115079	4.337217
74.09	0.395536	0.016589	4.378252
74.329	0.332778	0.336408	4.427071
74.568	0.393790	0.185206	4.460623
74.807	0.473204	0.072027	4.388433
75.046	0.407966	0.144065	4.390539
75.285	0.388769	-0.118631	4.254271
75.524	0.411823	-0.062280	4.294464
75.763	0.397754	0.110017	4.347815
76.002	0.355369	0.112727	4.380848
76.241	0.319139	-0.021515	4.299135
76.48	0.293493	-0.133412	4.376932
76.719	0.351868	0.027768	4.300554
76.958	0.398809	-0.081956	4.361769
77.197	0.400885	0.013900	4.408985
77.436	0.355234	-0.182119	4.225666
77.675	0.385901	-0.066466	4.313618
77.914	0.404721	0.192767	4.358395
78.153	0.405726	-0.130451	4.352928

78.392	0.386928	0.068808	4.282791
78.631	0.364319	-0.004560	4.358011
78.87	0.370324	-0.012427	4.309036
79.109	0.455291	-0.086286	4.364916
79.348	0.449642	-0.015829	4.377935
79.587	0.353419	0.046564	4.343019
79.826	0.299402	0.104147	4.271944
80.065	0.397931	-0.025750	4.281603
80.304	0.352945	0.022452	4.286303
80.543	0.358677	0.005581	4.289631
80.782	0.376914	0.040095	4.325378
81.021	0.395490	0.125381	4.303907
81.26	0.420978	0.202001	4.323006
81.499	0.374367	0.203989	4.315832
81.738	0.364316	-0.020965	4.286459
81.977	0.377250	0.084701	4.236921
82.216	0.317788	0.244919	4.321556
82.455	0.435008	-0.093324	4.328259
82.694	0.284444	0.196968	4.335943
82.933	0.367749	-0.019049	4.217632
83.172	0.426183	0.018075	4.239414
83.411	0.412831	0.093273	4.344559
83.65	0.467452	-0.089353	4.381861
83.889	0.355628	-0.155087	4.329443
84.128	0.378381	-0.071000	4.298260
84.367	0.401346	0.092370	4.293888
84.606	0.321340	0.101354	4.330868
84.845	0.489704	-0.038641	4.378223
85.084	0.456323	0.138796	4.330212
85.323	0.399213	0.038723	4.300674
85.562	0.400338	-0.007108	4.284430
85.801	0.422132	0.292713	4.410513
86.04	0.379660	0.302327	4.346687
86.279	0.419125	-0.094397	4.255207
86.518	0.488957	0.049940	4.377947
86.757	0.420141	-0.133567	4.325148
86.996	0.396279	0.085643	4.353249
87.235	0.438783	0.094980	4.308960
87.474	0.398747	0.133541	4.283596

87.713	0.446187	0.121611	4.345201
87.952	0.355626	-0.028134	4.291698
88.191	0.448110	-0.138918	4.383619
88.43	0.414988	0.081109	4.255013
88.669	0.454318	0.084908	4.289940
88.908	0.350272	0.128104	4.261612
89.147	0.468158	-0.047121	4.332211
89.386	0.376155	0.011352	4.274799
89.625	0.444605	0.044831	4.241007
89.864	0.423166	0.053628	4.257305
90.103	0.402448	0.295822	4.343182
90.342	0.411000	0.125222	4.202362
90.581	0.474338	0.101781	4.326208
90.82	0.415381	0.374590	4.345905
91.059	0.403458	-0.081768	4.207935
91.298	0.469007	0.115898	4.315102
91.537	0.365256	0.182462	4.280275
91.776	0.437204	0.208612	4.296219
92.015	0.382740	0.033865	4.240143
92.254	0.430932	0.102273	4.276848
92.493	0.454994	0.114482	4.269016
92.732	0.396641	0.087855	4.226246
92.971	0.415181	0.051081	4.341227
93.21	0.425301	-0.069906	4.255215
93.449	0.459221	0.058204	4.315695
93.688	0.429660	0.035868	4.244797
93.927	0.420582	0.114054	4.258631
94.166	0.350305	0.089127	4.239687
94.405	0.390548	0.041423	4.219395
94.644	0.494462	0.100030	4.351088
94.883	0.406164	0.086334	4.281746
95.122	0.386410	-0.005377	4.257872
95.361	0.402361	0.201864	4.331516
95.6	0.430779	0.085377	4.282351
95.839	0.413585	0.257267	4.361767
96.078	0.421346	0.071391	4.264494
96.317	0.467587	-0.070317	4.228420
96.556	0.487493	0.142729	4.331619
96.795	0.441041	0.020312	4.229120

97.034	0.509257	0.160602	4.394012
97.273	0.447811	0.176427	4.259272
97.512	0.477109	-0.016955	4.314466
97.751	0.412421	0.097911	4.332504
97.99	0.463910	0.130429	4.298843
98.229	0.438457	-0.001539	4.293737
98.468	0.331144	-0.152208	4.263216
98.707	0.358425	0.309829	4.313059
98.946	0.394758	-0.045888	4.255953
99.185	0.364842	0.321645	4.336439
99.424	0.439267	0.256914	4.352520
99.663	0.422263	0.115359	4.302944
99.902	0.459337	0.083596	4.307432
100.141	0.439055	0.235204	4.381475
100.38	0.406626	0.132079	4.320168
100.619	0.420890	0.246646	4.343466
100.858	0.440823	-0.183466	4.275837
101.097	0.381201	0.002343	4.319376
101.336	0.404585	0.086776	4.280251
101.575	0.443020	0.217793	4.322481
101.814	0.483182	0.026983	4.295210
102.053	0.357803	0.029339	4.267302
102.292	0.447086	-0.301469	4.135172
102.531	0.411621	0.175708	4.307888
102.77	0.509614	-0.030407	4.310249
103.009	0.447117	0.004237	4.269474
103.248	0.391425	0.089508	4.273888
103.487	0.495635	0.127854	4.247366
103.726	0.398355	0.176719	4.268957
103.965	0.438021	0.116911	4.304535
104.204	0.376034	0.020864	4.254524
104.443	0.311607	0.135672	4.289999
104.682	0.423382	0.187160	4.331549
104.921	0.405808	0.018996	4.314371
105.16	0.434831	0.033333	4.208399
105.399	0.389843	-0.035607	4.254543
105.638	0.407390	-0.191457	4.221060
105.877	0.438073	0.242812	4.302731
106.116	0.363818	0.058281	4.353144

106.355	0.450926	0.084967	4.253370
106.594	0.447023	0.042000	4.243010
106.833	0.434630	0.191539	4.327599
107.072	0.398223	-0.131570	4.237768
107.311	0.424982	0.221356	4.280407
107.55	0.388246	-0.011174	4.181017
107.789	0.479320	0.131613	4.299631
108.028	0.438894	-0.089986	4.284317
108.267	0.398327	-0.127103	4.279032
108.506	0.424616	0.367705	4.376863
108.745	0.485736	-0.021818	4.459827
108.984	0.415338	0.038351	4.324331
109.223	0.394296	-0.007525	4.272507
109.462	0.429225	-0.114087	4.360317
109.701	0.328498	-0.070012	4.296078
109.94	0.467627	-0.013547	4.396559
110.179	0.408128	0.093092	4.365992
110.418	0.394891	0.197387	4.350842
110.657	0.470851	-0.038241	4.357315
110.896	0.441703	-0.002712	4.335060
111.135	0.364968	0.080238	4.305431
111.374	0.433664	0.037895	4.417280
111.613	0.461609	-0.007055	4.496920
111.852	0.446792	0.207409	4.429581
112.091	0.405847	-0.013571	4.396667
112.33	0.419261	0.028875	4.332848
112.569	0.400479	0.035036	4.363432
112.808	0.351076	-0.025639	4.461443
113.047	0.449669	0.075476	4.380251
113.286	0.425650	0.266153	4.372128
113.525	0.348978	0.031545	4.306267
113.764	0.412473	0.045604	4.502090
114.003	0.329939	-0.034992	4.244255
114.242	0.446100	0.114462	4.476139
114.481	0.431570	0.064418	4.464985
114.72	0.410649	0.230383	4.460819
114.959	0.384757	-0.068292	4.309221
115.198	0.424867	0.110945	4.355022
115.437	0.409020	0.019488	4.381607

115.676	0.447534	0.074401	4.429459
115.915	0.376719	-0.006825	4.366262
116.154	0.433007	0.364673	4.480330
116.393	0.426533	0.069420	4.375120
116.632	0.354907	-0.042118	4.362474
116.871	0.284125	0.220312	4.378078
117.11	0.405574	0.139839	4.374428
117.349	0.434059	0.159524	4.461750
117.588	0.385356	0.239681	4.396517
117.827	0.355904	-0.028055	4.366388
118.066	0.454208	0.163362	4.502655
118.305	0.436785	0.187881	4.481264
118.544	0.388119	0.133863	4.335453
118.783	0.348979	0.186511	4.322376
119.022	0.405234	-0.048838	4.281754
119.261	0.448777	0.004272	4.343008
119.5	0.395351	0.333253	4.417566
119.739	0.394971	0.344162	4.440071
119.978	0.411927	0.172925	4.409449
120.217	0.365738	0.069541	4.285803
120.456	0.333651	0.265485	4.416388
120.695	0.364232	0.432804	4.356831
120.934	0.371040	0.170100	4.404339
121.173	0.423215	0.073101	4.285500
121.412	0.378033	0.294375	4.458948
121.651	0.396573	0.346091	4.424263
121.89	0.378943	0.107266	4.352041
122.129	0.400351	0.127770	4.330378
122.368	0.409762	-0.166879	4.355400
122.607	0.495571	-0.137277	4.430443
122.846	0.342236	0.122160	4.410355
123.085	0.369740	0.217066	4.358519
123.324	0.374531	0.032797	4.299274
123.563	0.424470	0.057004	4.420212
123.802	0.401988	-0.065528	4.198959
124.041	0.445007	0.191860	4.386227
124.28	0.441005	0.142626	4.349003
124.519	0.422579	-0.044245	4.349968
124.758	0.351536	0.099930	4.278988

124.997	0.392943	-0.045552	4.285694
125.236	0.445831	-0.074384	4.337172
125.475	0.431185	0.304385	4.388634
125.714	0.438433	0.105025	4.283638
125.953	0.369280	0.421975	4.410095
126.192	0.368180	0.089720	4.296219
126.431	0.389756	0.396852	4.406164
126.67	0.477177	0.149625	4.353323
126.909	0.415594	0.249904	4.310333
127.148	0.294875	0.218629	4.213539
127.387	0.392632	0.068755	4.230995
127.626	0.478483	0.192377	4.375544
127.865	0.366691	0.026924	4.288996
128.104	0.400370	0.129044	4.296019
128.343	0.481155	0.160622	4.317532
128.582	0.455485	0.198159	4.298553
128.821	0.410661	0.112035	4.358671
129.06	0.381775	0.049425	4.223656
129.299	0.444315	-0.021369	4.275656
129.538	0.394956	-0.018986	4.259756
129.777	0.388376	0.111914	4.383694
130.016	0.416946	-0.076107	4.274660
130.255	0.383646	0.047827	4.309456
130.494	0.430129	-0.031758	4.289360
130.733	0.447233	0.059828	4.345819
130.972	0.409766	0.177367	4.306026
131.211	0.456344	0.188063	4.392254
131.45	0.389826	-0.025318	4.270550
131.689	0.411394	0.112377	4.355715
131.928	0.449622	0.185345	4.275188
132.167	0.464935	-0.015577	4.287016
132.406	0.466877	-0.126122	4.241962
132.645	0.415522	0.033713	4.223923
132.884	0.404856	0.205383	4.360872
133.123	0.386098	-0.088962	4.217079
133.362	0.394957	-0.070632	4.159636
133.601	0.436960	0.213458	4.315819
133.84	0.345534	0.144125	4.324820
134.079	0.340605	0.162402	4.264067

134.318	0.425176	0.052845	4.308224
134.557	0.347062	0.184242	4.286524
134.796	0.411914	-0.134201	4.213379
135.035	0.396716	-0.083498	4.244703
135.274	0.415101	0.236979	4.350208
135.513	0.398436	0.023367	4.285948
135.752	0.351123	0.062777	4.312584
135.991	0.443179	0.071434	4.325176
136.23	0.385435	-0.057083	4.256285
136.469	0.411375	0.146633	4.329432
136.708	0.430515	0.100167	4.289059
136.947	0.389796	0.138810	4.265753
137.186	0.418207	0.138567	4.409300
137.425	0.445876	-0.131614	4.288191
137.664	0.497447	0.075917	4.331404
137.903	0.460399	0.136204	4.285387
138.142	0.306550	0.073118	4.261103
138.381	0.446793	0.003831	4.234459
138.62	0.462068	0.190775	4.474934
138.859	0.388968	0.150224	4.292696
139.098	0.415690	0.054519	4.369368
139.337	0.404736	0.063370	4.295616
139.576	0.384463	0.165480	4.333725
139.815	0.344115	0.173165	4.257607
140.054	0.399055	-0.055297	4.382891
140.293	0.354971	0.005165	4.221081
140.532	0.356322	0.179577	4.324219
140.771	0.425618	-0.007231	4.312174
141.01	0.421926	0.010200	4.349714
141.249	0.456877	0.038927	4.214275
141.488	0.488118	-0.053277	4.326298
141.727	0.359247	0.041524	4.373272
141.966	0.408548	0.032909	4.332903
142.205	0.398487	0.124891	4.340855
142.444	0.393427	0.098679	4.374380
142.683	0.366805	0.075661	4.281832
142.922	0.358674	0.034437	4.279129
143.161	0.413542	0.100959	4.358984
143.4	0.423599	0.033939	4.346989

143.639	0.391520	0.106780	4.237295
143.878	0.417107	0.112811	4.393259
144.117	0.412079	0.100415	4.347023
144.356	0.408709	0.073718	4.249483
144.595	0.344316	0.177036	4.343794
144.834	0.458095	0.156005	4.303219
145.073	0.376309	0.090403	4.299639
145.312	0.412874	0.167120	4.310923
145.551	0.508337	0.101822	4.317911
145.79	0.432714	0.012453	4.367260
146.029	0.333785	0.135887	4.189692
146.268	0.337135	0.028871	4.298733
146.507	0.378777	0.117810	4.195663
146.746	0.394907	0.152618	4.357183
146.985	0.391423	0.111698	4.336048
147.224	0.403475	-0.006572	4.294771
147.463	0.343951	0.399636	4.297491
147.702	0.426075	0.122180	4.382515
147.941	0.400929	0.055809	4.359095
148.18	0.363785	0.081462	4.266043
148.419	0.355298	-0.056532	4.162548
148.658	0.472675	0.048249	4.299459
148.897	0.398300	0.244344	4.248667
149.136	0.448470	0.152334	4.401360
149.375	0.436157	0.170344	4.422220
149.614	0.401458	0.023204	4.276449
149.853	0.378349	0.261703	4.275944
150.092	0.397179	0.155543	4.295647
150.331	0.453875	0.117130	4.285330
150.57	0.385330	0.105446	4.272236
150.809	0.377724	0.097345	4.206480
151.048	0.454575	0.398236	4.445671
151.287	0.454060	0.097585	4.360807
151.526	0.338270	0.186364	4.330347
151.765	0.403957	0.219942	4.253752
152.004	0.442160	0.039047	4.353899
152.243	0.344718	0.048712	4.289598
152.482	0.428867	0.005985	4.394930
152.721	0.358133	0.081378	4.313564

152.96	0.355187	0.201349	4.256203
153.199	0.368500	-0.002790	4.214060
153.438	0.430727	0.286592	4.314112
153.677	0.430470	0.073974	4.311459
153.916	0.368990	-0.141711	4.290520
154.155	0.423290	0.086911	4.284580
154.394	0.422884	0.227170	4.334379
154.633	0.442904	0.350896	4.408535
154.872	0.390833	0.134482	4.380739
155.111	0.361988	0.152284	4.250443
155.35	0.416567	0.115534	4.320240
155.589	0.433778	-0.012464	4.314432
155.828	0.374262	0.115768	4.338367
156.067	0.513406	-0.067316	4.344481
156.306	0.410073	0.046219	4.274607
156.545	0.356827	0.230724	4.200024
156.784	0.426109	0.045870	4.247059
157.023	0.415191	0.284971	4.336538
157.262	0.373348	0.105565	4.303991
157.501	0.404023	0.119754	4.312511
157.74	0.349790	0.072871	4.243427
157.979	0.431830	0.025161	4.293982
158.218	0.390975	0.207391	4.319384
158.457	0.473201	0.133276	4.259975
158.696	0.405481	0.015986	4.216431
158.935	0.354236	0.087516	4.330414
159.174	0.447459	0.095390	4.178724
159.413	0.440439	-0.010981	4.271704
159.652	0.365386	0.083763	4.173227
159.891	0.454226	-0.055986	4.236807
160.13	0.385350	0.187956	4.294783
160.369	0.519804	0.268199	4.334164
160.608	0.359859	0.280486	4.254330
160.847	0.426273	0.176227	4.363157
161.086	0.453853	0.172197	4.360094
161.325	0.387252	-0.008358	4.212448
161.564	0.402350	-0.120769	4.192070
161.803	0.338893	0.139690	4.283791
162.042	0.356167	0.096688	4.250284

162.281	0.425073	-0.025150	4.237463
162.52	0.478575	0.156774	4.451906
162.759	0.484913	0.225319	4.257807
162.998	0.451330	-0.137049	4.357624
163.237	0.421996	0.065898	4.267519
163.476	0.416577	0.044297	4.359274
163.715	0.321703	0.065185	4.333040
163.954	0.463434	0.298901	4.445244
164.193	0.422888	0.031145	4.309925
164.432	0.384378	0.000198	4.268015
164.671	0.456024	0.036206	4.315969
164.91	0.458355	0.069326	4.334101
165.149	0.438726	0.060404	4.314831
165.388	0.447303	0.073994	4.409126
165.627	0.430530	0.010981	4.298971
165.866	0.456362	-0.068575	4.337303
166.105	0.435322	0.005521	4.406704
166.344	0.427168	-0.030011	4.373358
166.583	0.437039	0.199718	4.307962
166.822	0.456373	0.003959	4.341528
167.061	0.457403	0.022224	4.379215
167.3	0.434942	0.053583	4.314859
167.539	0.439164	0.142769	4.379383
167.778	0.523984	0.289859	4.460896
168.017	0.430991	-0.062292	4.346708
168.256	0.463795	0.219046	4.433594
168.495	0.416998	-0.136485	4.323473
168.734	0.402342	-0.088321	4.348055
168.973	0.401967	-0.041058	4.351004
169.212	0.486005	0.003101	4.397799
169.451	0.480351	0.184768	4.509869
169.69	0.457033	-0.039081	4.364294
169.929	0.389350	0.216470	4.434303
170.168	0.437827	0.083471	4.391199
170.407	0.428423	0.042916	4.432915
170.646	0.365591	0.154632	4.304897
170.885	0.412542	-0.014996	4.408323
171.124	0.451884	-0.068520	4.372887
171.363	0.428009	0.004635	4.379583

171.602	0.346959	0.128819	4.263708
171.841	0.471078	-0.104208	4.405628
172.08	0.451019	0.208288	4.458712
172.319	0.456599	-0.061132	4.356855
172.558	0.351847	0.132371	4.288927
172.797	0.405757	0.057129	4.397459
173.036	0.354686	0.041662	4.219679
173.275	0.465693	-0.011014	4.441475
173.514	0.440513	0.113590	4.423475
173.753	0.408529	0.066820	4.382755
173.992	0.511026	-0.022672	4.423227
174.231	0.468949	-0.159673	4.301464
174.47	0.433139	-0.077478	4.328630
174.709	0.419651	0.061216	4.393812
174.948	0.434227	-0.018634	4.358255
175.187	0.421221	-0.209550	4.306479
175.426	0.435374	0.161830	4.352736
175.665	0.399242	0.034040	4.351242
175.904	0.456139	0.109140	4.332771
176.143	0.450643	0.066308	4.433107
176.382	0.431845	0.280184	4.423428
176.621	0.445533	0.069854	4.420370
176.86	0.427027	0.061444	4.379650
177.099	0.448111	0.115530	4.397539
177.338	0.446773	-0.063543	4.365580
177.577	0.401710	-0.059981	4.310339
177.816	0.460147	-0.047300	4.377060
178.055	0.493196	0.043235	4.422531
178.294	0.442938	-0.039390	4.352373
178.533	0.483972	0.260637	4.403227
178.772	0.421585	-0.155162	4.245564
179.011	0.453136	-0.000432	4.381186
179.25	0.468020	0.093051	4.362288
179.489	0.491873	-0.000303	4.480471
179.728	0.467237	0.167194	4.403416
179.967	0.443467	0.065349	4.365784
180.206	0.397677	-0.106421	4.311548
180.445	0.454161	-0.041011	4.488514
180.684	0.513370	-0.186591	4.289843

180.923	0.425751	-0.173248	4.335506
181.162	0.430370	0.032769	4.336164
181.401	0.455222	0.105990	4.405399
181.64	0.412694	0.134628	4.411270
181.879	0.403996	0.081311	4.353182
182.118	0.345375	0.026318	4.366737
182.357	0.455497	0.048316	4.391388
182.596	0.471863	0.135954	4.389408
182.835	0.482209	0.091390	4.414690
183.074	0.382518	0.114227	4.396448
183.313	0.476547	-0.055204	4.437706
183.552	0.497151	-0.010738	4.427952
183.791	0.459327	-0.025412	4.383175
184.03	0.514161	0.197074	4.407999
184.269	0.441210	0.203266	4.451927
184.508	0.441745	-0.095322	4.353413
184.747	0.484928	-0.040320	4.360807
184.986	0.476034	0.006383	4.401712
185.225	0.394085	0.039940	4.383533
185.464	0.490539	-0.074300	4.466219
185.703	0.450413	-0.011888	4.384295
185.942	0.431161	0.149317	4.373323
186.181	0.440145	-0.123382	4.394100
186.42	0.421438	-0.020715	4.315428
186.659	0.429920	-0.198371	4.291529
186.898	0.386535	-0.017535	4.297068
187.137	0.470982	-0.141585	4.353266
187.376	0.441919	0.036610	4.325766
187.615	0.494989	0.048549	4.474339
187.854	0.467541	-0.001113	4.414587
188.093	0.451154	-0.057902	4.396843
188.332	0.472082	0.248786	4.419239
188.571	0.398201	-0.068694	4.344732
188.81	0.441911	0.017032	4.377131
189.049	0.400438	0.043721	4.342834
189.288	0.436753	0.146157	4.375051
189.527	0.411592	-0.012921	4.358776
189.766	0.432546	0.088854	4.439701
190.005	0.481614	-0.025868	4.344988

190.244	0.421482	-0.002195	4.351088
190.483	0.443470	-0.085171	4.357624
190.722	0.306742	0.046658	4.320143
190.961	0.429390	0.027310	4.320177
191.2	0.374091	0.093582	4.361019
191.439	0.479558	0.024638	4.309591
191.678	0.365297	-0.132393	4.304703
191.917	0.385060	0.123227	4.356911
192.156	0.440381	-0.038750	4.288616
192.395	0.461304	0.107336	4.353083
192.634	0.457082	0.004752	4.413111
192.873	0.415038	0.050445	4.347868
193.112	0.430627	-0.005350	4.409092
193.351	0.483950	0.120967	4.330626
193.59	0.487062	0.113181	4.418587
193.829	0.441875	0.087721	4.308197
194.068	0.436664	0.000417	4.367672
194.307	0.430655	0.140268	4.394258
194.546	0.472829	-0.245456	4.344707
194.785	0.482082	-0.098176	4.383699
195.024	0.399263	0.126117	4.357410
195.263	0.428269	-0.132304	4.295492
195.502	0.404414	-0.120623	4.328558
195.741	0.396212	0.016450	4.330420
195.98	0.481095	-0.186423	4.366846
196.219	0.463359	-0.175570	4.370775
196.458	0.458925	0.060481	4.400023
196.697	0.416895	-0.004806	4.288158
196.936	0.433450	0.217568	4.381680
197.175	0.416988	-0.017693	4.339207
197.414	0.424623	-0.044180	4.323023
197.653	0.407236	0.026219	4.316839
197.892	0.389643	0.069715	4.310303
198.131	0.430492	0.027704	4.324240
198.37	0.404323	0.122602	4.327175
198.609	0.498147	0.027005	4.286465
198.848	0.417023	0.002398	4.307001
199.087	0.409329	0.145939	4.399399
199.326	0.390772	0.003690	4.311508

199.565	0.372326	-0.190801	4.222536
199.804	0.385307	0.064151	4.173996
200.043	0.417845	0.043258	4.352386
200.282	0.437389	-0.052894	4.305214
200.521	0.396886	0.071621	4.250147
200.76	0.359314	-0.029724	4.281893

B.2 Experimental data for the constrained wiggling unplugging experiment

Table B.2: Experimental data for force and torque changes in the 6-axis in the 9 mm-8 mm constrained unplugging with 4 N LF.

Time	F_x	F_y	F_z	T_x	T_y	T_z
0	-0.052228	0.015799	0.006901	0.003028	0.003396	0.003256
0.2358	0.218591	0.567404	1.028722	-0.143638	0.026849	0.003042
0.4716	0.195856	0.635496	1.179151	-0.146526	0.026171	0.004488
0.7074	0.338867	1.060430	1.825854	-0.245766	0.040621	0.004754
0.9432	0.305227	1.112686	1.950626	-0.289755	0.044697	0.001381
1.1790	0.415457	1.337118	2.453185	-0.332689	0.050203	0.002722
1.4148	0.466285	1.801304	2.699578	-0.413825	0.052447	0.001745
1.6506	0.596359	1.993001	2.987416	-0.451997	0.064006	0.004076
1.8864	0.597057	2.274405	3.303036	-0.520445	0.065326	0.003429
2.1222	0.692514	2.330750	3.464183	-0.536391	0.072113	0.001128
2.3580	0.769480	2.749814	3.719917	-0.639715	0.078715	0.001352
2.5938	0.778452	2.747055	3.728853	-0.636127	0.078908	0.003125
2.8296	0.969806	3.138582	4.225311	-0.724540	0.091573	0.000871
3.0654	0.948465	3.227544	4.273337	-0.739998	0.097423	0.004926
3.3012	1.005683	3.350896	4.556410	-0.793439	0.099361	0.003250
3.5370	1.071135	3.618145	4.674547	-0.842411	0.104585	-0.000026
3.7728	1.015693	3.576148	4.843744	-0.857305	0.102005	0.002958
4.0086	1.232745	3.787042	5.047933	-0.916851	0.118015	-0.004420

4.2444	1.107022	4.296207	5.097019	-0.965113	0.103687	0.000805
4.4802	1.257510	4.485554	5.278299	-1.034805	0.118260	0.000466
4.7160	1.254391	4.584656	5.259677	-1.040997	0.115141	0.003321
4.9518	1.177524	3.782820	5.755434	-0.884305	0.122014	0.003870
5.1876	1.078871	3.695930	5.900479	-0.830245	0.116960	0.001881
5.4234	1.080179	3.367563	6.135114	-0.742836	0.121994	-0.000933
5.6592	0.992304	3.078886	6.534036	-0.674039	0.122247	-0.000312
5.8950	0.911110	2.728821	6.695824	-0.609524	0.121454	-0.003712
6.1308	1.030472	2.354302	7.069266	-0.516034	0.141761	0.003635
6.3666	0.865117	2.469132	7.137334	-0.521290	0.123994	-0.000418
6.6024	0.751889	2.005250	7.448320	-0.403289	0.129601	-0.000631
6.8382	0.774884	2.060556	7.481416	-0.408106	0.133465	0.004549
7.0740	0.772313	1.541073	7.913927	-0.306458	0.134629	0.002353
7.3098	0.709894	1.514760	7.991761	-0.284959	0.132290	0.005037
7.5456	0.633963	0.938201	8.171576	-0.185438	0.134511	0.001695
7.7814	0.617978	1.127720	8.456439	-0.168903	0.132946	0.000997
8.0172	0.655536	0.926384	8.671544	-0.136908	0.138565	0.005876
8.2530	0.581546	0.344073	8.846180	-0.038076	0.142199	0.004245
8.4888	0.625831	0.429231	8.896154	-0.036914	0.148445	0.003205
8.7246	0.620619	-0.003937	9.187239	0.052344	0.147396	0.000120
8.9604	0.622794	-0.070145	9.206554	0.058862	0.152689	-0.000862
9.1962	0.480409	-0.366458	9.444407	0.140472	0.147618	0.002822
9.4320	0.614204	-0.471541	9.648932	0.153070	0.158391	0.001103
9.6678	0.633609	-1.246461	9.928724	0.252201	0.168534	0.004395
9.9036	0.605081	-1.221951	10.007480	0.260691	0.164211	0.001955
10.1394	0.630890	-1.336380	10.147070	0.299632	0.170016	-0.000906
10.3752	0.659933	-1.872796	10.374510	0.374055	0.174981	0.007256
10.6110	0.657735	-1.615663	10.311290	0.354510	0.176700	0.006070
10.8468	0.681330	-2.360565	10.692000	0.464065	0.183212	0.008577
11.0826	0.723350	-2.344677	10.544840	0.465760	0.181203	0.002581
11.3184	0.723708	-2.881654	10.908990	0.557780	0.187443	0.003508
11.5542	0.771627	-2.851565	10.807020	0.555464	0.192165	0.003618
11.7900	0.794398	-3.151340	11.015480	0.617103	0.192250	0.003076
12.0258	0.787250	-3.323462	11.099380	0.650653	0.201684	0.003643
12.2616	0.786055	-3.095791	11.250590	0.663698	0.201918	0.010158
12.4974	0.746605	-3.750811	11.199100	0.741000	0.201814	0.003789
12.7332	0.868389	-3.927008	11.206600	0.760344	0.211277	0.002569
12.9690	0.769803	-4.071033	11.390910	0.801416	0.204098	0.003791
13.2048	0.749033	-4.068032	11.579380	0.800114	0.204057	0.003510
13.4406	0.784971	-3.283856	11.938100	0.656393	0.207483	0.007277
13.6764	0.865663	-3.364345	11.921250	0.635424	0.212037	0.006326
13.9122	0.928999	-2.688344	12.282400	0.524609	0.221578	0.002853
14.1480	0.904198	-2.561791	12.298180	0.501557	0.222722	0.005819
14.3838	0.894668	-2.297608	12.613250	0.440629	0.226092	0.006380

14.6196	0.933192	-1.913136	12.897290	0.391157	0.232266	0.001462
14.8554	0.926238	-1.629921	12.890190	0.339457	0.230224	0.000656
15.0912	0.993884	-1.402783	13.261120	0.275079	0.236741	0.003729
15.3270	0.972327	-1.374339	13.212710	0.270864	0.238606	0.000285
15.5628	1.012980	-0.906360	13.461330	0.185240	0.239829	-0.000133
15.7986	1.000757	-0.701013	13.302330	0.168644	0.238724	-0.001054
16.0344	1.040871	-0.538642	13.661020	0.100434	0.247648	0.004485
16.2702	0.994893	-0.367738	13.520980	0.091722	0.250147	0.006607
16.5060	1.030075	-0.147975	13.678560	0.049423	0.248698	0.000687
16.7418	1.071440	0.116026	13.797320	0.011278	0.253843	0.005176
16.9776	1.072530	0.324308	13.879490	-0.017060	0.254247	0.007505
17.2134	1.164339	0.588796	13.983920	-0.079458	0.257284	-0.002657
17.4492	1.147966	0.605291	14.010320	-0.076452	0.262904	0.005174
17.6850	1.211840	0.836965	14.102830	-0.143933	0.260852	-0.002334
17.9208	1.214144	0.753155	14.030660	-0.136296	0.264037	-0.000593
18.1566	1.254629	1.304253	14.346490	-0.220802	0.267986	-0.000870
18.3924	1.314365	1.204827	14.196620	-0.223989	0.268506	-0.001297
18.6282	1.291890	1.333187	14.431320	-0.260326	0.274156	-0.002446
18.8640	1.296436	1.521413	14.521310	-0.295161	0.267993	-0.001767
19.0998	1.398837	1.910240	14.516130	-0.339817	0.273281	0.002709
19.3356	1.341781	2.161339	14.557060	-0.391220	0.270876	0.004125
19.5714	1.338814	2.027761	14.554800	-0.386211	0.272498	-0.000165
19.8072	1.449339	2.306920	14.764560	-0.453367	0.280308	0.006737
20.0430	1.467445	2.389112	14.589790	-0.454369	0.280377	0.003354
20.2788	1.551862	2.649340	14.871930	-0.524272	0.285300	0.001494
20.5146	1.510454	2.686975	14.743080	-0.524049	0.278211	-0.002898
20.7504	1.519888	2.702222	14.834960	-0.564396	0.281316	0.003247
20.9862	1.487625	2.748017	14.817480	-0.575929	0.278829	0.000200
21.2220	1.511306	2.911287	14.996910	-0.608029	0.280309	0.001779
21.4578	1.597214	3.230637	15.022210	-0.666116	0.285667	0.001930
21.6936	1.639336	3.216084	15.028830	-0.665354	0.287677	0.004043
21.9294	1.762364	3.414427	15.174040	-0.730665	0.294680	0.001545
22.1652	1.667080	3.528569	15.187880	-0.727613	0.291036	0.002543
22.4010	1.800206	3.656916	15.386440	-0.789033	0.296745	-0.005221
22.6368	1.818969	3.769042	15.306780	-0.790522	0.301929	0.001557
22.8726	1.895954	3.854634	15.520440	-0.831536	0.303370	0.001724
23.1084	1.840690	4.046613	15.425650	-0.855945	0.298693	-0.002547
23.3442	1.810002	3.714032	15.373540	-0.803436	0.302011	0.003728
23.5800	1.759099	3.515301	15.732420	-0.714312	0.303355	0.000154
23.8158	1.740623	3.120084	15.804960	-0.670786	0.303737	-0.003264
24.0516	1.631363	2.814031	16.153100	-0.587354	0.298825	0.002906
24.2874	1.703398	3.003543	16.218680	-0.587388	0.306501	-0.001638
24.5232	1.531925	2.520596	16.380810	-0.484391	0.300585	-0.000553
24.7590	1.581926	2.370373	16.532010	-0.471115	0.306044	-0.002231

24.9948	1.595505	2.226328	16.593600	-0.418024	0.303888	-0.002006
25.2306	1.547934	1.928738	16.749780	-0.369707	0.315796	-0.001115
25.4664	1.693373	1.796128	16.913380	-0.338006	0.328464	-0.000451
25.7022	1.575713	1.751919	17.050040	-0.303395	0.318243	0.001380
25.9380	1.523096	1.326706	16.910020	-0.253871	0.318564	-0.004923
26.1738	1.498471	1.419533	17.291870	-0.221151	0.317571	0.003497
26.4096	1.538854	1.094274	16.987470	-0.192595	0.324677	0.003269
26.6454	1.561321	0.721651	17.393240	-0.127255	0.327550	-0.003240
26.8812	1.459039	0.588574	17.225370	-0.103553	0.321181	0.005550
27.1170	1.505129	0.586385	17.388580	-0.078144	0.329485	0.004635
27.3528	1.522062	0.163902	17.411310	-0.026074	0.332440	-0.001146
27.5886	1.503049	0.066639	17.316120	0.004842	0.332776	0.006234
27.8244	1.398329	-0.042624	17.499320	0.036982	0.333373	0.006436
28.0602	1.423659	0.005591	17.517860	0.034458	0.332377	0.003648
28.2960	1.504053	-0.505023	17.794430	0.113183	0.344027	0.006706
28.5318	1.417762	-0.704414	17.403470	0.125361	0.333074	0.003906
28.7676	1.536685	-1.128204	17.813760	0.197058	0.342577	0.005867
29.0034	1.479668	-0.766853	17.608490	0.175073	0.337057	0.007557
29.2392	1.471179	-0.789179	17.805460	0.203240	0.340235	-0.001893
29.4750	1.467692	-1.359977	17.790860	0.258588	0.337317	0.000383
29.7108	1.366260	-1.293611	17.682250	0.264229	0.331946	0.007184
29.9466	1.508797	-1.743240	17.828400	0.327212	0.345117	0.006707
30.1824	1.457627	-1.635709	17.667820	0.318119	0.339711	0.004890
30.4182	1.515395	-2.102627	17.921580	0.397446	0.346517	0.007586
30.6540	1.415348	-1.981774	17.727310	0.380583	0.338917	0.007166
30.8898	1.563237	-2.062721	18.088580	0.417742	0.349009	0.000947
31.1256	1.453691	-2.349983	17.816860	0.447215	0.343076	0.003242
31.3614	1.441862	-2.504064	17.917930	0.487471	0.350974	0.005622
31.5972	1.459187	-2.655354	17.839860	0.506063	0.341102	0.007676
31.8330	1.559791	-3.167544	17.880630	0.565069	0.352409	0.007426
32.0688	1.505847	-3.019438	17.977150	0.575740	0.354065	0.003981
32.3046	1.526671	-3.137009	17.798580	0.581721	0.349303	-0.001415
32.5404	1.475564	-3.131456	17.970490	0.616140	0.348032	0.006891
32.7762	1.450013	-3.204846	17.790730	0.622190	0.343960	0.002941
33.0120	1.475162	-3.566344	18.041770	0.672267	0.346802	0.007773
33.2478	1.523365	-3.602839	17.830140	0.687253	0.353460	0.006318
33.4836	1.403269	-3.975184	17.806440	0.739611	0.340620	0.003605
33.7194	1.504771	-3.873099	17.884620	0.740682	0.343440	0.007991
33.9552	1.427688	-3.977224	17.836660	0.767860	0.345850	0.009375
34.1910	1.493589	-4.208669	17.994380	0.803463	0.353612	0.007355
34.4268	1.408343	-3.818278	18.064000	0.758832	0.340097	0.004965
34.6626	1.537721	-3.640599	18.198540	0.684196	0.352852	0.007817
34.8984	1.501494	-3.581915	17.976430	0.672430	0.349377	0.007874
35.1342	1.538031	-3.232889	18.291040	0.605150	0.356260	0.005499

35.3700	1.534890	-3.095428	18.132020	0.591666	0.360276	0.002860
35.6058	1.547863	-2.675298	18.292500	0.516139	0.354126	0.003361
35.8416	1.513743	-2.616342	18.212090	0.507929	0.356391	0.003607
36.0774	1.527705	-2.690934	18.346890	0.492245	0.360473	0.003636
36.3132	1.541817	-2.364004	18.247210	0.449832	0.360918	0.005101
36.5490	1.561284	-2.430845	18.180540	0.441416	0.358090	0.001432
36.7848	1.545337	-1.964547	18.318370	0.373194	0.362807	0.002835
37.0206	1.515610	-1.793453	18.103930	0.364539	0.360110	0.004288
37.2564	1.517479	-1.747156	18.200270	0.325343	0.362428	0.008443
37.4922	1.584246	-1.700730	18.042160	0.317050	0.366218	0.006105
37.7280	1.487890	-1.343744	18.320290	0.256717	0.367161	0.004701
37.9638	1.540500	-1.298178	17.938700	0.252820	0.362207	0.002430
38.1996	1.628785	-1.240249	17.992200	0.217115	0.367647	0.006715
38.4354	1.538568	-0.910191	17.857260	0.185976	0.359571	0.005071
38.6712	1.553487	-0.819410	17.801760	0.167008	0.359596	0.005762
38.9070	1.554239	-0.689963	17.735980	0.125334	0.359121	0.010732
39.1428	1.524264	-0.691743	17.554170	0.121748	0.357768	0.010070
39.3786	1.535792	-0.662548	17.570190	0.097410	0.357582	0.006553
39.6144	1.563596	-0.163547	17.434850	0.056507	0.360208	0.006652
39.8502	1.551626	-0.057088	17.413360	0.019756	0.357055	0.006544
40.0860	1.575096	-0.111981	17.201400	0.023543	0.358256	0.007712
40.3218	1.578943	-0.033119	17.341560	-0.011335	0.354285	0.001192
40.5576	1.540665	0.119260	17.199960	-0.025783	0.352763	0.006591
40.7934	1.611073	0.347768	17.188810	-0.059857	0.355018	0.000870
41.0292	1.577520	0.566063	17.021150	-0.100896	0.343970	0.000811
41.2650	1.595916	0.422422	16.966440	-0.082204	0.351658	0.005413
41.5008	1.618530	0.853698	17.062220	-0.152995	0.353796	0.004841
41.7366	1.658040	0.814870	16.898470	-0.138778	0.353472	0.003691
41.9724	1.559333	0.961084	16.968700	-0.182638	0.349532	0.005515
42.2082	1.590350	1.001263	16.615420	-0.189107	0.344840	0.001863
42.4440	1.625080	1.213334	16.728070	-0.231447	0.347179	0.005331
42.6798	1.691922	1.330122	16.646420	-0.246601	0.347417	0.000157
42.9156	1.629876	1.582514	16.655400	-0.285344	0.341660	0.005016
43.1514	1.690761	1.597933	16.645170	-0.305237	0.347080	-0.000144
43.3872	1.557018	1.605056	16.495590	-0.301675	0.336959	0.003864
43.6230	1.617942	1.828065	16.452000	-0.353079	0.337554	-0.001117
43.8588	1.650215	1.706659	16.345820	-0.339600	0.343366	0.002413
44.0946	1.731472	1.870807	16.346320	-0.378839	0.343417	0.005060
44.3304	1.692319	2.006854	16.133580	-0.383122	0.338939	0.000066
44.5662	1.677830	1.922228	16.136550	-0.408739	0.335539	0.001286
44.8020	1.741709	2.173699	16.086890	-0.431351	0.340795	0.004844
45.0378	1.777920	2.052713	16.096680	-0.425452	0.345386	0.005821
45.2736	1.740839	2.462029	16.020610	-0.477972	0.333735	-0.000449
45.5094	1.740000	2.380949	15.973900	-0.472347	0.335399	-0.000987

45.7452	1.791270	2.565063	16.011300	-0.518388	0.341843	-0.000695
45.9810	1.760832	2.825254	15.871970	-0.535417	0.331199	-0.000920
46.2168	1.781285	2.842755	15.806860	-0.563587	0.329917	-0.001508
46.4526	1.771388	2.760738	15.650620	-0.552301	0.329575	-0.000104
46.6884	1.855098	2.836130	15.787280	-0.576171	0.338047	-0.001778
46.9242	1.791606	2.792542	15.582410	-0.616017	0.333389	-0.000932
47.1600	1.765418	2.731733	15.555140	-0.589672	0.329969	0.002576
47.3958	1.834818	3.131818	15.586310	-0.640265	0.327528	-0.002669
47.6316	1.781704	3.225739	15.430730	-0.645276	0.322437	0.000857
47.8674	1.817461	3.290668	15.489870	-0.671723	0.328717	0.001307
48.1032	1.773149	3.204604	15.163380	-0.659100	0.321960	0.002118
48.3390	1.900681	3.388764	15.402250	-0.709009	0.331594	0.002148
48.5748	1.833749	3.360394	15.119650	-0.703997	0.323555	-0.003464
48.8106	1.841514	3.466491	15.119460	-0.728944	0.327214	0.000140
49.0464	1.888239	3.556489	15.113570	-0.750504	0.325478	-0.000292
49.2822	1.897331	3.619581	15.011150	-0.763041	0.320285	0.000637
49.5180	1.928788	3.605691	15.045030	-0.782763	0.324377	-0.002962
49.7538	1.945522	3.519855	14.835040	-0.766192	0.324636	-0.003098
49.9896	1.948104	3.919713	14.894440	-0.830219	0.322115	-0.002126
50.2254	1.926323	4.031950	14.765320	-0.834779	0.316851	-0.000604
50.4612	1.946167	4.039725	14.842150	-0.840629	0.325432	-0.002478
50.6970	1.929159	3.911113	14.553180	-0.846641	0.317403	-0.001146
50.9328	1.968722	3.898515	14.768870	-0.862209	0.322351	0.001331
51.1686	1.976331	4.073185	14.582300	-0.887064	0.319297	-0.001744
51.4044	1.876060	3.879504	14.321160	-0.859977	0.302423	-0.004484
51.6402	1.882311	3.513489	14.588930	-0.763713	0.318353	-0.000644
51.8760	1.883554	3.608294	14.482420	-0.765351	0.310997	-0.005021
52.1118	1.914296	3.428356	14.768170	-0.706959	0.319321	0.000002
52.3476	1.651165	3.306393	14.510850	-0.687787	0.298860	0.001356
52.5834	1.797596	3.096248	14.824900	-0.631176	0.313866	-0.002759
52.8192	1.734358	3.012599	14.675000	-0.614165	0.309100	0.004541
53.0550	1.582405	2.653434	14.743680	-0.559524	0.297346	-0.000410
53.2908	1.661615	2.747781	14.776570	-0.546428	0.307372	0.001000
53.5266	1.713410	2.531849	14.827710	-0.510453	0.314574	0.003220
53.7624	1.604283	2.218217	14.836610	-0.457303	0.308293	0.001303
53.9982	1.607376	2.539042	14.668640	-0.479964	0.304482	0.002737
54.2340	1.557079	2.180511	14.819990	-0.419079	0.303364	0.006230
54.4698	1.512906	2.251324	14.643240	-0.420078	0.301714	0.005560
54.7056	1.511374	1.889647	14.855750	-0.364985	0.300330	0.003421
54.9414	1.468735	1.816266	14.731690	-0.347516	0.298639	-0.002198
55.1772	1.446072	1.555995	14.757320	-0.305092	0.298016	0.002954
55.4130	1.505985	1.688138	14.779710	-0.299905	0.300395	0.001438
55.6488	1.374247	1.448207	14.706240	-0.258275	0.293761	-0.001225
55.8846	1.512705	1.250414	14.810160	-0.227476	0.305600	-0.001248

56.1204	1.433591	1.334280	14.559930	-0.235794	0.295690	0.002350
56.3562	1.382977	0.988139	14.780390	-0.174058	0.299547	-0.000930
56.5920	1.440588	1.067520	14.524200	-0.180445	0.294493	0.007235
56.8278	1.342914	0.862295	14.744040	-0.138751	0.295168	0.001052
57.0636	1.333325	0.944496	14.594500	-0.144797	0.289541	0.004711
57.2994	1.385227	0.610357	14.747220	-0.094326	0.298696	0.001257
57.5352	1.287815	0.544150	14.642630	-0.081233	0.289661	0.001679
57.7710	1.280419	0.815033	14.648070	-0.091265	0.288413	0.003429
58.0068	1.330341	0.409181	14.747550	-0.038720	0.299091	0.007608
58.2426	1.369048	0.459818	14.598740	-0.042405	0.297232	0.004665
58.4784	1.327814	-0.009444	14.708020	0.018929	0.293752	0.004996
58.7142	1.257489	0.233192	14.553430	-0.001080	0.290493	0.001123
58.9500	1.281924	-0.107610	14.614730	0.057098	0.291055	0.005603
59.1858	1.237712	-0.320469	14.440560	0.072625	0.288816	0.000208
59.4216	1.206455	-0.162781	14.707140	0.080734	0.290705	0.003521
59.6574	1.234836	-0.406268	14.622700	0.105497	0.291384	-0.000327
59.8932	1.259008	-0.601070	14.558030	0.137027	0.296319	0.005054
60.1290	1.214969	-0.756765	14.649180	0.158474	0.292218	0.006235
60.3648	1.247316	-0.809045	14.417550	0.166351	0.294724	0.002720
60.6006	1.257728	-0.826196	14.638830	0.179653	0.290814	0.001163
60.8364	1.221942	-1.054344	14.334260	0.206431	0.288533	0.003769
61.0722	1.163183	-0.895617	14.591110	0.212864	0.290434	0.002968
61.3080	1.221601	-1.176345	14.442830	0.225746	0.287046	0.000902
61.5438	1.166438	-1.352350	14.578620	0.264405	0.287340	0.002913
61.7796	1.237603	-1.367587	14.513580	0.267293	0.292347	0.003963
62.0154	1.166726	-1.381429	14.510550	0.289365	0.291126	0.002678
62.2512	1.207532	-1.479108	14.511650	0.304078	0.290123	0.000223
62.4870	1.122657	-1.433537	14.366290	0.306849	0.279563	0.001939
62.7228	1.247083	-2.125725	14.319980	0.374658	0.290928	0.002489
62.9586	1.242221	-1.994761	14.351460	0.366170	0.293307	0.007668
63.1944	1.229577	-1.602774	14.500110	0.352380	0.290587	0.007657
63.4302	1.186951	-1.957356	14.254180	0.385132	0.285052	0.004691
63.6660	1.119925	-2.090721	14.420010	0.415483	0.280915	-0.000070
63.9018	1.231266	-2.200644	14.328000	0.424070	0.287589	0.004190
64.1376	1.198787	-2.335229	14.354150	0.449690	0.289095	0.008567
64.3734	1.180552	-2.441525	14.198600	0.466048	0.284250	0.007601
64.6092	1.218145	-2.655210	14.202960	0.487950	0.288186	0.006267
64.8450	1.273014	-2.732438	14.319850	0.514392	0.295701	0.007366
65.0808	1.182983	-2.628802	14.093570	0.502568	0.286422	0.007624
65.3166	1.171508	-2.619452	14.130400	0.528237	0.280835	0.002919
65.5524	1.163624	-2.707507	14.059470	0.532421	0.284044	0.005841
65.7882	1.241332	-2.817658	14.203480	0.561656	0.291681	0.002451
66.0240	1.169548	-2.944660	14.042620	0.571712	0.285152	0.002093
66.2598	1.121529	-3.127679	14.154380	0.603417	0.281416	0.002962

66.4956	1.187489	-3.160748	14.007300	0.611995	0.284883	0.001438
66.7314	1.201701	-2.985098	14.003260	0.609335	0.286869	0.003895
66.9672	1.180933	-3.340322	13.979560	0.647289	0.286113	0.001679
67.2030	1.148937	-3.366084	13.803600	0.649857	0.282581	0.003106
67.4388	1.162834	-3.472233	13.867130	0.680195	0.282092	0.008283
67.6746	1.164013	-3.531362	13.694740	0.677624	0.281958	0.005868
67.9104	1.086092	-3.662865	13.848670	0.706070	0.277160	0.007137
68.1462	1.147305	-3.650482	13.676940	0.710325	0.282292	0.005104
68.3820	1.131069	-3.859865	13.723970	0.732624	0.278258	0.003208
68.6178	1.172589	-3.848778	13.556350	0.742260	0.278173	0.002751
68.8536	1.186299	-4.073457	13.544660	0.771572	0.284842	0.006996
69.0894	1.077126	-4.214924	13.507810	0.793067	0.271327	0.003322
69.3252	1.162792	-3.885349	13.479350	0.769829	0.280391	0.002883
69.5610	1.217421	-4.220047	13.502720	0.812031	0.283412	0.002091
69.7968	1.102563	-4.127952	13.319660	0.793497	0.270783	0.004388
70.0326	1.137556	-3.767131	13.369680	0.737946	0.274318	0.002828
70.2684	1.091923	-3.806095	13.114500	0.735534	0.271129	0.009020
70.5042	1.129889	-3.710677	13.237050	0.705253	0.276243	0.005707
70.7400	1.069246	-3.359175	13.058490	0.669629	0.268217	0.005629
70.9758	1.049076	-3.214296	13.166320	0.641336	0.263932	0.002506
71.2116	1.140403	-3.266836	13.236290	0.633114	0.278755	0.005140
71.4474	1.091401	-3.306626	13.014420	0.640000	0.270718	0.003654
71.6832	1.133766	-3.240590	13.231930	0.611073	0.276872	0.003173
71.9190	1.135204	-3.104462	13.045800	0.599226	0.272676	0.001521
72.1548	1.067173	-2.775303	13.120260	0.549879	0.271075	0.001389
72.3906	1.105280	-2.989770	12.928890	0.569341	0.265452	0.001517
72.6264	1.053826	-2.495497	12.918720	0.508062	0.264690	0.006568
72.8622	1.084031	-2.692845	12.943650	0.518993	0.269546	0.008882
73.0980	1.117886	-2.525456	12.822790	0.499133	0.271087	0.004765
73.3338	1.051758	-2.634273	12.852770	0.499811	0.264365	0.000958
73.5696	1.045120	-2.512221	12.887920	0.486636	0.267586	0.009549
73.8054	1.043018	-2.427157	12.855260	0.454481	0.266271	0.007533
74.0412	1.056138	-2.537395	12.714720	0.471350	0.262083	0.008369
74.2770	1.084326	-2.174179	12.771710	0.423701	0.271669	0.008020
74.5128	1.050436	-2.165624	12.670760	0.420240	0.266115	0.007340
74.7486	1.121529	-2.220742	12.793910	0.412756	0.270253	0.006591
74.9844	1.084630	-2.064236	12.620240	0.389756	0.262533	0.002691
75.2202	1.052219	-1.888884	12.615620	0.370301	0.267123	0.007945
75.4560	1.015679	-1.821031	12.641790	0.357840	0.264024	0.006755
75.6918	1.062331	-1.788719	12.565850	0.352272	0.264350	0.005922
75.9276	1.062793	-1.848083	12.605090	0.339816	0.261224	0.003211
76.1634	1.067665	-1.625880	12.354210	0.326430	0.262305	0.003666
76.3992	1.059634	-1.585195	12.487610	0.304100	0.261421	0.006661
76.6350	1.045843	-1.513018	12.294530	0.300364	0.259374	0.008765

76.8708	1.001390	-1.228843	12.322880	0.261852	0.257213	0.010441
77.1066	1.064960	-1.172506	12.206110	0.258591	0.259681	0.006808
77.3424	1.098211	-1.388722	12.296630	0.261569	0.261317	0.007679
77.5782	0.966499	-1.272037	12.184380	0.249703	0.257474	0.009285
77.8140	1.058696	-1.305492	12.186820	0.247183	0.258382	0.004873
78.0498	1.073369	-1.182117	12.158780	0.225765	0.262908	0.007690
78.2856	0.998147	-1.194745	11.930140	0.236218	0.250627	0.007005
78.5214	1.076887	-0.819981	12.076580	0.185105	0.258280	0.000359
78.7572	1.053593	-0.984346	11.916230	0.199719	0.257020	0.007551
78.9930	0.899340	-0.930992	11.916270	0.183438	0.245851	0.005675
79.2288	1.038305	-0.737121	11.846300	0.169715	0.256675	0.005313
79.4646	1.102154	-0.757444	11.930150	0.162394	0.258369	0.008642
79.7004	1.053343	-0.688274	11.738260	0.154201	0.257144	0.004897
79.9362	1.065882	-0.661138	11.639650	0.143139	0.251358	0.008466
80.1720	1.050204	-0.486885	11.645190	0.124095	0.249680	0.005192
80.4078	1.023875	-0.581558	11.566410	0.134227	0.253716	0.007842
80.6436	1.079480	-0.509007	11.598180	0.114910	0.252617	0.004439
80.8794	1.019211	-0.488937	11.390530	0.117308	0.246924	0.006635
81.1152	0.985291	-0.357738	11.497980	0.097100	0.244680	0.001328
81.3510	1.078994	-0.413764	11.328760	0.103799	0.256565	0.002769
81.5868	1.113109	-0.231708	11.375860	0.068835	0.251416	0.001927
81.8226	1.041068	-0.447710	11.160650	0.095321	0.244387	0.000415
82.0584	1.057579	-0.340441	11.224250	0.084271	0.249001	-0.002074
82.2942	0.972534	-0.347434	11.049560	0.077341	0.233979	0.001906
82.5300	1.084380	-0.229249	11.085400	0.060557	0.245410	0.001895
82.7658	1.080306	-0.093117	11.099610	0.043621	0.250210	0.001557
83.0016	1.127184	-0.206843	10.980720	0.048725	0.249752	-0.003162
83.2374	1.094166	-0.129540	10.961240	0.035702	0.247455	0.006452
83.4732	1.012118	-0.042274	10.725770	0.030042	0.242122	0.006024
83.7090	1.080564	0.052601	10.880480	0.012556	0.244188	0.001478
83.9448	1.117208	-0.069294	10.676050	0.019975	0.247626	0.002858
84.1806	1.180843	-0.035892	10.762000	0.017029	0.249118	0.000132
84.4164	1.096292	0.207692	10.611350	-0.010012	0.241157	0.000328
84.6522	1.084229	-0.079932	10.612290	0.011836	0.241214	-0.000973
84.8880	1.044942	0.269934	10.637540	-0.020364	0.243636	0.005214
85.1238	0.989406	0.184287	10.431110	-0.007449	0.231356	0.002797
85.3596	1.083148	0.237008	10.491380	-0.030959	0.234321	0.003984
85.5954	1.068932	0.158993	10.251700	-0.015978	0.236592	0.004282
85.8312	1.012856	0.195285	10.310990	-0.034869	0.228503	0.000602
86.0670	1.098132	0.215976	10.258290	-0.031334	0.240012	0.004287
86.3028	1.121947	0.176409	10.236390	-0.031166	0.240817	0.007188
86.5386	1.037234	0.600184	10.239400	-0.075100	0.228030	0.005426
86.7744	1.032054	0.184165	10.019060	-0.034974	0.230075	0.005436
87.0102	1.039390	0.303161	10.073790	-0.056509	0.230508	0.001628

87.2460	1.042889	0.331138	9.962479	-0.047515	0.234431	0.004266
87.4818	0.982231	0.303635	9.967030	-0.061221	0.225870	0.003109
87.7176	0.991839	0.389812	9.745571	-0.060884	0.224664	0.000329
87.9534	0.970333	0.391006	9.737831	-0.068456	0.224566	0.003295
88.1892	1.046094	0.149304	9.690487	-0.036563	0.234038	0.003310
88.4250	1.065917	0.542287	9.728113	-0.086123	0.231260	0.006451
88.6608	0.988735	0.390499	9.584087	-0.072182	0.226484	0.008332
88.8966	1.101748	0.475557	9.619687	-0.075715	0.236127	0.007689
89.1324	1.086452	0.353039	9.504519	-0.073445	0.230506	0.002748
89.3682	1.036168	0.360566	9.370166	-0.067401	0.225890	0.005093
89.6040	1.000669	0.535706	9.305988	-0.091852	0.223973	0.005551
89.8398	1.088329	0.426498	9.315235	-0.076849	0.231533	0.007771
90.0756	0.993703	0.630201	9.395387	-0.106137	0.223241	0.001388
90.3114	1.008636	0.353350	9.094779	-0.069700	0.222439	0.002318
90.5472	1.095096	0.463695	9.242865	-0.078290	0.235118	0.006232
90.7830	1.042127	0.400003	9.085094	-0.082825	0.223703	0.006436
91.0188	1.061118	0.517724	9.008820	-0.088680	0.226806	0.006246
91.2546	1.038779	0.433332	9.048936	-0.086398	0.227643	0.006978
91.4904	1.042420	0.367706	8.936823	-0.074965	0.224471	0.005584
91.7262	1.166574	0.461483	8.882554	-0.088570	0.232469	0.004075
91.9620	1.045306	0.453495	8.720898	-0.081510	0.222783	0.008225
92.1978	0.967378	0.575069	8.715433	-0.100568	0.218028	0.006416
92.4336	1.011806	0.416668	8.570075	-0.077581	0.221642	0.005960
92.6694	1.146504	0.403606	8.543975	-0.075260	0.229263	0.005918
92.9052	0.908354	0.437240	8.234096	-0.065657	0.212575	0.006029
93.1410	1.022635	0.368204	8.479191	-0.078465	0.224351	0.003920
93.3768	1.130717	0.380145	8.457668	-0.086311	0.228296	0.001888
93.6126	1.065793	0.505775	8.389209	-0.092141	0.222037	0.003978
93.8484	1.048781	0.638691	8.426540	-0.112563	0.225513	0.004211
94.0842	1.049471	0.414307	8.320354	-0.084494	0.221977	0.001463
94.3200	1.040224	0.691974	8.403084	-0.120320	0.221274	0.000714
94.5558	1.032658	0.533001	8.303312	-0.109542	0.222664	0.004626
94.7916	1.064496	0.700765	8.494891	-0.122949	0.235362	0.006428
95.0274	1.074272	0.629874	8.220976	-0.124344	0.227922	0.005844
95.2632	1.015067	0.372068	8.225803	-0.095108	0.224271	0.007436
95.4990	1.123227	0.487211	8.199961	-0.113608	0.230580	0.003940
95.7348	1.043001	0.469007	8.208364	-0.110587	0.224483	0.002497
95.9706	1.057669	0.608409	8.265036	-0.133271	0.225975	0.004333
96.2064	1.051570	0.759483	8.348259	-0.149415	0.226159	0.003330
96.4422	1.088711	0.747086	8.338917	-0.149680	0.227019	0.002333
96.6780	0.986644	0.572203	8.185095	-0.132439	0.218613	0.000305
96.9138	1.000829	0.646362	8.173628	-0.136887	0.224641	0.006466
97.1496	1.027903	0.788747	8.152763	-0.151755	0.220715	-0.000933
97.3854	1.103790	0.634204	8.196463	-0.141103	0.230631	0.004280

97.6212	1.068521	0.661432	8.113614	-0.148553	0.224423	0.001718
97.8570	1.087057	0.790738	8.159914	-0.155547	0.229522	0.001322
98.0928	1.120316	0.759758	8.060150	-0.162757	0.229977	-0.000249
98.3286	1.089447	1.016787	8.188911	-0.186087	0.224756	0.001117
98.5644	1.066955	0.671235	8.001987	-0.155014	0.223037	-0.000896
98.8002	1.082653	0.758811	8.093712	-0.162553	0.230505	0.007861
99.0360	1.065176	0.832821	8.129887	-0.164899	0.230436	0.006026
99.2718	1.119850	0.817685	7.979990	-0.172460	0.229501	0.004322
99.5076	1.043621	0.623303	8.030146	-0.159545	0.226639	0.006990
99.7434	1.065059	0.950756	8.065481	-0.190371	0.225191	0.007751
99.9792	1.146384	0.843986	8.088409	-0.179015	0.229808	0.005066
100.2150	1.084203	0.965497	8.053604	-0.197283	0.229227	0.006744
100.4508	1.110668	0.818967	8.001316	-0.178924	0.228302	0.000617
100.6866	1.143501	0.829069	7.980014	-0.180605	0.231068	0.000085
100.9224	1.034770	0.694792	7.899163	-0.171890	0.223791	0.008660
101.1582	1.078450	1.054438	8.171222	-0.210557	0.223812	0.006615
101.3940	1.125798	0.822276	7.974722	-0.188450	0.233152	0.006030
101.6298	0.982022	0.989581	7.951923	-0.201451	0.218253	0.000801
101.8656	1.210490	1.052056	7.993593	-0.208629	0.234607	0.000182
102.1014	1.069653	0.887960	7.905362	-0.193933	0.224671	0.004252
102.3372	1.028027	0.850383	7.900072	-0.195834	0.221509	-0.000397
102.5730	1.073864	0.876561	7.853551	-0.197298	0.224620	0.000586
102.8088	1.147919	1.097148	7.943334	-0.218476	0.230516	0.002171
103.0446	1.093727	0.842907	7.766543	-0.189990	0.230769	0.002463
103.2804	1.024911	1.095655	7.828289	-0.219352	0.221001	0.007629
103.5162	1.121928	0.961209	7.802579	-0.211348	0.230187	0.005800
103.7520	1.072173	1.066697	7.968173	-0.221145	0.225728	0.002830
103.9878	1.138305	1.019073	7.870606	-0.216451	0.232952	0.000696
104.2236	1.108603	0.887982	7.793540	-0.198814	0.229357	0.005715
104.4594	1.175166	0.979291	7.843665	-0.213392	0.232748	0.001565
104.6952	1.172004	1.173092	7.939817	-0.230883	0.235181	0.000797
104.9310	1.033068	1.181507	7.732716	-0.238241	0.217236	0.003379
105.1668	1.203878	1.109869	7.850416	-0.234868	0.234155	0.002694
105.4026	1.149730	1.107283	7.805227	-0.231283	0.231279	0.005695
105.6384	1.146148	1.029179	7.754345	-0.222973	0.232179	0.004787
105.8742	1.122456	1.232387	7.761471	-0.240962	0.226918	0.001156
106.1100	1.122315	1.057635	7.775016	-0.227247	0.229003	0.001199
106.3458	1.132956	1.038890	7.704210	-0.226819	0.224231	0.001241
106.5816	1.053456	1.079926	7.785179	-0.231379	0.224042	0.002905
106.8174	1.169725	1.169655	7.702609	-0.233974	0.236072	-0.000452
107.0532	1.188360	0.969844	7.732462	-0.221598	0.236699	0.001897
107.2890	1.128896	0.950281	7.652959	-0.217859	0.229221	0.002875
107.5248	1.240980	1.061860	7.683021	-0.237030	0.237256	0.002510
107.7606	1.150866	1.276972	7.753700	-0.254191	0.230146	0.000307

107.9964	1.191027	0.855187	7.617655	-0.218546	0.234270	0.007959
108.2322	1.100043	1.140745	7.597268	-0.234802	0.228377	0.001112
108.4680	1.105466	1.160298	7.735227	-0.238604	0.230654	0.001339
108.7038	1.100343	1.197266	7.594657	-0.245578	0.222213	0.000134
108.9396	1.138565	1.079690	7.639244	-0.230893	0.235112	0.005412
109.1754	1.148939	1.009655	7.675874	-0.226944	0.234517	0.001652
109.4112	1.061118	0.949342	7.465624	-0.220925	0.221711	0.001079
109.6470	1.153114	0.983737	7.585108	-0.231004	0.230675	0.007036
109.8828	1.131799	1.042385	7.473310	-0.233713	0.227905	0.007659
110.1186	1.080221	1.046351	7.477095	-0.234961	0.221062	0.004930
110.3544	1.080323	1.062536	7.503621	-0.231309	0.228287	0.006680
110.5902	1.087236	1.025807	7.510981	-0.227060	0.228026	0.008377
110.8260	1.108657	0.955041	7.477587	-0.221988	0.230555	0.005456
111.0618	1.109567	1.064434	7.448270	-0.230179	0.226787	0.007198
111.2976	1.122663	1.038088	7.549142	-0.235618	0.227788	0.007118
111.5334	0.983182	0.932455	7.295324	-0.214150	0.211268	0.001922
111.7692	1.116292	1.042193	7.488857	-0.226391	0.226795	0.001545
112.0050	1.168165	0.935678	7.355518	-0.217437	0.235892	0.003837
112.2408	1.130082	0.984150	7.301762	-0.221555	0.228051	-0.000057
112.4766	1.146793	1.004047	7.229210	-0.222549	0.230898	0.002124
112.7124	1.100418	0.666935	7.299870	-0.196248	0.228401	0.004902
112.9482	1.096853	1.122413	7.188536	-0.234270	0.219516	0.002584
113.1840	1.055731	0.877801	7.173708	-0.207050	0.224865	0.006883
113.4198	1.090539	1.077003	7.180192	-0.229815	0.224133	0.008413
113.6556	1.124580	0.816101	7.126955	-0.201339	0.229485	0.007054
113.8914	1.122256	0.614072	7.105707	-0.175850	0.231810	0.006272
114.1272	1.107315	0.682391	6.821781	-0.178102	0.228174	-0.000513
114.3630	1.110820	0.698589	6.802452	-0.179850	0.225218	0.005949
114.5988	1.019571	0.817569	6.779746	-0.182313	0.219072	0.004220
114.8346	1.078684	0.660027	6.634021	-0.164580	0.225029	0.007984
115.0704	1.048784	0.667357	6.519096	-0.150541	0.224218	0.009058
115.3062	1.005535	0.712023	6.393684	-0.146815	0.219797	0.004974
115.5420	0.912058	0.345602	6.008409	-0.107887	0.207311	0.004796
115.7778	0.884072	0.015690	5.249637	-0.022671	0.208643	0.006162
116.0136	0.864784	-1.262067	5.933780	0.246107	0.229484	0.004729
116.2494	0.987062	-2.317600	8.497533	0.456408	0.248978	0.004580
116.4852	0.928356	-2.425058	8.519954	0.469980	0.246244	0.003152
116.7210	0.894033	-2.285039	8.439880	0.459949	0.240248	0.002447
116.9568	0.866239	-2.347348	8.453560	0.463428	0.237916	0.000080
117.1926	0.940817	-2.317102	8.564166	0.459049	0.244719	0.003728
117.4284	0.896649	-2.263735	8.513962	0.458338	0.243753	0.003591
117.6642	0.855710	-2.458573	8.499940	0.472504	0.243908	0.002713
117.9000	0.888602	-2.175848	8.551859	0.448638	0.245452	-0.000547
118.1358	0.985532	-2.156241	8.640935	0.440218	0.250789	0.005197

118.3716	0.847021	-2.313866	8.542377	0.456676	0.238869	0.001907
118.6074	0.879943	-2.347714	8.627348	0.462144	0.241716	0.001896
118.8432	0.959713	-2.412716	8.500057	0.469157	0.249019	0.004452
119.0790	0.894965	-2.333084	8.548309	0.459235	0.245860	0.009509
119.3148	0.857462	-2.684525	8.368409	0.494211	0.243464	0.007893
119.5506	0.907146	-2.509515	8.509201	0.474157	0.246848	0.001008
119.7864	0.873017	-2.556319	8.401252	0.477655	0.239958	0.003800

Appendix C. Programming code for calculating variables in Chapter 5

This appendix provides the programming code for solving equations to obtain variables in Chapter 5.

The programming code is presented below:

```
% Define variables
syms L E F a k h1 h2 b H w Y1 Y2 Y3 Y4 Y5 Y6 Y7 Y8 Y9

% Bring in a set of experimental data
b=0.0005; L=0.009; H=0.01; a=0.01; F=5; E=2000000; w=0.008;

% Establish a system of equations
eqn1= L*F*a/(E*w) + k*h1^3/6 + k*h2^3/6 + b*h1^2/2 + b*h2^2/2 +b^3/(3*k^2)
+H*b^2/(2*k) == h2*b^2/(2*k)+h1*b^2/(2*k)+H*h2*b+k*h2^2*H/2;
eqn2= L*F/(E*w)==k*h1^2/2 - k*h2^2/2 + b*(h1-h2);
eqn3= k*(H-h1-h2)^2+2*(L-2*b)*(H-h1-h2)==k*(L-2*b)^2;
eqns=[eqn1 eqn2 eqn3];

% Compute analytic solution of a symbolic equation
solution = solve(eqns,[h1,h2,k],...
    "Real",true...
    "PrincipalValue",true);

% Display symbolic solution returned by solve
displaySymSolution(solution);

% Verify solution to determine if it is satisfactory
Expr1 =k*(H-h1-h2)^2+2*(L-2*b)*(H-h1-h2); Y1= subs(Expr1,solution)
Expr2 =k*(L-2*b)^2; Y2= subs(Expr2,solution)
Expr3 =L*F/(E*w); Y3= subs(Expr3,solution)
Expr4 =k*h1^2/2 - k*h2^2/2 + b*(h1-h2); Y4= subs(Expr4,solution)
Expr5 =L*F*a/(E*w) + k*h1^3/6 + k*h2^3/6 + b*h1^2/2 + b*h2^2/2 +b^3/(3*k^2)
+H*b^2/(2*k); Y5= subs(Expr5,solution)
Expr6= h2*b^2/(2*k)+h1*b^2/(2*k)+H*h2*b+k*h2^2*H/2; Y6= subs(Expr6,solution)

% Compare the effect of adding lateral forces on stress distribution
Expr7=-b*(h1+h2)+(k*h1^2+k*h2^2)/2+b^2/k;Y7=subs(Expr7,solution)

% Calculate the maximum friction force after applying lateral force
```

```
Expr8=(-b*(h1+h2)+(k*h1^2+k*h2^2)/2+b^2/k+2*b*H)/H/L*E*H*w*2*0.23;  
Y8=subs(Expr8,solution)
```

```
% Calculate the maximum friction force without lateral force
```

```
Expr9=2*b/L*E*H*w*2*0.4; Y9=subs (Expr9, solution)
```

References

- [1] V. Masson-Delmotte, P. Zhai, A. Pirani, et al., “Climate change 2021: The physical science basis,” Contribution of Working Group I to the Sixth Assessment Report of the Intergovernmental Panel on Climate Change, Cambridge University Press, 2021.
- [2] C. Le Quéré, R. M. Andrew, P. Friedlingstein, et al., “Global carbon budget 2018,” *Earth Syst. Sci. Data*, vol. 10, no. 4, pp. 2141-2194, 2018.
- [3] D. Lüthi, M. Le Floch, B. Bereiter, et al., “High-resolution carbon dioxide concentration record 650,000–800,000 years before present,” *Nature*, vol. 453, no. 7193, pp. 379-382, 2008.
- [4] H.-O. Pörtner, D. C. Roberts, V. Masson-Delmotte, et al., “IPCC special report on the ocean and cryosphere in a changing climate,” IPCC, 2019.
- [5] M. Collins, R. Knutti, J. Arblaster, et al., “Long-term climate change: Projections, commitments and irreversibility,” in *Climate Change 2013: The Physical Science Basis. Contribution of Working Group I to the Fifth Assessment Report of the Intergovernmental Panel on Climate Change*, T. F. Stocker, Ed. Cambridge University Press, 2013, pp. 1029–1136.
- [6] S. C. Sherwood and M. Huber, “An adaptability limit to climate change due to heat stress,” *Proc. Natl. Acad. Sci.*, vol. 107, no. 21, pp. 9552-9555, May 2010.
- [7] T. A. Carleton, M. Delgado, M. Greenstone, et al., “Valuing the global mortality consequences of climate change accounting for adaptation costs and benefits,” *The University of Chicago, Becker Friedman Institute for Economics Working Paper No. 2020-51*, 2020.
- [8] IPCC, "Climate Change 2022: Impacts, Adaptation and Vulnerability," 2022.
- [9] IPCC, "Climate Change 2022: Mitigation of Climate Change," 2022.
- [10] IPCC, *Global Warming of 1.5°C. An IPCC Special Report*, 2018.
- [11] C. Figueres, H. J. Schellnhuber, G. Whiteman, et al., “Three years to safeguard our climate,” *Nature*, vol. 546, no. 7660, pp. 593-595, June 2017.
- [12] O. D. Elisha, “Moving Beyond Take-Make-Dispose to Take-Make-Use for Sustainable Economy,” *International Journal of Scientific Research in Education*, vol. 13, pp. 497–516, June 2020.
- [13] J. Kirchherr, D. Reike and M. Hekkert, “Conceptualizing the circular economy: An analysis of 114 definitions,” *Resour. Conserv. Recycl.*, vol. 127, pp. 221-232, Sept. 2017.
- [14] M. Geissdoerfer, P. Savaget, N. M. P. Bocken and E. J. Hultink, “The circular economy—A new sustainability paradigm?,” *J. Clean. Prod.*, vol. 143, pp. 757-768, Feb. 2017.

- [15] Ellen MacArthur Foundation (EMF), Towards a Circular Economy: Business Rationale for an Accelerated Transition, EMF, 2015.
- [16] N. M. P. Bocken, E. J. Hultink, and C. B. Davis, "Product design and business model strategies for the circular economy," *J. Ind. Prod. Eng.*, vol. 38, no. 5, pp. 1605–1618, Apr. 2021.
- [17] Circle Economy, The Circularity Gap Report 2021, 2021. [Online]. Available: <https://www.circularity-gap.world/2021>.
- [18] W. Ijomah, "Addressing decision making for remanufacturing operations and design-for-remanufacture," *Int. J. Sustain. Eng.*, vol. 2, no. 2, pp. 91-102, June 2009.
- [19] R. Geyer and T. Jackson, "Supply loops and their constraints: The industrial ecology of recycling and reuse," *Calif. Manage. Rev.*, vol. 46, no. 2, pp. 55-73, Winter 2004.
- [20] D. Mangun and D. L. Thurston, "Incorporating component reuse, remanufacture, and recycle into product portfolio design," *IEEE Trans. Eng. Manag.*, vol. 49, no. 4, pp. 479-490, Nov. 2002.
- [21] K. Kim, I. Song, J. Kim and B. Jeong, "Supply planning model for remanufacturing system in reverse logistics environment," *Comput. Ind. Eng.*, vol. 54, no. 2, pp. 279-287, Mar. 2008.
- [22] V. D. R. Guide and L. N. Van Wassenhove, "The evolution of closed-loop supply chain research," *Oper. Res.*, vol. 57, no. 1, pp. 10-18, Jan.-Feb. 2009.
- [23] S. Statham, "Remanufacturing Towards a More Sustainable Future," Electronics-enabled Products Knowledge-transfer Network, Wolfson School of Mechanical and Manufacturing Engineering, Loughborough University, Loughborough, 2006.
- [24] S. Dowlatshahi, "A strategic framework for the design and implementation of remanufacturing operations in reverse logistics," *International Journal of Production Research*, vol. 43, no. 16, Aug. 2005,
- [25] P. Georgiadis and M. Besiou, "Environmental and economical sustainability of WEEE closed-loop supply chains with recycling: A system dynamics analysis," *Int. J. Adv. Manuf. Technol.*, vol. 47, no. 5-8, pp. 475–493, 2010.
- [26] A. Desai and A. Mital, "Evaluation of disassemblability to enable design for disassembly in mass production," *Int. J. Ind. Ergon.*, vol. 32, no. 4, pp. 265-281, Oct. 2003.
- [27] O. I. Avram and P. Xirouchakis, "Evaluating the use phase energy requirements of a machine tool system," *J. Clean. Prod.*, vol. 19, no. 6-7, pp. 699-711, Apr. 2011.
- [28] H. C. Fang, S. K. Ong, and A. Y. C. Nee, "Product Remanufacturability Assessment based on Design Information," *Procedia CIRP*, vol. 15, pp. 195-200, Dec. 2014.

- [29] S. Wu, N. Kaden, and K. Dröder, "A Systematic Review on Lithium-Ion Battery Disassembly Processes for Efficient Recycling," *Batteries*, vol. 9, no. 6, p. 297, May 2023.
- [30] S. Parsa and M. Saadat, "Intelligent selective disassembly planning based on disassemblability characteristics of product components," *The International Journal of Advanced Manufacturing Technology*, vol.104, no. 5-8, pp. 1769-1783, June 2019.
- [31] H. C. Fang, S. K. Ong, and A. Y. C. Nee, "Use of Embedded Smart Sensors in Products to Facilitate Remanufacturing," *Handbook of Manufacturing Engineering and Technology*, 2015
- [32] I. H. Sarker, "AI-Based Modeling: Techniques, Applications and Research Issues Towards Automation, Intelligent and Smart Systems," *SN Computer Science*, vol. 3, no. 158, Feb. 2022.
- [33] J. R. Duflou, J. W. Sutherland, D. Dornfeld, C. Herrmann, J. Jeswiet, S. Kara, M. Hauschild, and K. Kellens, "Towards energy and resource efficient manufacturing: A processes and systems approach," *CIRP Ann.*, vol. 61, no. 2, pp. 587–609, 2012.
- [34] S. Kara, P. Pornprasitpol and H. Kaebernick, "Selective disassembly sequencing: A methodology for the Disassembly of End-of-Life Products," *CIRP Ann.*, vol. 58, no. 1, pp. 37–40, 2006.
- [35] A. Priyono and K. H. Tan, "Disassembly for remanufacturing: A systematic literature review, new model development and future research needs," *Journal of Industrial Engineering and Management*, vol. 10, no. 3, pp. 596-630, 2017, doi: 10.3926/jiem.2053.
- [36] J. Liu, Z. Zhou, D. T. Pham, W. Xu, C. Ji, and Q. Liu, 'Robotic disassembly sequence planning using enhanced discrete bees algorithm in remanufacturing', *Int J Prod Res*, vol. 56, no. 9, pp. 3134–3151, 2018, doi: 10.1080/00207543.2017.1412527.
- [37] Y. Laili, F. Tao, D. T. Pham, Y. Wang, and L. Zhang, 'Robotic disassembly re-planning using a two-pointer detection strategy and a super-fast bees algorithm', *Robot Comput Integr Manuf*, vol. 59, no. April, pp. 130–142, 2019, doi: 10.1016/j.rcim.2019.04.003.
- [38] Q. Liu, Z. Liu, W. Xu, Q. Tang, Z. Zhou, and D. T. Pham, 'Human-robot collaboration in disassembly for sustainable manufacturing', *Int J Prod Res*, vol. 57, no. 12, pp. 4027–4044, 2019, doi: 10.1080/00207543.2019.1578906.
- [39] G. Foo, S. Kara, and M. Pagnucco, "Challenges of robotic disassembly in practice," *Procedia CIRP*, vol. 105, pp. 513-518, 2022.
- [40] D. W. Apley, G. Seliger, L. Voit, and J. Shi, 'Diagnostics in disassembly unscrewing operations', *International Journal of Flexible Manufacturing Systems*, vol. 10, no. 2, pp. 111–128, 1998, doi: 10.1023/A:1008089230047.
- [41] W. H. Chen, G. Foo, S. Kara, and M. Pagnucco, 'Application of a multi-head tool for robotic disassembly', *Procedia CIRP*, vol. 90, no. March, pp. 630–635, 2020, doi: 10.1016/j.procir.2020.02.047.

- [42] P. Schumacher and M. Jouaneh, "A force sensing tool for disassembly operations," *Robot. Comput. Integr. Manuf.*, vol. 30, no. 2, pp. 206–217, 2014.
- [43] P. Schumacher and M. Jouaneh, "A system for automated disassembly of snap-fit covers," *International Journal of Advanced Manufacturing Technology*, vol. 1, no. 15, pp. 2055–2069, 2013.
- [44] J. Huang, D. T. Pham, R. Li, K. Jiang, D. Lyu, and C. Ji, "Strategies for Dealing with Problems in Robotised Unscrewing Operations," in *Leveraging Technology for a Sustainable World*, Springer, Cham, pp. 93–107, 2019.
- [45] R. Li, D. T. Pham, J. Huang, Y. Tan, M. Qu, Y. Wang, M. Kerin, K. Jiang, S. Su, C. Ji, Q. Liu, and Z. Zhou, "Unfastening of Hexagonal Headed Screws by a Collaborative Robot," in *IEEE Transactions on Automation Science and Engineering*, vol. 17, no. 3, pp. 1455–1467, July 2020.
- [46] S. Vongbunyong, P. Vongseela, and J. Sreerattana-aporn, "A process demonstration platform for product disassembly skills transfer," *Procedia CIRP*, vol. 61, pp. 281–286, 2017.
- [47] M. Marconi, M. Germani, M. Mandolini, and C. Favi, "Applying data mining technique to disassembly sequence planning: A method to assess effective disassembly time of industrial products," *International Journal of Production Research*, vol. 57, no. 2, pp. 599–623, 2019, doi: 10.1080/00207543.2018.1472404.
- [48] M. Merdan, W. Lepuschitz, T. Meurer, and M. Vincze, "Towards ontology-based automated disassembly systems," 2010 IEEE 36th Annual Conference on Industrial Electronics Society, pp. 1392–1397, 2010.
- [49] F. Kecici, M. Tonko, H.-H. Nagel, and V. Gengenbach, "Improving visually servoed disassembly operations by automatic camera placement," in *Proceedings 1998 IEEE International Conference on Robotics and Automation (Cat. No.98CH36146)*, vol. 3, pp. 2947–2952, 1998.
- [50] J. Huang, D. T. Pham, R. Li, M. Qu, Y. Wang, M. Kerin, S. Su, C. Ji, O. Mahomed, R. Khalil, D. Stockton, W. Xu, Q. Liu, and Z. Zhou, "An experimental human-robot collaborative disassembly cell," *Computers & Industrial Engineering*, vol. 155, Art. no. 107189, 2021.
- [51] C. Klas, F. Hundhausen, J. Gao, C. R. G. Dreher, S. Reither, Y. Zhou, and T. Asfour, "The KIT Gripper: A Multi-Functional Gripper for Disassembly Tasks," 2021 IEEE/RSJ International Conference on Intelligent Robots and Systems (IROS), pp. 4582–4589, 2021.
- [52] H. Poschmann, H. Brüggemann and D. Goldmann, "Disassembly 4.0: A Review on Using Robotics in Disassembly Tasks as a Way of Automation," in *Chemie Ingenieur Technik*, vol. 92, no. 4, pp. 341–359, 2020.
- [53] M. Daneshmand, F. Noroozi, C. Corneanu, F. Mafakheri, and P. Fiorini, "Industry 4.0 and Prospects of Circular Economy: A Survey of Robotic Assembly and Disassembly," *arXiv preprint arXiv:2106.07270*, 2021.

- [54] H. McCallion, G. R. Johnson, and D. T. Pham, "A compliant device for inserting a peg in a hole," *Industrial Robot*, vol. 6, no. June, pp. 81–87, 1979, doi: <https://doi.org/10.1108/eb004754>.
- [55] D. E. Whitney, "Quasi-static assembly of compliantly supported rigid parts," *J Dyn Syst Meas Control*, vol. 104, no. 1, pp. 65–77, 1982, doi: 10.1115/1.3149634.
- [56] T. Lozano-Pérez, M. T. Mason, and R. H. Taylor, "Automatic synthesis of fine-motion strategies for robots," *International Journal of Robotics Research*, vol. 3, no. 1, pp. 3-24, 1984.
- [57] H. Zohoor and M. Shahinpoor, "Dynamic analysis of peg-in-hole insertion for manufacturing automation," *Journal of Manufacturing Systems*, vol. 10, no. 2, pp. 99-108, 1991.
- [58] N. Pitchandi, S. P. Subramanian and M. Irulappan, "Insertion force analysis of compliantly supported peg-in-hole assembly," *Assembly Automation*, vol. 37, no. 3, pp. 285-295, 2017.
- [59] Y. Zhang, H. Lu, D. T. Pham, Y. Wang, M. Qu, J. Lim, and S. Su, "Peg-hole disassembly using active compliance," *R Soc Open Sci*, vol. 6, no. 8, p. 190476, 2019, doi: 10.1098/rsos.190476.
- [60] X. Li, R. Li, H. Qiao, C. Ma and L. Li, "Human-Inspired Compliant Strategy for Peg-in-Hole Assembly Using Environmental Constraint and Coarse Force Information," in *Proceedings of the IEEE/RSJ International Conference on Intelligent Robots and Systems*, 2017, pp. 4743-4748.
- [61] M.W. Abdullah, H. Roth, M. Weyrich, J. Wahrburg, "An approach for peg-in-hole assembling using intuitive search algorithm based on human behavior and carried by sensors guided industrial robot," *IFAC-PapersOnLine*, vol. 48, no. 3, pp. 1476-1481, 2015.
- [62] J. Su, H. Qiao, Z. Ou, and Y. Zhang, "Sensor-less insertion strategy for an eccentric peg in a hole of the crankshaft and bearing assembly," *Assembly Automation*, vol. 32, no. 1, pp. 86–99, 2012.
- [63] J. Wang, A. Liu, X. Tao, and H. Cho, "Microassembly of micropeg and-hole using uncalibrated visual servoing method," *Precis. Eng.*, vol. 32, no. 3, pp. 173–181, 2008.
- [64] R. J. Chang, C. Y. Lin, and P. S. Lin, "Visual-Based Automation of Peg-in-Hole Microassembly Process," *J. Manuf. Sci. Eng.*, vol. 133, no. 4, 2011.
- [65] Y. Fei and X. Zhao, "An assembly process modeling and analysis for robotic multiple peg-in-hole," *J. Intell. Robot. Syst.*, vol. 36, no. 2, pp. 175–189, 2003.
- [66] K. Zhang, M. Shi, J. Xu, F. Liu, and K. Chen, "Force control for a rigid dual peg-in-hole assembly," *Assem. Autom.*, vol. 37, no. 2, pp. 200–207, 2017.
- [67] Y. Zhao, F. Gao, Y. Zhao, and Z. Chen, "Peg-in-Hole Assembly Based on Six-Legged Robots with Visual Detecting and Force Sensing," *Sensors*, vol. 20, no. 11, p. 3124, 2020.

- [68] W. Li, H. Cheng, C. Li, and X. Zhang, "Robotic assembly for irregular shaped peg-in-hole with partial constraints," *Appl. Sci.*, vol. 11, no. 16, p. 7394, 2021.
- [69] X. Zhang, Y. Zheng, J. Ota, and Y. Huang, "Peg-in-Hole Assembly Based on Two-phase Scheme and F/T Sensor for Dual-arm Robot," *Sensors*, vol. 17, no. 9, p. 2004, Sep. 2017, doi: 10.3390/s17092004.
- [70] R. S. Khurmi and J. K. Gupta, *Machine Design*. Ram Nagar, New Delhi, Eurasia Publishing House (PVT.) Ltd., 2005.
- [71] A. O. Lebeck, *Principles and design of mechanical face seals*. New York: John Wiley&Sons, Inc., 1991.
- [72] R. P. Goel, "Analysis of an interference-fit pin connection," *IEEE Trans. Compon. Hybrids Manuf. Technol.*, vol. 1, no. 3, pp. 248–251, 1978.
- [73] D. Song, Y. Li, K. Zhang, P. Liu, H. Cheng, and T. Wu, "Stress distribution modeling for interference-fit area of each individual layer around composite laminates joint," *Compos. Part B Eng.*, vol. 78, pp. 469-479, 2015.
- [74] J. F. Jiang and Y. B. Bi, "An elastic-plastic analysis of interference fit connection," in *Proc. 2nd Int. Workshop Mater. Sci. Mech. Eng.*, 2019, pp. 012071.
- [75] D. Croccolo and N. Vincenzi, "A generalized theory for shaft-hub couplings," *Proc. IMechE, Part C: J. Mechanical Engineering Science*, vol. 223, no. 9, pp. 2231-2239, Sep. 2009.
- [76] M. Paredes, N. Nefissi, and M. Sartor, "Study of an interference fit fastener assembly by finite element modelling, analysis and experiment," *Int J Interact Des Manuf*, vol. 6, no. 3, pp. 171-177, 2012.
- [77] S. Sen and B. Aksakal, "Stress analysis of interference fitted shaft–hub system under transient heat transfer conditions," *Mater. Des.*, vol. 25, no. 5, pp. 407–417, 2004.
- [78] Y. Zhang, B. McClain and X.D. Fang, "Design of interference fits via finite element method," *Int. J. Mech. Sci.*, vol. 42, no. 9, pp. 1835-1850, 2000.
- [79] J. Shen, D. Chen, G. Liu, D. Zhou and X. Du, "FEM analysis of stress on shaft-sleeve interference fits," *Adv. Mater. Res.*, vol. 668, pp. 495-499, 2013.
- [80] F. Lanoue, A. Vadean and B. Sanschagrin, "Finite element analysis and contact modelling considerations of interference fits for fretting fatigue strength calculations," *Simul. Model. Pract. Theory*, vol. 17, no. 10, pp. 1587-1602, 2009.
- [81] P. Pedersen, "On shrink fit analysis and design," *Computational Mechanics*, vol. 37, no. 2, pp. 121-130, 2006.
- [82] S. Niu, "Numerical simulation of interference assembly of shaft and sleeve," *Int. J. Eng. Adv. Res. Technol.*, vol. 1, no. 2, pp. 35-37, Aug. 2015.

- [83] J. Mackerle, "Finite element analysis of fastening and joining: A bibliography (1990–2002)," *International Journal of Pressure Vessels and Piping*, vol. 80, no. 4, pp. 253–271, 2003.
- [84] R. Lewis, M. B. Marshall, and R. S. Dwyer-Joyce, "Measurement of interface pressure in interference fits," *Proc. IMechE, Part C: J. Mech. Eng. Sci.*, vol. 219, no. 10, pp. 1039–1046, Oct. 2005.
- [85] L. Bottini and A. Boschetto, "Interference fit of material extrusion parts," *Additive Manufacturing*, vol. 25, pp. 335–346, Jan. 2019.
- [86] J. Jiang et al., "Influence of interference fit size on hole deformation and residual stress in hi-lock bolt insertion," *Proc. IMechE Part C: J. Mechanical Engineering Science*, vol. 228, no. 18, pp. 3296–3305, 2014.
- [87] B. Parsons and E. K. Wilson, "A method for determining the surface contact stresses resulting from interference fits," *Journal of Engineering for Industry*, vol. 92, no. 1, pp. 208–218, 1970.
- [88] I. Sogalad and N. G. S. Udupa, "A comparative study of stress distribution in interference fitted assemblies," *Indian Journal of Engineering and Materials Sciences*, vol. 13, pp. 397–404, 2006.
- [89] H. Hüyük, O. Music, A. Koç, C. Karadogan, and Ç. Bayram, "Analysis of elastic-plastic interference-fit joints," *Procedia Eng.*, vol. 81, pp. 2030–2035, 2014.
- [90] Z. Liu, L. Song, Z. Hou, K. Chen, S. Liu, and J. Xu, "Screw insertion method in peg-in-hole assembly for axial friction reduction," *IEEE Access*, vol. 7, pp. 148313–148325, 2019.
- [91] D. Croccolo, M. De Agostinis, and N. Vincenzi, "Design of hybrid steel-composite interference fitted and adhesively bonded connections," *Int. J. Adhes. Adhes.*, vol. 37, pp. 19–25, 2012.
- [92] G. M. Yang, J. C. Coquille, J. F. Fontaine, and M. Lambertin, "Contact pressure between two rough surfaces of a cylindrical fit," *J. Mater. Process. Technol.*, vol. 123, no. 2, pp. 490–497, Apr. 2002.
- [93] J. Madej and M. Sliwka, "Analysis of interference-fit joints," *Appl. Sci.*, vol. 11, no. 23, p. 11428, Nov. 2021.
- [94] X. Wang, Z. Lou, X. Wang, and C. Xu, "A new analytical method for press-fit curve prediction of interference fitting parts," *J. Mater. Process. Tech.*, vol. 250, pp. 16–24, Sep. 2017.
- [95] J. A. Regalbuto and O. E. Wheeler, "Stress distributions from interference fits and uniaxial tension," *Exp. Mech.*, vol. 10, no. 7, pp. 274–280, Jul. 1970.

- [96] T. Wu, K. Zhang, H. Cheng, P. Liu, D. Song, and Y. Li, "Analytical modeling for stress distribution around interference fit holes on pinned composite plates under tensile load," *Compos. Part B Eng.*, vol. 100, pp. 176–185, Sep. 2016.
- [97] M. Qu, D. T. Pham, F. Altumi, A. Gbadebo, N. Hartono, K. Jiang, M. Kerin, F. Lan, M. Micheli, S. Xu and Y. Wang, "Robotic Disassembly Platform for Disassembly of a Plug-In Hybrid Electric Vehicle Battery: A Case Study," *Automation*, vol. 5, pp. 50–67, 2024.
- [98] K. Wegener, W. Chen, F. Dietrich, K. Dröder and S. Kara, "Robot Assisted Disassembly for the Recycling of Electric Vehicle Batteries," *Procedia CIRP*, vol. 29, pp. 716-721, 2015.
- [99] K. Wegener, S. Andrew, A. Raatz, K. Dröder and C. Herrmann, "Disassembly of Electric Vehicle Batteries Using the Example of the Audi Q5 Hybrid System," *Procedia CIRP*, vol. 23, pp. 155-160, 2014.
- [100] A. Pražanová, V. Knap and D.-I. Stroe, "Literature Review, Recycling of Lithium-Ion Batteries from Electric Vehicles, Part II: Environmental and Economic Perspective," *Energies*, vol. 15, no. 7356, 2022.
- [101] "Unplug." Collins English Dictionary, HarperCollins Publishers. Available: <https://www.collinsdictionary.com/dictionary/english/unplug>. Accessed 22 Sept. 2023.
- [102] R. G. Budynas, J. K. Nisbett, *Shigley's Mechanical Engineering Design*. 9th ed. New York: McGraw-Hill, 2011. p. 229.
- [103] N. Laghzale and A. Bouzid, "Analytical Modelling of Elastic-Plastic Interference Fit Joints," *International Review on Modelling and Simulations*, vol. 9, no. 3, pp. 191-199, June 2016, doi: 10.15866/iremos.v9i3.8703.
- [104] D. Askeland, P. Fulay, *The Science & Engineering of Materials*, 5th ed. Boston: Cengage Learning, 2006.
- [105] S. Timoshenko, *Strength of Materials*, 2nd ed. New York, D. Van Nostrand Company, Inc., 1940.
- [106] W. C. Young, R. G. Budynas, and A. M. Sadegh, *Roark's Formulas for Stress and Strain*, 8th ed. New York, NY, USA: McGraw-Hill, 2011.
- [107] R. L. Norton, *Machine Design: An Integrated Approach*. Upper Saddle River, NJ: Pearson/Prentice Hall, 2004.
- [108] Dassault Systèmes, "ABAQUS Unified FEA - SIMULIA by Dassault Systèmes®," [Online]. Available: <https://www.3ds.com/products-services/simulia/products/abaqus>. [Accessed: May 31, 2023].
- [109] Dassault Systèmes, *Abaqus 6.11: Abaqus/CAE User's Manual*. Providence, RI: Dassault Systèmes Simulia Corp, 2011.

- [110] Ansys, "Ansys Granta EduPack | Software for Materials Education," [Online]. Available: <https://www.ansys.com/products/materials/granta-edupack>. [Accessed: May 31, 2023].
- [111] C. A. Harper, "Connectors and Sockets," in Handbook of Wiring, Cabling, and Interconnecting for Electronics, New York: McGraw-Hill, 1972, pp. 1-136–1-147.
- [112] S. K. De and J. R. White, Eds., Rubber Technologist's Handbook, vol. 1, 1st ed. Shrewsbury, UK: Smithers Rapra Publishing, 2001.
- [113] R. Askeland and W. Wright, The Science and Engineering of Materials, 7th ed. Boston, MA: Cengage Learning, 2016.
- [114] R.C. Hibbeler, Mechanics of Materials, 10th ed. Boston, MA: Pearson, 2016.
- [115] IEEE Standard Reference Designations for Electrical and Electronics Parts and Equipments, IEEE Std 200-1975, 1975.
- [116] R. Resnick, D. Halliday, and J. Walker, Fundamentals of Physics, 10th ed. Hoboken, NJ: Wiley, 2014.
- [117] H. D. Young and R. A. Freedman, University Physics with Modern Physics, 14th ed. Boston, MA: Pearson, 2015.
- [118] Abaqus Acumen, "Boundary Conditions in Abaqus Using Reference Points," YouTube, May 20, 2021. [Online]. Available: <https://www.youtube.com/watch?v=3mZzTpajh70>
- [119] The MathWorks, Inc., MATLAB version: 9.13.0 (R2022b). Natick, MA: The MathWorks, Inc., 2022. [Online]. Available: <https://www.mathworks.com>